MODELLING INHERITED PRION DISEASES IN MICE

Submitted by

Bernie Simone Owusu-Yaw

MRC Prion Unit at UCL

This thesis is submitted for the degree of Doctor of Philosophy

Declaration

I, Bernie Simone Owusu-Yaw confirm that the work presented in this thesis is my own. Where information has been derived from other sources, I confirm that this has been indicated in the thesis.

Abstract

Prion diseases are fatal neurodegenerative diseases of mammals, caused by a misfolded infectious protein. There are 3 aetiological forms namely sporadic, acquired or inherited. The genetic component makes it possible for transgenic technology to be applied to the modelling of prion diseases. In 2013 Mead *et al*. reported a novel prion disease linked to a stop codon mutation at residue 163 (Y163X) in the human prion protein gene (*PRNP*). This mutation results in the production of a truncated prion protein (PrP) lacking both glycosylation sites and GPI anchor, and it is associated with an atypical prion disease phenotype including diarrhoea, autonomic neuropathy and the accumulation of PrP amyloid in peripheral organs and blood vessels. Typically, prion diseases predominantly affect the nervous system so the uniqueness of the Y163X disease phenotype makes it a good candidate for the study of prion therapeutics. The aim of this project was therefore to develop mouse models expressing human PrP Y163X that recapitulate human disease and then to study ageing cohorts of homozygous and heterozygous mice for spontaneous amyloid deposition. Two different approaches were pursued as follows: (1) Conventional transgenic approach (2) Gene targeted approach (CRISPR- Cas9 and knock-in technology). Six transgenic lines expressing HuPrP 163X under the control of the ubiquitous CAG promoter were generated alongside transgenic wild-type controls expressing wild-type human PrP. Y163X knock-in mice and control knock-in mice expressing wild-type human PrP generated from blastocyst injection of embryonic stem cells were made commercially. These lines were characterised for expression of the truncated 163X human prion protein using techniques such as western blotting, ELISA, fluorescent immunohistochemistry and RT-PCR. Aging cohorts from homozygous lines were set up in long term observation experiments. A panel of CNS and peripheral tissues has been isolated at defined time points for immunohistochemical analysis to determine if the expression of HuPrP Y163X in transgenic and knock-in mice is sufficient to cause spontaneous PrP amyloid deposition.

Impact Statement

Inherited prion diseases account for approximately 15% of human prion diseases. These diseases are associated with autosomal dominant mutations in *PRNP* that can usually be classified as Creutzfeldt Jakob disease (CJD), Gerstmann–Sträussler–Scheinker (GSS) or Fatal familial insomnia (FFI), based on clinical symptoms and neuropathology. Over 40 pathogenic mutations have been discovered. These mutations can be separated into 3 groups: missense, nonsense and octapeptide repeat insertion mutations and they are usually associated with CJD, GSS or FFI. However, stop codon mutations are associated with atypical phenotypes that cannot be classified as FFI, CJD or GSS. These mutations are associated with neurofibrillary tangles and the deposition of prion protein (PrP) as amyloid in the brain and blood vessels. In 2013, Mead and colleagues reported a novel prion disease associated with the Y163X stop codon mutation. This mutation leads to the production of truncated PrP without a GPI anchor. Patients harbouring this mutation presented an unusual clinical phenotype of chronic diarrhoea and peripheral neuropathy. This disease is very debilitating and it has a slow disease progression over 20 years. The mechanisms involved in this unique disease are not fully understood and there are no disease modifying treatments available for this condition. Two novel mouse models expressing human PrP 163X have been generated to model this unique prion disease. Transgene expression has been confirmed at mRNA and protein level in control lines expressing wild-type human PrP, however, detection of protein in the Y163X lines proved to be difficult to achieve. Notably, similar difficulties are observed with patient brain samples confirming the appropriateness of the newly generated models. Murine cell lines expressing human PrP 163X were also generated in this project as part of the characterisation of this truncated protein. Abnormal trafficking of the mutant was protein observed in the cell lines expressing human PrP 163X compared to the control lines expressing wild-type human PrP.

These findings suggest that glycosylation and the GPI anchor play a role in the cellular trafficking of PrP. Primary neuronal cells could be derived from these new mouse models in future to further investigate the impact of PrP trafficking defects in the pathogenesis of this disease. Several experimental groups have been set up as ageing cohorts to study spontaneous deposition of amyloid plaques in the CNS and peripheral organs. These new mouse models can be used as tools to dissect the molecular mechanisms involved in this atypical prion disease. Patients with the Y163X mutation have presented with symptoms from as early as 27 years of age. Treating this cohort of patients as early as possible could potentially slow down the disease progression and improve the survival of these patients. Once the time point for onset of spontaneous PrP plaques has been determined through the long-term observation experiments, these new models can be used to evaluate efficacy and safety of small molecules and immunotherapeutics developed at the Institute of Prion Diseases, before progressing to clinical trials.

Acknowledgements

First and foremost I would like to thank Jesus my Lord and personal saviour for always seeing me through.

I would also like to thank my supervisors Dr Emmanuel Asante and Dr Jonathan Wadsworth for their continued support, guidance and mentorship throughout this PhD.

Next, I would like to thank my colleagues Shyma Hamdan and Tatiana Jakubcova for training me in the lab and for being a constant source of support and encouragement. Thank you to Andrew Tomlinson for helping me breed and maintain the mouse lines and for performing all the microinjections. I am very grateful for all your contributions to this project. Thank you to all the staff at the Biological Services Facility for animal husbandry and tissue collection.

I would also like to thank Professor Parmjit Jat for all the advice and assistance throughout this PhD and for providing the CAD5 cells. I am very grateful to Nunu Arora for taking the time to train me in tissue culture and for helping me to generate the CAD5 cell lines. Thank you to Aline Marinho for all her advice on primary neuronal cultures.

In addition, I would also like to thank Adam Wenborn for training me to perform ELISA's. Thank you to Juan Ribes and Hazim Halim for their assistance with immunostaining and the confocal microscope. Also, thank you to Peter Kloehn and Azadeh Khalili-Shirazi for providing anti-PrP antibodies.

I would like to thank Professor Simon Mead for making it possible for me to meet patients with this novel prion disease, to which I am grateful. Thank you to Emmanuelle Vire for all the RNA advice.

Thank you to Professor John Collinge for being so supportive of this project and for all of his contributions to this project.

Lastly, I would like to thank my amazing family who have been a solid support system. Thank you to Daniel Owusu-Yaw, Evelyn Owusu-Yaw, Joseph, Owusu-Yaw, Danielle Owusu-Yaw, Elizabeth Serwaa, Kofi Acheampong, Agnes Acheampong, Sophia Acheampong, Anita Osei-Poku, Richard Owusu-Ansah, Nicholas Kotei, Ken and Elizabeth Aduhene, Festus and Rita Mensah. Thank you all for your constant support.

Table of Contents

List of figures

List of tables

List of abbreviations

Abbreviation	Meaning
BCA	Bicinchoninic acid
BSA	Bovine serum albumin
CAA	Cerebral amyloid angiopathy
CAG	Cytomegalovirus (CMV) enhancer fused to the chicken beta-actin promoter
Cas-9	CRISPR-associated protein 9
cDNA	Complementary DNA
CJD	Creutzfeldt-Jakob disease
CMV	Cytomegalovirus
CRISPR	Clustered regularly interspaced short palindromic repeats
crRNA	Crispr RNA
ctRNP	crRNA + tracrRNA + Cas9 Protein complex
CWD	Chronic wasting disease
DAPI	4′,6-diamidino-2-phenylindole
dCt	Delta Ct
ddCt	Delta-Delta-Ct
ddH_2O	Double-distilled water
DMEM	Dulbecco's Modified Eagle Medium
DMEM-FBS	Dulbecco's Modified Eagle Medium supplemented 10% Fetal Bovine Serum + 1% PenStrep
DNA	Deoxyribonucleic acid
DPBS	Dulbecco's phosphate-buffered saline
dsDNA	Double-stranded DNA
E. coli	*Escherichia coli*
ELISA	Enzyme-Linked Immunosorbent Assay

FBS	Fetal Bovine Serum
FFI	Fatal Familial Insomnia
FSH	Follicle-stimulating hormone
GPI	Glycosylphosphatidylinositol
GSS	Gerstmann-Sträussler-Scheinker Disease
iCJD	Iatrogenic CJD
IF	Immunofluorescence
IHC	Immunohistochemistry
INDELs	Insertions and deletions
*iv*RT	*In vitro* transcription and reverse transcription
KI	Knock-in
LB	Lysogeny broth
LH	Luteinising hormone
mRNA	Messenger RNA
NCAM	Neural cell adhesion molecule
NHEJ	Non-homologous end joining
OBGS	OptiMEM supplemented 10% Bovine Growth Serum + 1% PenStrep
ORF	Open reading frame
PAM	Protospacer adjacent motif
PBS	Phosphate buffered saline
PBST	Phosphate buffered saline with tween 20
PCR	Polymerase chain reaction
PK	Proteinase K
PRNP	Human Prion Protein Gene
PrP	Prion protein

PrP $^{o/o}$	PrP-null
PVDF	Polyvinylidene fluoride
qPCR	Quantitative real-time PCR
RBPs	RNA-binding proteins
RNA	Ribonucleic acid
RT-PCR	Reverse transcription polymerase chain reaction
RV	Relative value
SDS-PAGE	Sodium dodecyl sulfate polyacrylamide gel electrophoresis
sgRNA	Single guide RNA
SOD1	Superoxide Dismutase 1
ssDNA	Single-stranded DNA
ssODN	Single-strand oligodeoxynucleotide
TE	Tris-EDTA
Tg	Transgenic
tracrRNA	Trans-activating CRISPR RNA
vCJD	Variant CJD
VGCCs	Voltage-gated calcium channels
WB	Western blot

1. Chapter 1: Introduction

Prion diseases are fatal transmissible neurodegenerative disorders that affect humans and a variety of animals (Collinge, 2001). The first prion disease to be identified was scrapie which affects both sheep and goats (Jeffrey and González, 2007). Other prion diseases affecting animals include bovine spongiform encephalopathy (BSE) in cattle, transmissible mink encephalopathy in mink and chronic wasting disease in deer and elk. Human prion diseases include Creutzfeldt Jakob disease (CJD), Kuru, Gerstmann–Sträussler–Scheinker (GSS) disease and fatal familial insomnia (FFI) (Table 1.1 and 1.2).

Table 1.1 Prion diseases in humans

Humans	Year	Country of first report	Reference
Sporadic Creutzfeldt Jakob disease	1920	Germany	(Jakob, 1921)
Familial CJD	1924	Germany	(Meggendorfer, 1930)
Gerstmann–Sträussler–Scheinker	1936	Austria	(Gerstmann et al., 1936)
Kuru	1957	New Guinea	(Gajdusek and Zigas, 1959)
Iatrogenic Creutzfeldt Jakob disease	1974	USA	(Duffy, 1974)
Fatal familial insomnia	1986	Italy	(Lugaresi et al., 1986)
Variant Creutzfeldt Jakob disease	1996	UK	(Will et al., 1996)

Table 1.2 Prion diseases in animals

Animals	Year	Country of first report	Reference
Scrapie (Sheep and goats)	1732	England	(McGowan, 1922)
Transmissible Mink encephalopathy	1947	USA	(Hartsough and Burger, 1965)
Chronic wasting disease (Elk and deer)	1967	USA	(Williams and Young, 1980)
Bovine spongiform encephalopathy (Cattle)	1986	UK	(Wells et al., 1987)

Prion diseases are also experimentally transmissible to a range of different animal species including mice, ferrets, hamsters and non-human primates (Imran and Mahmood, 2011).

1.1 The Cellular Prion Protein

The cellular prion protein (PrP^C) is an N-glycosylated protein that is attached to the cell surface via a glycosylphosphatidylinositol (GPI)-anchor (Puig et al., 2019)

The gene encoding PrP^C in humans, *PRNP*, is located on the short (p) arm of chromosome 20 (20p12-ter) (Makrinou et al., 2002). PrP^C is a 253 amino-acid protein that is post-translationally processed to remove the first 22 amino acid residues, encoding a signal peptide at the amino terminal (Chen et al., 1995). The last 23 amino acid residues located at the carboxyl-terminal are also cleaved off and replaced with a glycosyl phosphatidylinositol (GPI) anchor, resulting in mature PrP^C anchored to the cell surface, consisting of 208 amino acids (Büeler et al., 1993; Chen et al., 1995).

1.2 The Role of PrP^C

Studies have demonstrated that the expression of PrP^C is essential for development of prion disease; however, the function of PrP^C remains enigmatic. Experiments carried out using PrP-null ($PrP^{o/o}$) mice demonstrated that these mice develop normally without any gross abnormalities (Büeler et al., 1992, 1993). $PrP^{o/o}$ mice challenged with mouse-adapted scrapie prions were resistant to infection and did not develop prion disease (Büeler et al., 1993). The absence of an overt phenotype in the PrP-null mice may be due to compensation by Doppel and Shadoo, which are both proteins that belong to the PrP family. Nonetheless, subsequent electrophysiological studies in PrP-null mice showed several functional abnormalities including, impaired long-term potentiation, reduced GABAergic synaptic transmission, the disruption of slow calcium activated potassium currents and alterations in sleep and circadian rhythms (Collinge et al., 1994; Colling et al., 1996; Tobler et al., 1996; Curtis et al., 2003).

PrP^C has the ability to bind to copper ions to the N-terminal octarepeat domain (Figure 1.1) and it has been implicated in the regulation of copper metabolism (Brown et al., 1997a; Stöckel et al., 1998). The concentration of copper in synaptosomal fractions is 50 % lower in PrP-null mice compared to wild-type mice, therefore it has been suggested that PrP^C may regulate the concentration of copper at pre-synaptic terminals (Herms et al., 1999) .

Figure 1.1: Schematic diagram of PrP^C with the octarepeat domain marked in purple and GPI anchor marked in green. The two glycosylation sites, Asn-181 and Asn- 197 are in the C-Terminal domain. NTD= N-Terminal domain, CTD= C-Terminal domain.

Oxidative stress is a common feature of neurodegenerative diseases and several lines of evidence suggest the involvement of PrP^C in the protection of cells from oxidative stress. Tissue culture experiments revealed that cerebellar neurons cultured from PrP-null mice were more sensitive to oxidative stress compared to wild-type neurons (Brown et al., 1997b). *In vivo* experiments also demonstrate that there is a reduction in the enzymatic activity of copper/zinc-dependent superoxide dismutase 1 (SOD1) in the brains of PrP-null mice (Brown et al., 1997b). The protective mechanisms of PrP^C are yet to be determined but it has been suggested that PrP^C may indirectly protect cells by controlling the activities of anti-oxidant enzymes such as SOD1 (Brown et al., 1997b; Brown and Besinger, 1998).

PrP^C also interacts with a diverse range of proteins involved in cell adhesion such as the neural cell adhesion molecule (NCAM) and laminin (Graner et al., 2000a; Santuccione et al., 2005).

Experiments have demonstrated that PrP^C binds to NCAM at the neuronal cell surface. This interaction promotes the redistribution of NCAM to lipid rafts, neurite outgrowth and leads to the activation of Fyn kinase, an enzyme involved in NCAM signalling. The disruption of the interaction between PrP^C and NCAM by PrP antibodies or in PrP-deficient and NCAM-deficient neurons inhibits neurite outgrowth (Santuccione et al., 2005).

Laminin is located in the basement membrane and it plays a role in neuronal cell migration, survival and differentiation. PrP^C has been identified as a binding partner of laminin and studies have demonstrated that the binding of PrP^C promotes neurite outgrowth in hippocampal neurons and PC-12 cells (Graner et al., 2000a). Graner *et al*. have also shown that laser ablation of PrP^C on the cell –surface of PC-12 cells induced neurite retraction (Graner et al., 2000b).

1.3 The Protein Only Hypothesis

It is widely accepted that prions are the unconventional transmissible agents that cause prion disease (Prusiner, 1982). Prions are self-propagating, infectious multi-chain assemblies of misfolded host-encoded PrP (Collinge, 2016). The first proposal that the disease agent could be a protein was by Griffith in 1967 (Griffith, 1967).

The protein-only hypothesis proposes that prions are principally or entirely composed of a protease-resistant, misfolded isoform of the host-encoded PrP^{C}, designated as PrP^{Sc} (Prusiner, 1998). According to this hypothesis, prion replication occurs via the conversion of PrP^{C} to PrP^{Sc} (Prusiner, 1982, 1998; Poggiolini et al., 2013).

During this process, PrP^{Sc} acts as a seed or template for the recruitment and conversion of PrP^{C} to further PrP^{Sc} (Telling et al., 1996).

Prions were originally thought to be composed of PrP^{Sc} but more recent evidence suggests that prions are composed of several multi-molecular assemblies of misfolded PrP, including protease sensitive PrP isoforms (Pastrana et al., 2006; Cronier et al., 2008; Collinge, 2016).

1.4 The Role of the GPI anchor in Prion Disease

The role of the GPI anchor in prion disease remains elusive. Tissue culture experiments suggest that the conversion of PrP^{C} to PrP^{Sc} occurs at the plasma membrane and/or in endocytic pathways (Béranger et al., 2002; Goold et al., 2011).

A study that involved the expression of epitope tagged PrP^{C} in a PrP-knockdown neuroblastoma line, reported de novo formation of epitope-tagged PrP^{Sc} on the plasma membrane minutes after the cells had been infected with Rocky Mountain Laboratory (RML) mouse prions (Goold et al., 2011).

In this study the researchers also discovered that PrP^{Sc} formation was inhibited when cells were treated with reagents that disrupt the integrity of lipid rafts. These findings suggest that the conversion of PrP^{C} to PrP^{Sc} depends on the presence of lipid raft domains in the plasma membrane (Goold et al., 2013).

Further experiments revealed that PrP^{Sc} is internalised via endosomes after it is formed at the cell surface, where it has different fates. Some PrP^{Sc} is recycled back to the plasma membrane and used as a template for PrP^{C} conversion, whereas the remaining PrP^{Sc} is subject to retrograde transport to the Golgi apparatus and degradation in lysosomes (Goold et al., 2013).

Studies have also shown that expressing GPI-anchorless PrP^{C} in scrapie-infected N2a mouse neuroblastoma (ScN2a) cells abrogated PrP^{Sc} formation. In this study the GPI anchor was replaced with transmembrane regions from mouse CD4, which led to the chimeric PrP (CD4 PrP^{C}) being transported outside the lipid raft domains (Taraboulos et al., 1995).

Overall, these findings suggest that the anchoring and localisation of PrP^{C} in lipid raft domains is important for the conversion of PrP^{C} to PrP^{Sc}.

Chesebro *et al.*2005 generated transgenic mice expressing low levels of anchorless PrP^{C}, to investigate the role of the GPI anchor in prion disease pathogenesis *in vivo* (Chesebro et al., 2005) . In earlier experiments, transgenic (Tg) mice expressing low levels of anchorless PrP ($GPI^{-/-}$) did not develop clinical signs of prion disease, however, prion propagation accompanied by the additional formation of PrP amyloid was observed in the brains of these mice following inoculation with RML or 22L-mouse adapted scrapie prions. Although the GPI-anchorless PrP^{C} was not present in lipid rafts, it was still converted into amyloidogenic forms of disease-associated PrP. This study suggested that the GPI anchor is not required for prion replication (Chesebro et al., 2005).

In a follow-up study Chesebro and colleagues generated transgenic mice expressing two-fold more anchorless PrP compared to the mice in the previous experiment (Chesebro et al., 2010). They reported that the inoculation of these mice with RML or 22L mouse prions produced a distinct clinical phenotype when compared to non-transgenic mice inoculated with the same mouse prions. In the transgenic mice expressing two-fold more anchorless PrP, they observed longer incubation periods (~300-480 days) and PrP amyloidosis without gray matter spongiosis.

However the non-transgenic mice were characterised by shorter incubation periods (~150-160 days) and the deposition of abnormal forms of non-amyloidogenic PrP with gray matter spongiosis (Chesebro et al., 2010).

In another study, transgenic mice expressing higher levels of anchorless PrP developed spontaneous disease, accompanied by the deposition of amyloidogenic PrP. The transgenic mice were then crossed with wild-type mice to generate transgenic mice co-expressing wildtype PrP and anchorless PrP. The co-expression of anchorless PrP and wild-type PrP^C resulted in accelerated disease progression (Stöhr et al., 2011).

These results implicate membrane-anchored PrP^C in the pathogenesis of prion disease, and demonstrate that the presence or absence of the PrP-GPI anchor can influence the pathogenesis of prion disease (Stöhr et al., 2011).

1.5 The Role of Glycosylation in Prion Disease

Glycosylation refers to the process in which a carbohydrate (glycan) is covalently attached to a protein or a lipid to form a glycoconjugate (Reily et al., 2019). Glycosylation can influence the different properties of a protein including: structure, function, localisation and stability (Roth et al., 2012; Lee et al., 2015). N-linked glycosylation involves the enzymatic transfer of glycans to selected asparagine residues (Breitling and Aebi, 2013). This process occurs at the consensus sequence NXT/S where N is asparagine, S is serine, T is threonine and X is any amino acid other than aspartic acid or proline (Rao and Wollenweber, 2010). Human PrP^{C} contains two N-glycosylation sites (Asn 181 and Asn 197). Variable occupancy at these sites produces different glycoforms of PrP: un-glycosylated (with no glycan attachment), di-glycosylated (when both sites at 181 and 197 are occupied), mono-glycosylated (when either residue 181 or residue 197 is occupied) (Lawson et al., 2005).

The function of PrP glycosylation under normal conditions and in the disease process remains elusive (Tuzi et al., 2008). Studies in transgenic mice suggest that PrP glycosylation influences the cellular location of PrP. Cancellotti and colleagues generated three lines of transgenic mice with mutations at the first, second or both glycosylation sites - designated as G1 (N180T), G2 (N196T) and G3 (N180T-N196T) (Cancellotti et al., 2005). G1 and G2 mice express unglycosylated and monoglycosylated forms of PrP but lack diglycosylated PrP, whereas G3 mice only express unglycosylated forms of PrP (Tuzi et al., 2008).

In G1 and G2 mice they found that PrP was located on the cell surface, however in G3 mice PrP was mainly localised intracellularly (Cancellotti et al., 2005). When these three lines were inoculated with two different prion strains, 79A and ME7 there were differing responses between the lines. They reported that all three homozygous lines were susceptible to 79A, however the incubation periods were longer for G3 mice (435 ± 92 d) compared to G1 (194± 21d) and G2 mice (167±9.3d). Clinical disease was observed in all G1 and G2 mice, whereas only 4/21 G3 mice were scored as clinically positive. G1 and G3 mice were resistant to infection with ME7 but all G2 mice developed clinical disease following inoculation with ME7.

Despite the absence of spongiform degeneration and PK-resistant PrP in the brains of G3 mice, PrP-positive plaques were detected in the corpus callosum of some of these mice. Further sub passage experiments need to be carried out to determine whether these mice are propagating infectious PrP assemblies alongside fibrillar PrP amyloid assemblies (Terry and Wadsworth, 2019).

The authors reported that these findings demonstrate that PrP glycosylation is not essential for susceptibility to prion disease. They also show that PrP glycosylation influences incubation period and the ability of strains to induce prion disease in the host (Tuzi et al., 2008).

1.6 Introduction to Human Prion Diseases

Human prion diseases can be inherited, occur sporadically or be acquired by infection (Collinge and Clarke, 2007).

Sporadic Creutzfeldt-Jakob disease (sCJD)

The most common form of human prion disease is sporadic Creutzfeldt-Jakob disease and it accounts for~ 85% of cases of human prion disease (D'Aignaux et al., 2002). Clinical symptoms of sCJD include myoclonus, rapidly progressive cognitive decline, pyramidal and extrapyramidal signs and cerebellar ataxia (Zanusso et al., 2016). The neuropathological features of sCJD include spongiform degeneration, astrocytosis and neuronal loss (Belay, 1999). sCJD often has a rapid disease course with a mean survival of six months (Lahiri et al., 2019).

Acquired human prion diseases

Acquired prion diseases include iatrogenic CJD, kuru and variant CJD and they account for ~1% of cases of human prion disease (Table 1.3) (Jackson and Krost, 2014).

Table 1.3 Acquired human prion diseases

Acquired human prion disease	Aetiology	Neuropathological features	Reference
Iatrogenic CJD (iCJD)	Accidental transmission of CJD prions via surgical or medical procedures: human dura matter grafts, human growth hormone treatment, contaminated electroencephalographic electrodes and corneal transplantation	Resembles sCJD	(Wadsworth and Collinge, 2011) (Collinge, 2001)
Variant CJD (vCJD)	Human exposure to BSE prions	Florid plaques	(Wadsworth and Collinge, 2011) (Collinge, 2001)
Kuru	Cannibalism	Amyloid plaques	(Wadsworth and Collinge, 2011) (Collinge, 2001)

1.7 Inherited Prion Diseases

Inherited Prion Diseases (IPDs) are associated with autosomal dominant mutations in the human prion protein gene (*PRNP*) and account for approximately 10-15% of human prion disease (Wang et al., 2019). Over 30 pathogenic mutations in *PRNP* have been reported, and these mutations can be separated into three groups: missense mutations, nonsense mutations and octapeptide repeat insertion mutations (Windl et al., 1999; Mead, 2006; Capellari et al., 2011) (Figure 1.2).

How *PRNP* mutations cause prion disease remains to be determined. However, it has been suggested that some *PRNP* mutations increase the tendency of PrP^{C} to spontaneously fold into disease-associated conformers of misfolded PrP (Apetri et al., 2004).

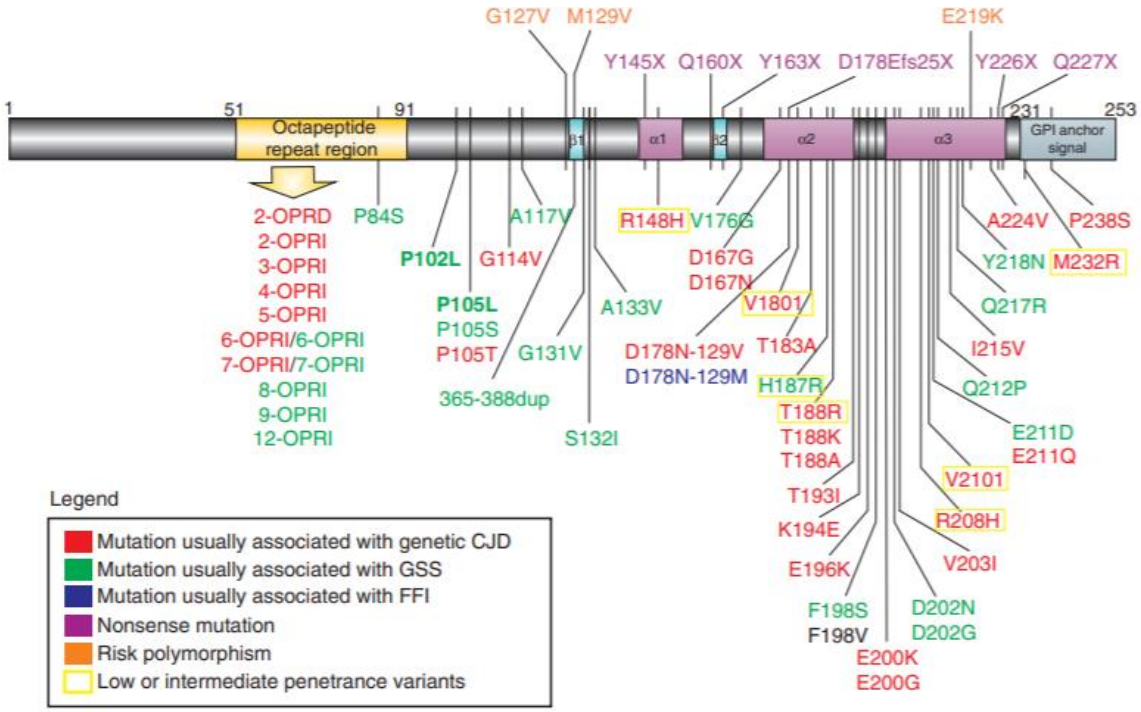

Figure 1.2: Schematic of *PRNP* associated variants. Adopted from Kim *et al.*, 2018 (Kim et al., 2018)

Inherited prion diseases can be sub-classified by clinical or pathological phenotypes as fatal familial insomnia (FFI), CJD or Gerstmann-Sträussler Scheinker disease (GSS) (Kovács et al., 2002).

FFI is characterised by insomnia, dementia, dysautonomia and thalamic atrophy (Lugaresi et al., 1986; Parchi et al., 1995). GSS typically presents as an ataxic disorder with the later development of dementia and it is associated with the histopathologic presence of PrP amyloid plaques in the brain (Masters et al., 1981; Hudson et al., 1983; Kovács et al., 2002). Although inherited prion diseases can be sub-classified into these groups, there are instances in which patients with the same mutation present different clinicopathological phenotypes (Poulter et al., 1992). Also, in some cases there is an overlap in symptoms of the different genetic forms of prion disease (Poulter et al., 1992; Hainfellner et al., 1995).

Inherited prion diseases can be caused by a variety of point mutations that result in the substitution of a single nucleotide, which causes a single amino acid change in PrP (Table 1.4).

Table 1.4 *PRNP* Missense mutations

PRNP Mutation	*PRNP* codon 129	Amino acid change	Phenotype	Reference
P102L	M	Proline to Leucine	GSS	(Tesar et al., 2019)
P102L	V	Proline to Leucine	GSS	(Young et al., 1997)
P105L	V	Proline to Leucine	GSS	(Kitamoto *et al*., 1993)
A117V	V	Alanine to Valine	GSS	(Mallucci *et al*., 1999)
D178N	M	Aspartic acid to Asparagine	FFI	(Medori et al., 1992)
D178N	V	Aspartate to Asparagine	CJD	(Goldfarb et al., 1992)
E200K	M/V	Glutamic acid to Lysine	CJD	(Goldgaber et al., 1989)

1.8 Nonsense mutations in *PRNP*

Nonsense mutations in *PRNP* are accompanied by a variety of atypical phenotypes (Table 1.5), which cannot be classified as FFI, CJD or GSS (Mead and Reilly, 2015; Bagyinszky et al., 2018). These mutations are very rare and they lead to the integration of a stop codon, resulting in the expression of truncated forms of PrP without a GPI anchor (Mead et al., 2013). Truncating mutations have been associated with unique phenotypes including chronic diarrhoea, cerebral amyloid angiopathy and neurofibrillary tangles, similar to those reported in Alzheimer's disease (Ghetti et al., 1996; Mead et al., 2013).

Table 1.5 *PRNP* nonsense mutations

PRNP Mutation	Pathological features	Clinical features	Reference
Y145X	PrP-CAA, neurofibrillary tangles, PrP amyloid deposits	Slowly progressive dementia	(Ghetti et al., 1996)
Q160X	Neurofibrillary tangles, PrP amyloid deposits	Slowly progressive dementia, Orbitofrontal syndrome Sensorimotor polyneuropathy	(Fong et al., 2016)
Y226X	PrP CAA, PrP amyloid deposits	Dementia Hallucinations	(Jansen et al., 2010)
Q227X	PrP Amyloid deposits, PrP CAA, neurofibrillary tangles	Dementia Extrapyramidal signs	(Jansen et al., 2010)
Y163X	PrP CAA, PrP amyloid deposits, neurofibrillary tangles	Chronic diarrhoea, sensorimotor polyneuropathy	(Mead et al., 2013)

1.9 Octapeptide Repeat Insertions in the Prion Protein Gene

The octapeptide repeat region in PrP normally contains four octapeptide repeats and one nonapeptide repeat (Renner et al., 2004; Miura et al., 2005). Insertions of additional octapeptide repeats in this region between codons 51 and 91 can be pathogenic (Beck et al., 2001; Croes et al., 2004). Insertional mutations resulting in the addition of one or up to twelve octapeptide repeats have been identified in patients (Schmitz et al., 2017). It has been reported that disease onset occurs earlier in some patients with insertional *PRNP* mutations compared to other inherited forms of prion disease and longer disease duration has been reported in some cases (Gelpi et al., 2005).

In 1990 a new PRNP disease was reported that was associated with six octapeptide repeat insertions (Owen et al., 1990; Gelpi et al., 2005). Core features identified in the British and Basque-French family members include, cortical dementia, myoclonus and cerebellar ataxia (Gelpi et al., 2005) (Mead, 2006). The deposition of PrP in the cerebellum has been consistently reported in patients with this mutation but a spectrum of clinical and neuropathological changes have been reported between individuals and also within members of the same family carrying the same mutation (Gelpi et al., 2005; Xiao et al., 2013).

Evidence suggests that the polymorphism at codon 129 in *PRNP (*M129V*)* that results in a methionine or valine allele influences the disease phenotype (King et al., 2003). The codon 129 polymorphism status of individuals could therefore contribute to the phenotypic variability observed between and within families (Mead, 2006). Studies have also demonstrated that the wild-type *PRNP* allele can contribute to the disease pathogenesis which could also account for phenotypic heterogeneity observed in inherited prion diseases (Chen et al., 1997; Wadsworth et al., 2006).

1.10 Prion Strains

Prion strains can be defined as conformational variants that produce distinct phenotypes when transmitted into inbred rodents with an identical *PRNP* genetic background (Telling et al., 1996; Safar et al., 1998; Collinge and Clarke, 2007). A wide variety of distinct prion strains exist and they are distinguished by differences in incubation periods, clinical signs and neuropathological profiles, following passage of prions into experimental animals (Morales, 2017).

Distinct prion strains are associated with different conformations of PrP^{Sc} and strains can also be distinguished biochemically based on glycosylation profiles and electrophoretic mobility following digestion with PK (Collinge et al., 1996; Parchi et al., 1996, 1999) (Parchi et al., 1996) (Parchi et al., 1999, 2009; Hill et al., 2003; Wadsworth et al., 2003).

Different PrP^{Sc} types can be differentiated using western blot analysis by differences in fragment size following PK digestion and the ratio of unglycosylated, monoglycosylated and diglycosylated PrP (Wadsworth et al., 1999, 2003; Hill et al., 2003).

Sporadic and iatrogenic CJD (jointly designated classical CJD) are associated with four major types of PrP^{Sc} (Collinge et al., 1996; Hill et al., 2003). PrP^{Sc} types 1-3 are observed in classical CJD brain, whereas type 4 PrP^{Sc} is observed in variant CJD brain (Collinge et al., 1996; Hill et al., 2003). The PrP^{Sc} types seen in inherited prion diseases vary and they are different from those observed in classical and variant CJD (Telling et al., 1996; Piccardo et al., 1998, 2001; Hill et al., 2006).

1.11 Modelling Prion Diseases in Mice

Until transgenic technology made it possible to design animal models with specific genetic modifications, prion transmission studies were initially performed using wild-type mice (Chandler, 1961). Wild type mice were inoculated with different strains of prions and following an incubation period, which varies depending on prion strain, levels of PrP^C expression and genetic background of the host, mice begin to develop clinical signs of prion disease (Carlson et al., 1986; Sandberg et al., 2011). Clinical signs of prion disease in mice include ataxia, kyphosis and rigidity of the tail (Carlson et al., 1986; Flechsig et al., 2000).

Wild type mouse bioassays can be used to measure prion infectivity in biological samples using two different approaches: 1) End-point titration bioassay 2) Incubation time bioassay. In the end-point titration assay mice are inoculated with a series of 10-fold dilutions of the sample of interest and the prion titer is determined in terms of the dilution at which 50% of the animals inoculated develop prion disease (Prusiner et al., 1981, 1982).

Incubation time is defined as the time interval between exposure to prions and the development of prion disease (Collinge, 2005). The incubation time bioassay uses fewer animals and is less time consuming than the end-point titration assay, however, it is less accurate (Prusiner et al., 1982). This bioassay determines prion infectivity by comparing the incubation periods in prion-inoculated mice with a calibration curve generated using a sample of known prion titer (Prusiner et al., 1982; Watts and Prusiner, 2014).

One of the drawbacks of using wild-type mice to study prions is that the transmission of human prions in these mice is less efficient and produces prolonged incubation periods, partly due to the so-called species barrier effect (Telling et al., 1994). The species barrier describes the inefficient transmission of prions from one species to another when compared to intraspecies transmissions (Collinge, 2005; Wadsworth et al., 2010).

The similarity of the amino acid sequences between the donor and recipient influences cross-species conversion of PrP^C and species barriers arise due to differences in the primary structure of PrP in the prion strain being investigated between the donor and the recipient (Scott et al., 1989).

The generation of transgenic mice expressing human PrP permitted the analysis of a variety of human prion strains in the absence of a species barrier. The first transgenic mouse model of prion disease was developed by Scott and colleagues in 1989 (Scott et al., 1989). These transgenic mice expressed hamster PrP and retained the endogenous mouse PrP so they were susceptible to both hamster and mouse prions, whereas control wild type mice remained resistant to hamster prions (Scott et al., 1989).

The concept of transmission barriers was introduced for situations where despite the abrogation of the species barrier through transgenic technology, prion propagation in animal models is still inefficient (Collinge and Clarke, 2007).

Prion diseases were initially modelled in transgenic mice expressing human PrP transgenes on a mouse *Prnp*$^{+/+}$ background (Telling et al., 1994, 1995). However the mouse PrP gene interfered with the efficient propagation of human prions in these mice (Collinge et al., 1995; Telling et al., 1995). The generation of PrP null (PrP$^{0/0}$) (Büeler et al., 1992) mice enabled ‘’humanised’’ transgenic mouse models to be developed without interference of the endogenous mouse PrP (Büeler et al., 1992; Telling et al., 1995; Wadsworth et al., 2010).

1.12 Transgenic Mouse Models of Prion Disease

Different approaches are used to generate animal models and each approach has its own advantages and disadvantages.

In conventional transgenic mouse models the transgene is randomly integrated into the host genome (Bryda et al., 2006; Asante et al., 2015). Mouse models generated using this approach can produce variable levels of PrP. Examples of some commonly used transgenic mouse models expressing different levels of PrP are listed in Table 1.6. This is advantageous for prion disease modelling purposes as increasing PrP expression reduces incubation time compared to wild-type mice (Prusiner et al., 1990). Therefore PrP overexpression models are useful as the lifespan of a mouse is limited and in some instances the incubation period may exceed the natural lifespan of a mouse which is approximately two years depending on the mouse strain (Dickinson et al., 1975; Wang et al., 2020).

However, as the transgene is randomly inserted into the genome, position effects can interfere with transgene expression (Feng et al., 2001). This can lead to variable spatial expression patterns of PrP in different lines (Kaczmarczyk and Jackson, 2015; Kaczmarczyk et al., 2016).

Table 1.6 Expression levels of transgenic mice overexpressing human PrP^C

Mouse line	PrP genotype	Fold expression above endogenous levels of PrP^C	Reference
Tg152	HuPrP 129V	4-8	(Telling et al., 1994)
Tg35	HuPrP 129M	2	(Asante et al., 2002)
Tg45	HuPrP 129M	4	(Asante et al., 2002)
Tg650	HuPrP 129M	6	(Béringue et al., 2008)

Several different experimental models of inherited prion diseases have been produced via the transgenic approach (Table 1.7).

Table 1.7 Transgenic mouse models of inherited prion disease

PRNP Mutation	Mouse line	PrP sequence	Fold expression above endogenous levels of PrP^{C}	Spontaneous formation of prions?	Reference
P102L	Tg174	Mouse	8x	Yes	(Hsiao et al., 1990)
P102L	Tg27	Human	3x	No	(Asante et al., 2009)
A117V	Tg30	Human	3x	Yes	(Asante et al., 2020)
E200K	Tg23	Human	3x	No	(Asante et al., 2009)
D178N, M129	FFI	Mouse	2x	Yes	(Bouybayoune et al., 2015)
D178N, V129	CJD	Mouse	2x	Yes	(Dossena et al., 2008)
A224V	Tg (HuPrP, V129, A224V)	Human	1.5-3.2 x	No	(Watts et al., 2015)

Some models express human PrP whereas others express mouse homologues of the human pathogenic mutations. Many of these lines expressing mouse homologue of human *PRNP* mutations on the mouse prion protein develop spontaneous prion disease accompanied with disease specific neuropathological changes (Hsiao et al., 1990; Jackson et al., 2009, 2013). However, contrasting results have been obtained using models generated from direct modelling of human PrP mutations on the human prion protein, compared with mouse models expressing mouse PrP with the mouse equivalent of the human mutation (Manson et al., 1999; Asante et al., 2015).

Prions generated in gene-targeted mice expressing mouse PrP 101L that had been challenged with human GSS-102L prions were capable of transmitting disease to wild-type mice and 101L PrP knock-in mice upon serial passage (Manson et al., 1999). However, prions produced in transgenic mice expressing human PrP 102L challenged with GSS-102L were unable to infect transgenic mice expressing wild-type human PrP (Asante et al., 2015). These contrasting findings question the relevance of data obtained from models that superimpose human PrP mutations onto rodent PrP (Asante et al., 2015).

1.13 Knock-in models of Prion Disease

Gene targeted models are produced by the insertion of the transgene into a specific locus in the host genome via homologous recombination (Jackson et al., 2009; Kaczmarczyk et al., 2016). The classical approach to generating gene-targeted mouse models involves the electroporation of a targeting vector into embryonic stem cells (Bouabe and Okkenhaug, 2013a). The transgene is flanked by sequences from the mouse genome on both sides (Noguchi et al., 2004).

This flanking sequence induces homologous recombination at the target site, leading to the insertion of the transgene at a specific locus (Bouabe and Okkenhaug, 2013a) (Bouabe and Okkenhaug, 2013b).

Models using this technology are more precise and better reflect inherited mutations as the endogenous gene is replaced by the transgene at a specific locus, therefore the transgene is under physiological control and endogenous expression levels are obtained (Kaczmarczyk and Jackson, 2015).

Fewer mouse models of inherited prion diseases have been generated using the gene targeted approach (Table 1.8).

Table 1.8 Knock-in mouse models of inherited prion disease

PRNP Mutation	Tg Line	PrP sequence	Spontaneous formation of prions?	Reference
P102L	101LL	Mouse (P101L)	No	(Manson et al., 1999)
D178N, M129	Ki-3F4-FFI	Mouse (D177N, M128)	Yes	(Jackson et al., 2009)
E200K	Ki-3f4-CJD	Mouse (E199K)	Yes	(Jackson et al., 2013)

Knock-in mice expressing endogenous levels of MoPrP (P101L) failed to develop spontaneous disease (Manson et al., 1999), however transgenic Tg174 mice overexpressing MoPrP (P101L) at 8x levels developed a spontaneous neurological disease (Hsiao et al., 1990).

This difference may be due to the fact that in the knock-in model, the required incubation period exceeded the normal mouse lifespan. Jackson and colleagues developed two knock-in lines, Ki-3F4-FFI and Ki-3f4-CJD that developed spontaneous disease with neurological symptoms that mirrored those observed in patients. Gliosis and neuronal loss was observed in the thalamus of Ki-3F4-FFI mice and Ki-3f4-CJD line developed spongiform degeneration and PrP deposits in the brain (Jackson et al., 2013).

High levels of PrP overexpression may be pathogenic in some instances and lead to the development of abnormal pathologies that are not typically associated with prion diseases (Westaway et al., 1994; Marín-Moreno et al., 2020). Increasing protein expression beyond physiological levels can also disrupt the function of genes near the transgene insertion site and introduce artefacts (Kuang et al., 2006).

Some of these pitfalls could be avoided by using knock-in mice that express physiologically relevant levels of PrP. However as the incubation period is inversely proportional to level of PrP expression, endogenous levels of PrP may result in prolonged incubation periods that do not enable prion disease to be observed during the short lifespan of a mouse (Sandberg et al., 2011, 2014; Marín-Moreno et al., 2020).

For example human PrP knock-in mice were resistant to infection with BSE but were susceptible to vCJD prions (Bishop et al., 2006). In contrast, both BSE and vCJD prions successfully infected transgenic mice overexpressing human PrP 129M producing a vCJD-like phenotype (Asante et al., 2002). In this instance the knock-in models were not able to report BSE infection and the author would have reached the conclusion that BSE was not the cause of vCJD, but overexpression models proved otherwise. These findings demonstrate that in some cases overexpression is required for transmission (Wadsworth et al., 2010).
There are also instances where PrP knock-in mice recapitulate human prion diseases better compared to transgenic models.

Bian *et al*. 2019 reported that transgenic mice expressing cervid PrP^{C} were relatively resistant to intraperitoneaal challenges with different chronic wasting disease (CWD) isolates whereas PK-resistant PrP accumulated in the spleens of knock-in mice expressing cervid PrP^{C} following intracerebral and intraperitoneal challenges with CWD prions (Bian et al., 2019).

The authors concluded that the greater efficiency in disease induction observed in the gene targeted mice was due to the more accurate control of cervid PrP expression in the periphery by *PRNP* regulatory sequences in these mice (Bian et al., 2019).
Therefore in this instance knock-in mice were more suitable for investigating the peripheral pathogenesis of CWD.

Further experiments have also demonstrated that the transmission of a CWD isolate (M-N O2) from Norwegian moose was more efficient in knock-in mice expressing elk or deer PrP compared to transgenic counterparts. They also observed that the transmission efficiency of Norwegian reindeer CWD prions was equally efficient or faster in the PrP knock-in mice compared to the transgenic counterparts (Bian et al., 2021).
These findings highlight the importance of using both transgenic and knock-in mouse models in prion disease modelling

1.14 Generating mouse models using CRISPR/Cas9 technology

Generating knock-in mice using embryonic stem cells is expensive, time consuming and labour intensive compared to using CRISPR technology as it requires culturing of embryonic stem cells and chimera breeding (Kaczmarczyk and Jackson, 2015).

The development of programmable nucleases such as clustered regularly interspaced short palindromic repeat (CRISPR) – CRISPR-associated protein 9 (Cas9) into gene editing tools has enabled the development of knock-in mice without culturing embryonic stem cells (Kaczmarczyk and Jackson, 2015).

The CRISPR/Cas9 system has recently transformed genome editing (Hsu et al., 2014).This system exists in bacteria and archaea as a defence mechanism against invading bacteriophages (Kaczmarczyk and Jackson, 2015). It has been developed into a gene editing tool for the generation of precise animal models of disease (Hsu et al., 2014) .

The native bacterial CRISPR/Cas9 system utilises a dual guide RNA (gRNA) system that consists of CRISPR RNA (crRNA) and trans-activating CRISPR RNA (tracrRNA). The crRNA and tracrRNA form the interference complex with Cas9 that targets and cleaves foreign nucleic acids (Charpentier et al., 2015). However, the dual gRNA system can be engineered as a single guide RNA for experimental purposes (Jinek et al., 2012; Saayman et al., 2015). The Cas9/sgRNA complex recognises the downstream protospacer-adjacent motif (PAM) sequence and the complementary 20 bp target DNA sequence (Figure 2A). The PAM sequence recognised by Cas9 is 3-bp NGG, where N= any nucleotide (Zhang et al., 2014).

This short sequence is located next to the target DNA sequence and it is required in distinguishing between bacterial self and non-self DNA (Gleditzsch et al., 2019). The Cas9 protein cuts approximately 3 base pairs upstream of the PAM sequence resulting in DNA double-strand breaks (Figure 1.3A) (Mou et al., 2015).

This leads to the activation of the DNA repair system which can occur via two mechanisms: 1) Non-homologous end joining (NHEJ) 2) Homology directed repair (HDR) (Figure 1.3B). Non-homologous end joining introduces small insertions and deletions (INDELs) into the genome. Whereas, homology directed repair can be used to generate precise genome edits through the incorporation of a DNA donor template that contains the desired genomic modification at the target site (Mou et al., 2015; Aird et al., 2018).

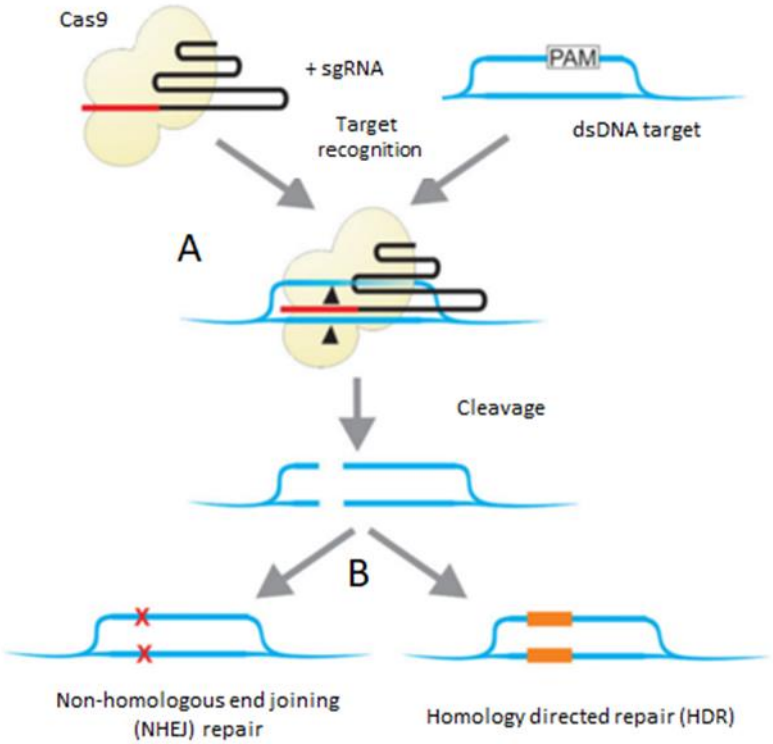

Figure 1.3: CRISPR/Cas9-directed cleavage using sgRNA. Adapted from Saayman *et al.*, 2015. (Saayman et al., 2015)

A. The PAM sequence and the target genomic sequence is recognised by the Cas9/sgRNA complex, and then Cas9 induces a double-strand break at the targeted genomic region.

B. B. Then the DNA is repaired via non-homologous end joining (NHEJ) or homology directed repair (HDR).

The CRISPR/Cas9 system has high therapeutic potential but it is hindered by the off-target effects (Aird et al., 2018). Off-target effects refer to the unintended cleavage and introduction of point mutations at sites other than the target site which have a sequence which is non-identical but similar to the target site (Modrzejewski et al., 2019, 2020).

Another one of the drawbacks using this approach is genetic mosaicism in founder animals (Yang et al., 2013; Mizuno et al., 2014; Mehravar et al., 2019).

The CRISPR/Cas9 components are often injected directly into fertilised zygotes as RNA, DNA or protein molecules and sustained activity of the Cas9/sgRNA complex can lead to the cleavage of different genes during different stages of embryonic development, leading to genetic mosaicism in founders (Yang et al., 2013; Yen et al., 2014; Mehravar et al., 2019).

CRISPR/Cas9 technology can be used to generate knock-out and knock-in mice. Knock-out mice can be generated by designing sgRNAs that direct Cas9 to the genomic target site (Hall et al., 2018). Once Cas9 has been recruited to the target site it creates a double-stranded break that can be repaired by NHEJ which introduces INDELs (Horii and Hatada, 2016; Hall et al., 2018). These NHEJ mediated mutations lead to the production of knock-out mice (Horii and Hatada, 2016; Hall et al., 2018).

The generation of knock-in mice is technically more challenging as knocking in a gene requires precise repair via HDR and an exogenous DNA template (Salsman et al., 2017; Lee et al., 2018; Ranawakage et al., 2021). HDR is less efficient than NHEJ in mammalian cells whereas NHEJ is more efficient but less accurate compared HDR (Salsman et al., 2017; Lee et al., 2018; Ranawakage et al., 2021).

Many different strategies have been developed by researchers to increase knock-in efficiency and studies suggest that the design of the donor template is crucial in determining the success of HDR (Bollen et al., 2018; Ranawakage et al., 2021).

There are different types of donor templates including, double-stranded DNA donors (dsDNA), single-stranded oligo DNA nucleotides (ssODNs), single-stranded DNA donors (ssDNA) and viral or plasmid based donors (Quadros et al., 2017; Bollen et al., 2018; Roth et al., 2018; Okamoto et al., 2019).

Knock-in efficiency is higher using ssDNA donors compared with dsDNA donors (Miura et al., 2015; Codner et al., 2018; Zhang et al., 2021). This is due to the fact that ssDNA donors require shorter homology arms so they can be inserted into the genome more efficiently than dsDNA donors that require longer homology arms (Miura et al., 2015, 2018; Quadros et al., 2017).

Efficient additions with ssDNA inserts-CRISPR (Easi-CRISPR) was developed to improve the efficiency of DNA donor insertion into the genomic target site (Quadros et al., 2017) (Miura et al., 2018). This strategy uses *in vitro* Transcription and Reverse Transcription (*iv*TRT) to generate long ssDNA donors that are assembled with crispr RNA (crRNA), trans-activating crispr RNA (tracrRNA) and Cas9 protein. This ssDNA+crRNA + tracrRNA + Cas9 complex is then microinjected into mouse zygotes (Quadros et al., 2017; Miura et al., 2018). Miura *et al*. (2018) reported that the insertion efficiency of the long ssDNA donor was 2.5 times higher compared to a dsDNA donor (Miura et al., 2018).

The synthesis of the long ssDNA donor remains a challenge using this strategy. Long ssDNA donors can be synthesised commercially or generated in house, however the stability of ssDNA sequences varies (Erwood and Gu, 2020). Single stranded DNA structures can also form secondary structures within a long ssDNA donor which could cause the donor sequence to be skipped during the DNA repair process (Pal and Levy, 2019; Erwood and Gu, 2020). There have been no reports of any mouse models of prion disease generated using the CRISPR-Cas9 system to date. With the development of many different strategies to boost HDR efficiency and the insertion of DNA donor templates this technique could be used to generate mouse models of inherited prion diseases.

1.15 Aims of the project

A unique phenotype associated with Y163X *PRNP* truncation mutation

Mead *et al*. (2013) identified the Y163X-129V stop codon mutation in a large British family (Mead et al., 2013). This *PRNP* truncation mutation is associated with unusual symptoms referred to as PrP systemic amyloidosis (Mead and Reilly, 2015). Reported clinical symptoms include chronic diarrhoea, autonomic neuropathy and the accumulation of amyloidogenic PrP in peripheral organs and blood vessels (Cerebral amyloid angiopathy (CAA). The disease progression for this mutation is slow (>20 years) and cognitive decline occurs in the later stages of the disease (Mead et al., 2013).

The transmission of brain tissue from patients with the Y163X mutation into transgenic mice expressing wild type human PrP-129V resulted in negative transmissions (Mead et al., 2013). However, these negative transmission results may be due to different PrP sequences between the donor and recipient (Asante et al., 2013). Previous experiments have demonstrated that transmission barriers may be due to incompatibility between the host and donor PrP. Therefore transgenic mice expressing the homologous mutant PrP may be required to demonstrate the transmissibility of prions produced in patients with the Y163X mutation (Asante et al., 2013, 2015).

This novel prion disease is distinct from previously reported inherited prion diseases due to the presence of a non-neurologic phenotype. The uniqueness of the disease phenotype associated with the Y163X mutation, characterised by the deposition of PrP amyloid in peripheral organs makes this mutation a good candidate for the study of prion therapeutics.

Modelling the Y163X *PRNP* truncation mutation in mice

Previous studies demonstrate that the accurate control of PrP expression by endogenous regulatory elements may be necessary to study peripheral pathogenesis of prion diseases (Bian et al., 2019) (Bian et al., 2021).

Against this background, the aims of this thesis were to generate and characterise mouse models expressing human PrP Y163X that recapitulate human disease using two different approaches:

1) Conventional transgenic approach

2) Gene targeted approach – Gene Knock-in and CRISPR-Cas9 technology

Cell lines expressing human PrP 163X will also be generated as part of the characterisation of this unique inherited prion disease to investigate the subcellular localisation of this mutant protein.

2. Chapter 2: Materials and Method

2.1 Materials and reagents

Luria broth (LB), 1L

25 g LB powder (Invitrogen, Massachusetts, USA)

1 L double-distilled water (ddH_2O)

2-YT broth, 1L

25 g 2-YT broth powder (Invitrogen, Massachusetts, USA)

1 L double-distilled water (ddH_2O)

LB Agar Plates

3 g Agar powder (Invitrogen, Massachusetts, USA)

200 ml LB media (Invitrogen, Massachusetts, USA)

Lysis buffer

10 ml RIPA buffer (Sigma-Aldrich, Missouri, USA)

1 ml Protease inhibitor cocktail (100 µl/ ml) (Sigma-Aldrich, Missouri, USA)

Sample buffer

200 µl Novex Tris-Glycine SDS Sample Buffer (2X) (Invitrogen, Massachusetts, USA)

10 µl β-mercaptoethanol (Sigma-Aldrich, Missouri, USA)

20 µl

Sterile H_2O (Global Life Sciences Solutions Operations UK Ltd, Sheffield, UK)

PBST (0.05%)

100 ml 10X PBS (VWR International Ltd, Pennsylvania, USA)

0.5 ml Tween 20 (Sigma-Aldrich, Missouri, USA)

899.5 ml dd H_2O

PBST (1%)

5 ml 10X PBS (VWR International Ltd, Pennsylvania, USA)

0.5 ml Tween 20 (Sigma-Aldrich, Missouri, USA)

44.5 ml ddH_2O

Carbonate coating buffer

2.93 g Sodium bicarbonate (Sigma-Aldrich, Missouri, USA)

1.59 g Sodium carbonate (Sigma-Aldrich, Missouri, USA)

In 1L of dd H_2O

IP Capture Buffer

0.4 g Sarkosyl (Sigma-Aldrich, Missouri, USA)

0.4 g BSA (Sigma-Aldrich, Missouri, USA)

0.4 ml Triton X-100 (Sigma-Aldrich, Missouri, USA)

1 ml 1.0M Tris (VWR International Ltd, Pennsylvania, USA)

Made up to 20 ml with ddH_2O

2.2 Restriction enzymes

Restriction enzymes (Table 2.1) were purchased from New England Biolabs, Massachusetts, USA and Thermo Fisher Scientific, Massachusetts, USA.

Table 2.1 List of restriction enzymes used

Enzyme	Recognition sequence (5'-3')	Incubation temperature (°C)	Company
BamHI	GGATCC	37	New England Biolabs
HindIII	AAGCTT	37	New England Biolabs
NotI	GCGGCCGC	37	New England Biolabs
SmaI	CCCGGG	30	Thermo Fisher Scientific
SalI	GTCGAC	37	New England Biolabs
SalI	GTCGAC	37	Thermo Fisher Scientific
XbaI	TCTAGA	37	Thermo Fisher Scientific
XhoI	CTCGAG	37	New England Biolabs

2.3 Primers

Oligonucleotide primers used for cloning, PCR, RT-PCR and qPCR (Table 2.2) were designed using the Eurofins Genomics PCR Primer Design Tool (https://eurofinsgenomics.eu/en/ecom/tools/pcr-primer-design/). Primers were ordered from Eurofins Genomics and diluted with TE (Thermo Fisher Scientific, Massachusetts, USA) to a stock concentration of 100μM.

Table 2.2 List of oligonucleotide primers used for sub-cloning, PCR and RT-PCR

Name	Sequence
Cloning Primers	
Not-Sal_Sn3	GGCCGCGGTACCCTCGAGCCCGGGGTCGACC
Not-Sal_Asn3	TCGAGGTCGACCCCGGGCTCGAGGGTACCGC
Bam-Xho linker	GATCGCTCGAGG
HuPrP_ORF_Sn2	CTGCAGGTCGACGCCACCATGGCGAACCTTGGCTGCTGGA
HuPrP_ORF_Asn2	CCCGGGTCTAGATCATCCCACTATCAGGAAGATG
PCR Primers	
Hu1	GTGGCCACATGGAGTGACCTGGGCCTC
Hu2	GGCACTTCCCAGCATGTAGCCG
P10	GTACCCATAATCAGTGGAACAAGCCCAGC
315	GTGCTGCTGGATCTTCTCCCGTC
P3	ATTCGCAGCGCATCGCCTTCTATCGCC
CAG_ASN3	CCAGTGTTCCATCCTCCAG
CAG_SN3	GCCTCTGCTAACCATGTTC
F2	AGGAGATTCTTGGCTTTGTGCTTA
R2	TGTGAGTTCTAATACATCTGGGCT
KI-F3	GGCTGGTAAGGGATATTTGCCTG
KI-R3	CCAGCCTAGACCACGAGAATGCG
KO-Sn2	TGCCCATTTCCAAATTCCAC
KO-Asn6	ATCGAAAGACACCCCCAAG
Sn2	GAGGATGGGATGAGCTGTG
Asn3	GACCTGAAGCAAAGAGCAAC

RT-PCR and qPCR Primers	
RT-primer MoPrP-20 (V2)	CACAGAGAAGCAAGAATGAG
HuPrP pLNCX2 Forward	AAGCCTGGAGGATGGAACAC
HuPrP pLNCX2 Reverse	ATGTTGGTTTTTGGCTTACTCG
Tyx_pCAG-TaqMan_Sn	TGCACGACTGCGTCAATATCA
Tyx_pCAG-TaqMan_Asn	TCGGTCTCGGTGAAGTTCTCC
Tyx_pCAG-Probe	TCACCACAACCACCA (FAM/TAMRA)

2.4 CRISPR Guide RNA sequences

The CRISPR guides (Table 2.3) were designed using the online platform called "Breaking Cas" (https://bioinfogp.cnb.csic.es/tools/breakingcas/?gset=8x1_GENOMES_Ensembl_104) and synthesised by Integrated DNA Technologies (IDT, Iowa, USA).

Table 2.3 CRISPR Guide RNA sequences

Mo PrP Left Guide:	TCAGTCATCATGGCGAACCT
Mo PrP Right Guide:	GCCTCCCTCATCCCACGATC

2.5 Antibodies

2.5.1 ICSM anti-prion protein monoclonal antibodies

Briefly, the ICSM anti-prion antibodies (Table 2.4) were produced by immunising F10_FVB/PrP null mice with human recombinant α- or β-$PrP^{91–231}$ (Khalili-Shirazi et al., 2005).

Table 2.4 ICSM anti-prion antibodies

	Epitope	Host	Reactivity	Use
ICSM 17	140-159	Mouse	Human	WB
ICSM 18	143-153	Mouse	Human	WB
ICSM 35/ICSM35-biotin	93–105	Mouse	Human, Mouse	WB
ICSM 37	96-105	Mouse	Human	WB
ICSM 61	96-105	Mouse	Human	WB
ICSM 62	96-105	Mouse	Human	WB

The rest of the antibodies used for this project are described in Table 2.5

Table 2.5 Other Primary and secondary antibodies used

	Epitope	Host	Reactivity	Manufacturer	Use
Primary antibodies					
Anti-Alpha 1 Na^+/K^+-ATPase	*N/A	Mouse	Canine, Human, Monkey, Mouse, Pig, Rabbit, Rat, Sheep, Xenopus	Merck	IF
Anti-Prion Protein-SAF32	57–88	Mouse	Bovine, Hamster, Human, Mouse, Ovine	Bertin Bioreagent	WB
Anti-Prion Protein-3F4	109-112	Mouse	Human	BioLegend	WB,ELISA
Anti-Prion Protein-6D11	95-110	Mouse	Human	BioLegend	WB, IF

Secondary antibodies

Antimouse IgG Alkaline phosphatase	Goat	Mouse	Merck	WB
Anti-mouse IgG1 Rhodamine	Goat	Mouse	Jackson ImmunoResearch	IF
Anti-mouse IgG2a Alexa Fluor488	Goat	Mouse	Jackson ImmunoResearch	IF

*Not Available

2.6 DNA methods

2.6.1 Restriction enzyme digestions

Restriction enzyme digestions were performed in a volume of 50-70µl per reaction with 2-5µg of template DNA, 5U of enzyme and the appropriate volume of 10x restriction enzyme buffer. The reactions were incubated overnight in a water bath at 37°C (with exception of SmaI at 30°C for 1hr). This was followed by agarose gel electrophoresis and DNA purification using the Zymoclean™ Gel DNA Recovery Kit (Zymo Research, USA), following the manufacturer's instructions to purify DNA fragments from agarose gels.

2.6.2 Filling-in reactions to blunt sticky ends

The sticky end of digested DNA with a 5' overhang was blunted using the Klenow fragment of DNA Polymerase I (New England Biolabs, Massachusetts, USA) filling in the sticky end. Briefly, 19µl of restriction enzyme digested DNA, 3ul of 10x NEB buffer 2 (New England Biolabs, Massachusetts, USA), dNTPs (10mM) (New England Biolabs, Massachusetts, USA), Klenow enzyme was brought up to a final volume of 30µl with dH_2O and incubated for 15 minutes at 25°C. The reaction was stopped by adding EDTA (ITW Reagents, Barcelona, Spain) to a final concentration of 10mM and heating for 20 minutes at 75°C in a heating block to inactivate the Klenow enzyme.

2.6.3 DNA End Modification: Dephosphorylation

Phosphate groups from 5'-ends of the digested DNA were removed using Calf intestinal alkaline phosphatase (CIAP) enzyme (New England Biolabs, Massachusetts, USA). DNA was digested in a 20µl volume and added to 5µl of 10x Cut Smart buffer (New England Biolabs, Massachusetts, USA), 1µl of alkaline phosphatase and brought up to a final volume of 50µl with dH_2O. The reaction was then incubated for 30min at 37°C in a water bath, followed by incubation at 65°C for 10 min on a heating block to heat inactivate the enzyme.

2.6.4 Annealing oligonucleotides for cloning

Equal amounts (in µg) of the oligonucleotides were added together and brought up to a final volume of 20µl with TE buffer in an Eppendorf tube. The tube containing the oligonucleotides was then incubated at 70°C for 5 min to denature the strands. Following the incubation period, the tube was transferred into a beaker containing water at 65°C and was allowed to cool slowly until the temperature was below 30°C.

2.6.5 Agarose gel electrophoresis

Agarose gels (1-2%) were used to separate digested plasmid DNA, for DNA quantification, fragment purification and for the analysis of PCR products. Agarose was dissolved in 1x TAE buffer (Geneflow Ltd, Lichfield, UK) and heated until the agarose completely dissolved. Ethidium bromide solution (Merck Life Science , New Jersey, USA) was added to a final concentration of 0.2 µg/mL once the agarose solution had cooled down to approximately 50°C. GeneRuler 1kB DNA ladder (Thermo Fisher Scientific, Massachusetts, USA) was included in every run as reference for determining DNA fragment sizes, and an image of the gel was acquired using the Bio-Rad *Gel Doc ™ XR+* documentation system (Bio-Rad Laboratories, California, USA).

2.6.6 Gel extraction

The agarose gel was placed on a UV transilluminator (Analytik Jena, Germany) and the desired DNA fragment was excised from the agarose gel using a scalpel blade. The DNA was then extracted using the Zymoclean™ Gel DNA Recovery Kit (Zymo Research, USA) according to the manufacturer's instructions.

2.6.7 Purification of DNA fragments

The Zymoclean™ Gel DNA Recovery Kit (Zymo Research, USA) was used to purify DNA fragments. The excised DNA fragment was placed into a 1.5ml microcentrifuge tube. Then 3 volumes of buffer ADB was added to 1 volume of gel slice (volume: weight).

The gel slice was then incubated in ADB for 5-10 minutes, or until the agarose completely dissolved at 55°C. Once the gel slice had completely dissolved, the melted agarose solution was transferred to a Zymo-Spin™ Column, incubated for 5-10 minutes and centrifuged for 1 minute at 13,000 x g. The flow through was discarded and the column was washed by adding wash buffer to the column and centrifugation at 13,000 x g. After the wash steps the DNA was eluted in elution buffer.

2.6.8 Purification of PCR products

PCR products were purified using the Wizard® SV Gel and PCR Clean-Up System (Promega, Wisconsin, USA). The excised PCR product was placed into a 1.5ml microcentrifuge tube and membrane binding solution was added at a ratio of 10µl of solution per 10mg of agarose gel slice. The mixture was then vortexed and incubated between 50–65°C for 10 minutes, or until the agarose completely dissolved. The dissolved gel slice was then transferred into a SV Minicolumn in a collection tube and incubated for 1 minute at room temperature. This was followed by centrifugation at 16,000 × g for 1 minute, then the flow-through was discarded and the membrane was washed by adding Membrane Wash Solution and centrifugation at 16,000 × g for 1 minute. The SV minicolumn was then transferred into a clean 1.5ml microcentrifuge tube and the DNA was eluted by adding 20 µl TE (Thermo Fisher Scientific, Massachusetts, USA) and centrifugation at 16,000 × g for 1 minute.

2.6.9 Preparation of competent bacterial cells

Escherichia coli SCS110 (Agilent Technologies, California, USA) glycerol stock was streaked onto an LB-agar plate with no antibiotics. The plate was incubated overnight at 37°C and the next morning a colony was picked and used to inoculate 10ml of LB.

The culture was then incubated overnight at 37°C in a shaking incubator. The following morning 250ml of LB (with no antibiotic) was inoculated with 6.25ml of the overnight culture and incubated at 37°C in a shaking incubator until the absorbance read at A550 reached 0.4-0.5.

Next, the culture was transferred into a centrifuge tube and incubated on ice for 30 minutes. This was followed by centrifugation between 4000 x g for 10 minutes at 4°C. Then the supernatant was discarded and the pellet was resuspended in 50ml of ice-cold 100 mM $CaCl_2$ (Merck Life Science, New Jersey, USA) incubated on ice again for 30 minutes. This was followed by centrifugation at 4000 x g for 10 minutes at 4°C. The supernatant was discarded and the pellet was resuspended in 6ml of ice cold 100mM $CaCl_2$ containing 15% glycerol (VWR International Ltd, Pennsylvania, USA). The cells were then aliquoted into sterile 1.5ml microcentrifuge tubes and kept on ice at 4°C overnight. After the overnight incubation the cells were snap frozen on dry ice and stored at -70°C.

2.6.10 Ligation and transformation

The vector and insert were ligated in a ratio of 1:4 respectively; the two fragments were added to 1 µl of 10x ligation buffer (Promega, Wisconsin, USA), brought up to 9µl with ddH_2O and incubated at 37°C for 10 min on a heating block before adding 1ul of T4 DNA ligase (Promega, Wisconsin, USA). This was followed by overnight incubation at 15°C in a water bath.

The following day, SCS110 competent cells (Agilent Technologies, California, USA) were thawed on ice before adding the 2 ul ligation mix, then mixed and incubated on ice for 60 min. The cells in the transformation reaction were then heat shocked at 42°C for 80 sec, chilled on ice for 10 min and left at room temperature for 10 min.

Following the addition of 850µl of LB, the cells were incubated at 37°C for 1hr with shaking at 200-300rpm. Then 150µl of the cells were spread onto LB-agar plates containing 100 µg/ml of Ampicillin or Kanamycin (Merck Life Science, New Jersey, USA), depending on the antibiotic resistance gene in the plasmid. The plates were incubated overnight at 37°C and checked in the morning for the presence of bacterial colonies.

2.6.11 Screening of colonies

Single colonies were picked and transferred into 5ml of 2-YT (Invitrogen, Massachusetts, USA) containing 100 µg/ml of Ampicillin/Kanamycin (Life Science UK Limited, Dorset, UK) and incubated at 37°C overnight. The bacterial cells were then harvested by centrifugation at 16,000 x g for 10 seconds and DNA was isolated using the QIAprep Spin Miniprep Kit (Qiagen Ltd, Hilden, Germany), following the manufacturer's instructions. Diagnostic restriction digestions were performed to identify positive clones. Purified DNA was digested with different restriction endonucleases and the reactions were run on an agarose gel and compared to the vector backbone to determine recombinant plasmids containing the correct insert.

2.6.12 Mini-Preps of plasmid DNA

Minipreparations of plasmid DNA were made using the QIAprep Spin Miniprep Kit (Qiagen Ltd, Hilden, Germany). After harvesting the cells, the pellet was resuspended in buffer P1 and the cells were lysed in buffer P2. Cell lysis was then neutralised by the addition of buffer N3 which lead to protein precipitation. The white precipitate was removed following centrifugation for 10 minutes at 16,000 x g. The supernatant containing the plasmid DNA was applied to a QIAprep spin column containing a silica membrane. The flow-through was discarded and endonucleases and salts were removed by adding buffer PB and buffer PE sequentially to the column followed by centrifugation at 16,000 x g for 1 minute.

DNA was eluted was by adding 20µl buffer EB to the column and centrifugation at 16,000 x g for 1 minute.

2.6.13 Maxi-preps of plasmid DNA

Maxipreparations of plasmid DNA were made using the Hi Speed Plasmid Maxi Kit (Qiagen Ltd, Hilden, Germany). Briefly, after harvesting the cells, the pellet was resuspended in buffer P1 and the cells were lysed in buffer P2. Cell lysis was then neutralised by the addition of buffer P3 and the lysate was transferred into a QIAfilter maxi cartridge and incubated for 10 min. A plunger was then inserted into the QIAfilter maxi cartridge and the lysate was filtered into a previously equilibrated HiSpeed Maxi Tip. Once the lysate had completely passed through the resin of the HI Speed Maxi Tip, the resin was washed with Buffer QC. Then the DNA was eluted in Buffer QF and precipitated by adding 10.5ml of isopropanol to the eluted DNA suspension. The mixture of DNA and isopropanol was incubated for 5 minutes.

This was followed by centrifugation at 4000 x g for 30 minutes at 4°C, then the isopropanol was discarded and the DNA pellet was washed by adding 70% ethanol and centrifugation for 10 minutes at 4000 x g. The ethanol was discarded and the pellet was then dried for 10 minutes and resuspended in 100-200 µl TE (Thermo Fisher Scientific, Massachusetts, USA).

2.6.14 TaqMan Quantitative Polymerase Chain Reaction (qPCR) assays

The probes and PCR primers used in the TaqMan qPCR assays were designed using Eurofins Genomics qPCR assay design software. TaqMan qPCR reactions were performed in triplicate according to Table 2.6.

Table 2.6 Reaction mixture for the TaqMan qPCR assay

Reagent	Per Sample (µl)
Qiagen mix	12.5
Tyx_pCAG-TaqMan_Sn (10µM)	1.0
Tyx_pCAG-TaqMan_Asn (10µM)	1.0
Tyx_pCAG Probe (10µM)	0.5
GAPDH forward (10µM)	0.25
GAPDH reverse (10µM	0.25
GAPDH forward probe (10µM)	0.25
DNA (15ng)	9
Water	0.25
Final volume	25

The TaqMan reactions were set up in optical 96-well reaction plates (Applied Biosystems, Massachusetts, USA) and run in an ABI Prisma 7000 sequence detection system (Applied Biosystems, Massachusetts, USA) .The following thermal profile was used for the reactions: 95°C 10 min (Hot start), (94°C 15min, 94°*C 15* sec, 60°C 60 sec) x40.

2.6.15 qPCR data analysis using the double delta Ct (ddCt) method

The C_T values were exported from the QuantStudio™ 12K Flex software (Applied Biosystems, Massachusetts, USA) into a Microsoft Excel spreadsheet for analysis. Experimental values were corrected by subtracting the GAPDH control C_T value from the CAG C_T value to obtain the delta Ct (dCt) value. The dCt value for the heterozygous control sample was also calculated by subtracting its GAPDH control C_T value from the corresponding CAG C_T value.

The averaged dCt value for the heterozygous control sample was then subtracted from the experimental dCt values to calculate the ddCt values. The ddCt value of each experimental sample was then raised to the power of 2 to determine the relative value (RV) and the mean RV was calculated for each sample analysed in triplicate. DNA extracted from heterozygous animals from the same line being analysed were used as control samples for the qPCR assays. Heterozygous animals were identified as having a mean RV of 1.00 and homozygous animals were identified by having a mean RV of 2.00 (Figure 2.1).

Tg377qPCR analysis								
Sample Name	GAPDH	CAG	dCt		ddCt	RV	mean RV	
C1	22.119	27.044	4.92453	4.784531	0.139999	0.90752	1.011202	Heterozygous Control
C1	22.625	27.110	4.485		-0.29964	1.230836		
C1	22.240	27.184	4.94417		0.159639	0.895249		
S1	21.957	25.749	3.791		-0.993	1.990454	2.192832	Homozygote
S1	22.200	25.826	3.626497		-1.15803	2.231531		
S1	22.399	25.947	3.547878		-1.23665	2.356512		

Figure 2.1 Identification of homozygous Tg377 mouse by TaqMan qPCR assay

2.7 RNA methods

2.7.1 Purification of total RNA from tissues

**All centrifugation steps were performed at 16,000 x g for 30 seconds unless stated otherwise.*

Total RNA was extracted from mouse tissues stored in RNAlater (Invitrogen, Massachusetts, USA) using the Direct-zol™ RNA Miniprep Kit (Zymo Research, USA) according to the manufacturer's instructions. The tissue sample was removed from the RNAlater stabilisation solution and transferred onto an RNase free cell culture dish (Eppendorf , Hamburg, Germany). Tissue samples were then weighed and 20-30 mg of tissue was cut and placed into a Precellys lysing tube (Bertin Instruments, France) containing 600µl of TRI Reagent®.

This was followed by sample homogenisation in a Minilys Personal Homogenizer (Bertin Instruments, France) for 2 minutes and 30 seconds. One volume of 100% ethanol was mixed thoroughly with the sample lysed in TRI Reagent and transferred into a Zymo-Spin™ IICR Column that had been placed in a collection tube and centrifuged. The flow-through was discarded and the column was transferred into a new collection tube.

Next, 400 µl Direct-zol™ RNA PreWash was added to the column and centrifuged. Once the flow through had been discarded the column was washed again by adding 700 µl RNA Wash Buffer to the column and centrifugation for two minutes to ensure the wash buffer was removed completely. The spin column was then placed into a new RNase-free tube and the RNA was eluted in 50 µl of RNase free TE (Invitrogen, Massachusetts, USA).

2.7.2 DNase treatment of RNA

**All centrifugation steps were performed at 16,000 x g for 30 seconds unless stated otherwise.*

The DNase I Reaction Mix was set up according to Table 2.7 in an RNase free-tube and incubated at room temperature for 30 minutes

Table 2.7 DNase I Reaction Mix

Sample	40 µl
DNase I (1 U/ µl) (Zymo Research)	5 µl
DNA Digestion Buffer (Zymo Research)	5 µl

The RNA was then recovered using the RNA Clean & Concentrator™ kit (Zymo Research, USA). Each sample was mixed with two volumes of RNA binding buffer and then an equal volume of 100% ethanol was added to the mixture. The sample was then transferred into a Zymo-Spin™ IC Column in a Collection Tube and centrifuged. The flow-through was discarded and the column was transferred into a new collection tube.

Next, 400 µl RNA Prep Buffer was added to the column and centrifuged. Once the flow-through had been discarded the column was washed again by adding 700 µl, then 400 µl RNA Wash Buffer was added to the column and centrifuged for two minutes to ensure the wash buffer was removed completely. The spin column was then placed into a new RNase-free tube and the RNA was eluted in 15 µl of RNase free TE (Invitrogen, Massachusetts, USA).

2.7.3 RNA synthesis using the mMESSAGE mMACHINE T7 Ultra Kit (Ambion, Texas, USA)

RNA was synthesised using the mMESSAGE mMACHINE T7 Ultra Kit (Ambion, Texas, USA). The *in vitro* transcription reaction was set up on ice according to Table 2.8.

Table 2.8 Reaction mixture for in vitro transcription reaction

Component	Volume per reaction (µl)
*T7 2X NTP/ARCA	10
10X T7 Reaction Buffer	2
T7 Enzyme Mix	2
Linear template DNA, up to 1µg	Variable
Nuclease-free Water	Variable
Final reaction volume	20

* A neutralized buffered solution containing:15mM ATP, 15mM CTP, 15mM UTP, 3mM GTP and 12mM ARCA.

The reaction mix was then incubated at 37 °C for 4 hours in a thermomixer. After 4 hours the reaction was terminated by adding 1 µl of TURBO DNase. The synthesised RNA was then purified using the MEGA clear Kit (Ambion, Texas, USA), following the 15- minute incubation with TURBO DNase at 37 °C.

2.7.4 RNA purification using the MEGA clear Kit (Ambion, Texas, USA)

RNA synthesised via *in vitro* transcription was purified using the MEGA clear Kit (Ambion, Texas, USA). The RNA sample was brought up to 100 µl with Elution Solution. Then 350 µl of Binding Solution Concentrate and 100% ethanol were added to the sample sequentially. The mixture was then transferred into a Filter Cartridge and centrifuged at 13, 000 x g for 1 minute. The flow-through was discarded and the filter was washed twice with 500 µl of Wash Solution followed by centrifugation at 13, 000 x g for 1 minute. After the wash step, the filter was transferred into an RNase-free tube and eluted in 20-50 µl of Elution Solution.

2.7.5 Complementary DNA (cDNA) synthesis using the QuantiTect ReverseTranscription Kit

cDNA was synthesised using the QuantiTect ReverseTranscription Kit (Qiagen Ltd, Hilden, Germany) according to the manufacturer's instructions. The genomic DNA elimination reaction was set up on ice according to Table 2.9 and incubated for 10 minutes at 42°C in a thermomixer.

Table 2.9 gDNA Wipeout reaction mix

Component	Volume per reaction (µl)
gDNA Wipeout Buffer, 7x	2
Template RNA, up to 1µg	Variable
RNase-free water	Variable
Total reaction volume	14

The reaction tube was then immediately placed on ice and the reverse-transcription reaction mix was then prepared according to Table 2.10. Separate reaction mixes without the reverse transcriptase enzyme were prepared for each sample being analysed as negative controls. Another reaction without template RNA was set up as an additional negative control. The reaction mix was then incubated at 42 ℃ for 30 minutes in a thermomixer. The reaction mix was then incubated at 95℃ for 3 minutes, then *2.5* µl of RNase H (New England Biolabs, Massachusetts, USA) to the reaction mix and was incubated for 40 minutes at 37°*C* in a thermomixer.

Table 2.10 Reverse transcription reaction mix using the QuantiTect Reverse Transcription Kit

Reagent	Volume per reaction (µl)
Template RNA	14
Quantiscript RT Buffer, 5x	4
Gene specific primers	1.5
Quantiscript Reverse Transcriptase	1
Total reaction volume	20.5

The cDNA was purified from the enzymatic reaction using the ssDNA/RNA Clean & Concentrator purification kit (Zymo Research, USA), according to the manufacturer's instructions. The reaction volume was adjusted to 50 µl with RNase-free water and two volumes of DNA/RNA binding buffer to the reaction and mixed by pipetting. The mixture was then transferred into a Zymo-Spin™ IIC Column and centrifuged at 16, 000 x g for 1 minute.

Then one volume of ethanol was added to the flow through and mixed by pipetting. The mixture was then transferred back into the Zymo-Spin™ IIC Column and centrifuged at 16, 000 x g for 1 minute and the flow-through was discarded. Next, 400 µl of DNA/RNA Prep Buffer was added to the column and centrifuged at 16, 000 x g for 1 minute. The spin column was then washed twice by adding DNA/RNA Wash Buffer to the column and centrifuging at 16, 000 x g for 1 minute. After the wash step, the spin column was centrifuged at full speed to dry the membrane. The column was then transferred into an RNase-free tube and the cDNA was eluted in 20-50 µl of RNase free TE (Invitrogen, Massachusetts, USA).

2.7.6 cDNA synthesis using the SuperScript™ VILO™ cDNA Synthesis Kit

cDNA was synthesised using the SuperScript™ VILO™ cDNA Synthesis Kit (Invitrogen, Massachusetts, USA). The reverse transcription reaction was set up on ice according to Table 2.11.

Table 2.11Reverse transcription reaction mix using the SuperScript™ VILO™ cDNA Synthesis Kit

Component	Volume per reaction (µl)
5X VILO™ Reaction Mix	4
10X SuperScript™ Enzyme Mix	2
RNA (up to 2.5 µg)	Variable
Nuclease-free Water	Variable
Final volume	20

The reaction mixture was then incubated at 25°C for 10 minutes, then at 42°C for 60 minutes. The reaction was terminated by heating at 85°C for 5 minutes. The synthesised cDNA was then purified by ethanol precipitation.

2.7.7 Ethanol precipitation

The DNA solution was brought up to an appropriate volume with sterile H_2O (Global Life Sciences Solutions Operations UK Ltd, Sheffield, UK) (minimum volume of 50 µl). Then 1/10 volume of sodium acetate (3 M final concentration, pH 5.2). (Sigma-Aldrich, Missouri, USA). This was followed by the addition of 2.5 volumes of 100% (ice-cold) ethanol (Thermo Fisher Scientific, Massachusetts, USA). The nucleic acid/salt/ethanol mixture was then incubated for 20 minutes at -20 °C and centrifuged at 13,000 × g for 15 minutes (4°C). Then the supernatant was discarded and the pellet was washed 3 times with 500 µl of 70% ethanol, followed by centrifugation at 13,000 × g for 5 minutes (4°C). The pellet was then air dried (~5-10 minutes) and resuspended in an appropriate volume of TE (Thermo Fisher Scientific, Massachusetts, USA), depending on downstream applications.

2.7.8 Reverse transcription-polymerase chain reaction (RT-PCR)

cDNA prepared using the method described in 2.7.3 was used as a template in PCRs. The 25 µl PCR reaction mix consisted of 2 µl cDNA (10ng/ µl), 12.5 µl MangoMix™ (Meridian Bioscience, Ohio, USA) and primers Hu1and Hu2 or HuPrP pLNCX2 Reverse and HuPrP pLNCX2 Forward oligonucleotide primers at 10 uM.

The human only PCR assay was run with the cycling conditions listed in Table 2.12. Hu1 and Hu2 amplify a sequence in the HuPrP open reading frame (ORF) to produce a 400bp PCR product.

Table 2.12 Human only PCR cycling conditions

Cycle	Temperature	Time	Cycles
Initial denaturation	94°C	5 min	1
Denaturation	94°C	30s	
Annealing	61.5°C	45s	34
Extension	72°C	1 min	
Final extension	72°C	10 min	1

The cycling conditions for the HuPrP pLNCX2 assay are listed in Table 2.13. The HuPrP pLNCX2 Reverse and HuPrP pLNCX2 Forward primers amplify a sequence in the HuPrP ORF to produce a 248 bp PCR product.

Table 2.13 HuPrP pLNCX2 PCR cycling conditions

Cycle	Temperature	Time	Cycles
Initial denaturation	94°C	5 min	1
Denaturation	94°C	1 min	
Annealing	58.8°C	1 min	
Extension	72°C	1 min	
Final extension	72°C	10 min	1

PCR products were run on a 1% agarose gel to confirm the presence of the expected band sizes.

2.8 Biochemistry techniques

2.8.1 Tissue homogenisation

Mouse tissue samples were snap-frozen in liquid nitrogen after collection and stored at -70°C until needed. Prior to homogenisation the tissue was placed on a petri dish on ice and chopped into smaller pieces. Next, the tissue was weighed and transferred into a Precellys lysing tube (Bertin Instruments, France) and the appropriate volume of lysis buffer was added to the sample to obtain a 20% (w/v) tissue homogenate. The sample was then homogenised in a Minilys Personal Homogenizer (Bertin Instruments, France) for 1 minute and 45 seconds. Following this, the lysate was then kept on ice for 10 minutes to reduce foam and then an equal volume of lysis buffer was added to the sample to obtain a 10% (w/v) tissue homogenate. The 10% (w/v) tissue homogenates were then centrifuged at 16,000 x g for 10 minutes at 4°C. The supernatant was then aliquoted into Eppendorf tubes and stored at -20°C.

2.8.2 Sodium Dodecyl Sulphate–Polyacrylamide (SDS-PAGE) Electrophoresis

The mouse tissue homogenate was centrifuged at 300 xg for 1 minute and an equal volume of sample buffer was added to the homogenate in a fume cupboard. The samples were then denatured at 100°C for 10 minutes and centrifuged at maximum speed for 1 minute before loading them onto a 16% Tris-Glycine gel (Invitrogen, Massachusetts, USA). Samples were then run alongside the SeeBlue™ Pre-stained Protein Standard marker (Invitrogen, Massachusetts, USA) for 80 minutes at 200V in Tris-Glycine SDS running buffer (Geneflow Ltd, Lichfield, UK).

2.8.3 Western blot

After SDS-PAGE electrophoresis, the gels were blotted onto a Polyvinylidene Fluoride (PVDF) membrane (Merck Life Science, New Jersey, USA) that had been activated by soaking it in 100% methanol for 2-3 minutes. The membrane was then equilibrated in Tris Glycine electroblotting buffer (Geneflow Ltd, Lichfield, UK) before use. The gel and PVDF membrane were assembled into a transfer sandwich along with several sheets of Whatman paper (Merck Life Science, New Jersey, USA) and transfer blotting pads. The transfer sandwich was prepared in a cassette submerged in transfer buffer. Electrotransfer was performed at 35V for 2 hrs.

Once the transfer was complete, the membranes were blocked for 1 hour in 5 % (w/v) non-fat milk powder (Oxoid Limited, Hampshire, UK) prepared in PBST to reduce background and block-non-specific binding of antibodies. The membranes were then washed thoroughly in PBST and then incubated with a primary antibody diluted in 20 ml of PBST, to give a final concentration of 0.25µg*/ ml,* for 1 hour at room temperature or overnight at 4°C on a rocking shaker. After incubation the membranes were washed in PBST once for 2 minutes, once for 15 minutes and then 3 times for 5 minutes.

The membrane was then incubated for 40 minutes at room temperature with Antimouse IgG Alkaline phosphatase diluted 1:20,000 in 40 ml of PBST on a rocking shaker. After incubation the membranes were washed in PBST once for 2 minutes, once for 15 minutes and then 3 times for 5 minutes. This was then followed by 2 x 3-minute washes in 1x TAB buffer to remove excess antibody (Applied Biosystems).

The blots were developed with Tropix CDP-Star (Applied Biosystems, Massachusetts, USA) which detects alkaline phosphatase- labelled molecules. After incubation with CDP-Star® for 5 minutes, the membranes were exposed to BioMax MR Film (Carestream Health, New York, USA) for different durations and developed manually using GBX Developer and Fixer (Carestream Health, New York, USA).

2.8.4 Total protein quantitation using the bicinchoninic acid assay

Total protein quantitation was carried out using the Pierce™ bicinchoninic acid (BCA) assay kit (Thermo Fisher Scientific, Massachusetts, USA). Albumin (BSA) standards were diluted in the lysis buffer used to extract the protein). The BCA working reagent was prepared by mixing Reagent A with reagent B (50:1, Reagent A: B). Then 200 µl of the working reagent was pipetted into a 96-well microplate. After this, 25 µl of each standard or sample was pipetted in triplicate into the same 96-well microplate. The contents of the microplate wells were then mixed on a microplate shaker for 30 seconds and then incubated at 37°C for 30 minutes in an incubator. The plate was then left to cool down to room temperature before the absorbance was measured. Absorbance was read at 560nm with the Tecan Infinite 200 PRO microplate reader (Tecan UK Ltd, Ireland). The final absorbance measurements were determined by averaging the replicate absorbance readings for each sample and then subtracting the average absorbance reading from the blank (working reagent and lysis buffer used for protein extraction). These final absorbance readings and the absorbance reading of the BSA standards were used to generate a standard curve. The concentrations of the protein samples were calculated using a standard curve.

2.8.5 ELISA (Enzyme-Linked Immunosorbent Assay)

**All wash steps were performed using the BioTek 50 TS automated microplate washer (BioTek, Vermont, USA)*

The wells of mictotitre plates (Greiner Bio-One Ltd, Frickenhausen, Germany) were coated with 100 µl of 2.5 µg/ ml of the capture antibody and incubated overnight at 4°C. The next morning, the plates were washed 3x with 300 µl PBST (0.05%). After this, the plates were blocked by adding 300 µl of Superblock (1x) (Thermo Fisher Scientific, Massachusetts, USA) to each well and incubated in a microplate shaker for 1 hour at 37°C with shaking at 300 rpm. Following this incubation step the plates were washed 1x with 300 µl PBST and 50 µl of each sample prepared in IP capture buffer was added to each well and incubated for 1 hour at 37°C with shaking. Then the plates were washed 3x with 300 µl PBST (0.05%) and 100 µl of ICSM35B (1 µg/ml) diluted in 1% PBST was added to each well and incubated for 1 hour at 37°C with shaking.

After this step the plates were washed 3x with 300 µl PBST then 100 µl of a 1: 100 000 dilution of Neutravidin-HRP (Thermo Fisher Scientific, Massachusetts, USA) was added to each well and incubated for 30 minutes at 37°C with shaking. The plates were then washed with 4x PBST and developed with 100 µl per well of QuantaBlu working solution (Thermo Fisher Scientific, Massachusetts, USA). Absorbance was then determined at 450 nm with the Tecan Infinite 200 PRO microplate reader (Tecan Männedorf, Switzerland).

Serial dilutions of recombinant mouse prion protein (23-231) were used to create a standard curve in order to quantify the amount of PrP^C in the tissue homogenates. The absorbance readings of samples of known concentrations were fed into GraphPad Prism 9 (GraphPad Software Inc, California, USA) and linear regression analyses were performed to determine PrP^C concentration.

2.9 Animals used

All experiments and procedures involving mice were carried out in accordance with the UK Animals (Scientific Procedures) Act 1986 and conformed to the ARRIVE (www.nc3rs.org.uk/ARRIVE/) and University College London institutional guidelines. Inbred FVB/N mice were supplied by Charles River UK.

F10_FVB/PrP null $^{(0/0)}$ mice were generated by backcrossing ZH1 PrP null mice (Büeler et al., 1992) to FVB/N mouse background for 10 generations.

2.10 Microinjection

2.10.1 Preparation of mice before microinjection

Superovulation was induced in female FVB/N mice (4-6 weeks old) by intraperitoneal administration of Follicle Stimulating Hormone (FSH) (Merck Life Science, New Jersey, USA) at 5U per mouse. Female FVB/N mice were superovulated to produce embryos for the CRISPR knock-in lines, whereas F10_FVB/PrP null mice were superovulated for the generation of pCAG transgenics. After 46-48 hours the female mice were injected intraperitoneally with 5U of Luteinising hormone (LH) (Merck Life Science, New Jersey, USA) (5 IU/female) and set up with a fertile male of the same strain overnight. The next morning, female mice were checked for vaginal plugs before embryo collection.

2.10.2 Microinjection day

On the day of microinjection, plugged females were euthanized by cervical dislocation and their oviducts were excised and transferred into a sterile 30 mm petri dish containing M2 medium (Merck Life Science, New Jersey, USA). The oviduct was then torn apart above the ampulla under a microscope and the cumulus cells and embryos were released into the M2 medium. Hyaluronidase (Merck Life Science, New Jersey, USA) was then added to the M2 medium at a concentration of 1.2 mg/ml to digest the cumulus cells away. The embryos were then picked up using a mouth-controlled pipette and washed by passing them through five 100 µl droplets of M2 medium. The washed embryos were then transferred into petri dishes containing M16 medium and stored in an incubator at 37°C until the microinjection procedure.

2.10.3 Pronuclear DNA microinjection

The purified DNA construct was diluted to 1ng/ µl using filtered TE buffer (Invitrogen, Massachusetts, USA) and centrifuged at 16,000 x g for 10-15 minutes prior to microinjection to pellet any particulate matter. The embryo was held in place with a holding pipette while the DNA construct was injected into the male pronucleus using an injection needle (Figure 2.2).

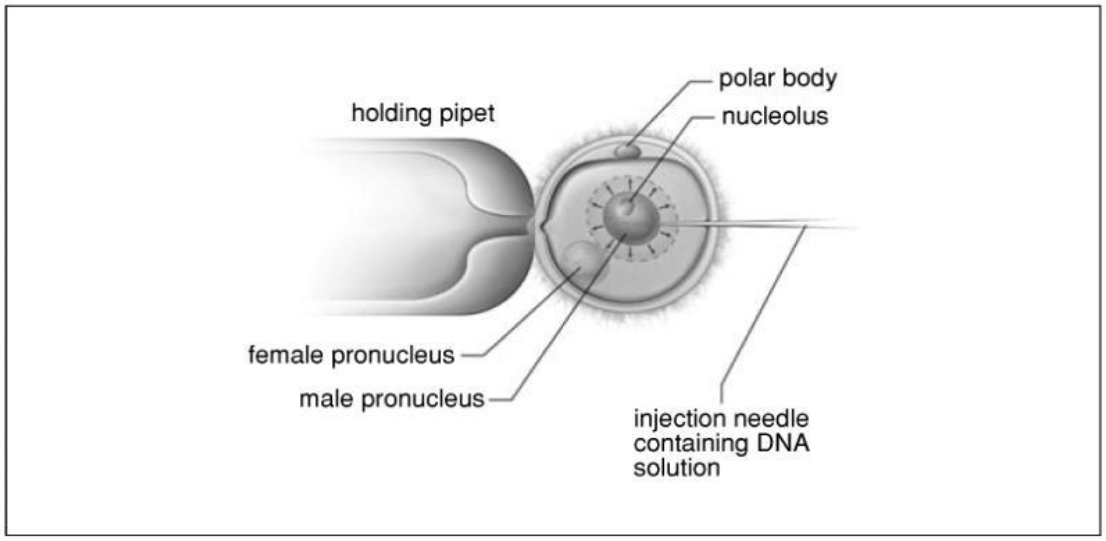

Figure 2.2: Microinjection of DNA construct into male pronucleus. Adopted from Cho *et al*., 2009 (Cho et al., 2009)

Transgenic mice were generated by microinjecting DNA constructs into the male pronucleus of F10_FVB/PrP-null single cell embryos. Following microinjection, the embryos were cultured to the two-cell stage and surgically transferred into C57BL/6 pseudo-pregnant recipient female mice (Charles River UK) to produce transgenic founder mice.

2.11 Genotyping

DNA for genotyping was obtained from ear biopsies. Each ear biopsy was transferred into the well of a 96-well plate and 200 µl of Proteinase K (PK)-ATL buffer was added to each well. PK-ATL buffer was prepared by mixing 1 part of PK (Qiagen, Hilden, Germany) with 9 parts of ATL buffer PK (Qiagen, Hilden, Germany). The ear biopsies were then incubated in the buffer overnight at 56°C in a Thermoshaker (Thermo Fisher Scientific, Massachusetts, USA) set to 300rpm. DNA was then extracted the following morning from the samples using the automated QIAcube-HT system (Qiagen, Hilden, Germany). The DNA was then used as a template in the appropriate PCR assay depending on the line being analysed.

2.12 Cell culture methods

2.12.1 Cell lines

CAD5 cells are murine catecholaminergic lines derived from mouse neuroblastoma tissue (Mahal et al., 2007). CAD5 cells expressing Human PrP 163X or WT 129V were generated using CAD5KDB3 cells, a gift from Parmjit Jat (MRC Prion Unit, UCL, UK). CADKDB3 cells were made by knocking-down the expression of mouse PrP in CAD5 wild-type cells with a small interfering RNA.

Phoenix Ecotropic packaging cell lines (Nolan Lab, Standford University School of Medicine, USA) derived from the HEK 293T human cell line were used for virus production (Pear et al., 1993) (Yang et al., 1999).

2.12.2 General cell culture

Generally, adherent cells were grown in an incubator set at 37°C containing 5% CO_2 and split every 3-4 days. Adherent cells were split by removing the spent cell culture media from the cell culture dish and then pipetting fresh pre -warmed medium into the dish. The cells were then detached from the surface of the plate by re-suspending them in the fresh medium using a pipetboy (INTEGRA Biosciences Ltd, Zizers, Switzerland) set to a high speed. Then the required amount of cell suspension was removed from the dish using a pipetboy and transferred into a new dish containing pre-warmed fresh medium.

The culturing conditions for CAD5KDB3 and Phoenix Ecotropic packaging cells are described in Table 2.14.

Table 2.14 Culturing conditions of CADKDB3 and Phoenix Ecotropic packaging cell lines

Cell Line	Medium	Split ratio
CAD5KDB3	OBGS: OptiMEM supplemented 10% Bovine Growth Serum + 1% PenStrep 500 ml OptiMEM (Thermo Fisher Scientific, Massachusetts, USA) 10% (v/v) Hyclone Bovine Growth Serum (Global Life Sciences Solutions, USA) 1% Penicillin (10,000 units/mL) -Streptomycin (10,000 µg/mL) (Thermo Fisher Scientific, Massachusetts, USA)	1:8
Phoenix Ecotropic packaging cells	DMEM-FBS : Dulbecco's Modified Eagle Medium supplemented 10% Fetal Bovine Serum + 1% PenStrep 500 ml Dulbecco's Modified Eagle Medium (Thermo Fisher Scientific, Massachusetts, USA) 10% Fetal Bovine Serum (Thermo Fisher Scientific, Massachusetts, USA) 1% Penicillin (10,000 units/mL) -Streptomycin (10,000 µg/mL) (Thermo Fisher Scientific, Massachusetts, USA)	1:10

2.12.3 Cell counting

Cell counts were performed manually using the C-Chip (Labtech, East Sussex, UK), a disposable plastic haemocytometer by loading 10 µl of the cell suspension into the sample injection area and then the number of cells were counted under the Motic AE20 binocular inverted microscope (Motic, Xiamen, China).

Cells per ml = average count per square x dilution factor x volume factor

2.12.4 Cell thawing

The vial containing frozen cells was removed from liquid nitrogen and thawed rapidly at 37°C in a water bath. The thawed cells were then transferred into a 15 ml sterile conical screw cap tube containing 2 ml of pre-warmed OBGS. After 5 minutes 8 ml of OBGS was added to the tube containing the cells and the cells were centrifuged at 500 x g for 4 minutes. Following this, the supernatant was discarded and the pellet was resuspended in 10 ml OBGS and cultured in 10 cm petri dishes at 5% CO_2 and 37 °C.

2.12.5 Cell freezing

The cells were frozen by being resuspended in 1 ml freezing medium (50 % bovine growth serum, 10 % DMSO and 40% OBGS) per 10^6 and then transferred into cryogenic vials (approximately 1.5ml per vial). The vials were stored in a freezing container overnight at -80°C and then transferred into liquid nitrogen the next day.

2.12.6 Transfection of cells via fuGENE transfection reagent

Phoenix ecotropic packaging cells were cultured in DMEM-FBS for a week before transfections and 1.5 million Phoenix cells were plated a day prior to transfections. The Phoenix cells were transfected with 3 μg of the retroviral vector construct and 2 μg of the VSV-G envelope expressing plasmid, pMD.G (a gift from Parmjit Jat (MRC Prion Unit, UCL, UK) using fuGENE transfection reagent (Promega, Wisconsin, USA) and maintained in culture for 24 hours.

The medium was changed the following day and viral supernatants were harvested and filtered 48 hours post-transduction through a 0.45 μM filter (Pall Corporation, New York, USA). The viral supernatants were stored at -80°C for later infection.

2.12.7 Retroviral transduction of CADKDB3 cells

For the retroviral transduction experiments, 1 x10^6 CADKDB3 cells were seeded in 10 ml of OBGS+Puromycin (2 μg/ml) (Sigma-Aldrich, Missouri, USA) and following overnight incubation polybrene (8μg/ml) (Sigma-Aldrich, Missouri, USA) was mixed with the cell culture medium that the cells were growing in to give a final concentration of (8μg/ml). The cells were then overlaid with 2 ml of retrovirus-containing supernatants and then incubated at 37°C and 5% CO_2 for 4 hours. After 4 hours the culture medium was removed and replaced with 10 ml OBGS+Puromycin (2 μg/ml). The cells were split 1:3 and cultured in selective medium (OBGS+Puromycin (2 μg/ml)+ Geneticin (400 μg/ml) (Life Technologies, California, USA) 72- hours post-transduction, in order to select for stable activated clones. The medium was replaced every 3-4 days until antibiotic resistant clones were identified.

2.12.8 Preparation of cell lysates

The cells were pelleted by centrifugation at 400 x g for 5 min in 10 ml of ice-cold PBS and then the PBS was discarded. The cell pellet was then resuspended in 200 µl of ice-cold RIPA buffer (Sigma-Aldrich, Missouri, USA) and subjected to three freeze-thaw cycles to lyse the cells. The cell suspension was frozen on dry ice and thawed in a water bath set at 37°C. The cell lysate was centrifuged at 11,000 x g for 10 min to remove debris and the supernatant was aliquoted and stored at -20°C until needed. Protein concentration was determined using the BCA assay and the protein concentration was adjusted to 2.0 mg/ml.

2.12.9 Sodium Dodecyl Sulphate–Polyacrylamide (SDS-PAGE) Electrophoresis

The cell lysates were thawed and an equal volume of sample buffer was added to the lysates in a fume cupboard. The samples were then centrifuged at 600 x g for 1 min and denatured at 100°C for 10 minutes. The lysates were centrifuged again for 1 min at 16, 000 x g prior to loading them onto a 16% Tris-Glycine gel (Invitrogen, Massachusetts, USA). Samples were electrophoresed alongside the SeeBlue™ Pre-stained Protein Standard marker (Invitrogen, Massachusetts, USA) for 80 minutes at 200V in Tris-Glycine SDS running buffer (Geneflow Ltd, Lichfield, UK).

2.13 Preparation and fluorescent immunocytochemistry staining of cells on coverslips

2.13.1 Coating of coverslips with Poly-L-Lysine (PLL)

Borate buffer was made by adjusting 0.1 M of boric acid (Sigma-Aldrich, Missouri, USA) with 0.1 M of sodium tetraborate (Sigma-Aldrich, Missouri, USA) to pH 8.5 and filter-sterilised through a 0.2 μm filter (Pall Corporation, New York, USA).

PLL was prepared by diluting the 10 mg/ml stock of PLL (Sigma-Aldrich, Missouri, USA) in 9.9 ml of 1x borate buffer to give a final concentration of 0.1 mg/ml. Ten sterilised coverslips were placed into 6 cm dishes and each 6 cm dish was filled with 6 ml of PLL and incubated overnight at 37°C in an incubator.

2.13.2 Plating cells on coverslips

The next day the PLL was removed from the 6 cm dishes and the coverslips were washed twice with distilled water (Thermo Fisher Scientific, Massachusetts, USA) and replaced with 6 ml of OBGS containing approximately 150K cells. The cells were grown on top of the cover slips in the 6 cm dishes for two days then the coverslips were placed into individual wells in a 24-well plate using forceps and the cells were washed three times for 5 min in ice cold 1x Dulbecco's phosphate-buffered saline (DPBS) (Thermo Fisher Scientific, Massachusetts, USA) . The cells were then fixed in 4% paraformaldehyde PFA (Sigma-Aldrich, Missouri, USA) diluted in 1x DPBS and stored at 4°C.

2.13.3 Immunofluorescence

Non-specific staining was blocked by adding 500 µl of 5% BSA (Sigma-Aldrich, Missouri, USA) in DPBS to each well in the 24-well plate with coverslips containing fixed cells and incubated for 1 hour at room temperature. The 5% BSA in DPBS was aspirated and 500 ul of the primary antibody diluted in 1% BSA (1:1000) was added to each well and incubated for 1 hour at room temperature. The coverslips were then washed with 1x DPBS 3 times: 1x 10 min wash and 2x 15 min washes. Then 500 ul of the secondary antibody diluted in 1% BSA (1:1000) containing DAPI (Sigma-Aldrich, Missouri, USA) (1:5000) was added to each well and incubated for 1 hour at room temperature. After 1 hour the coverslips were then washed with 1x DPBS 3 times: 1x 10 min wash and 2x 15 min washes. The coverslips were then removed from each well and dried with tissue paper before mounting them onto microscope slides. To mount the coverslips, 1 drop of mounting medium (Agilent Technologies, California, USA) was dispensed onto each slide (Knittel Glass, Germany) and then the cells were placed face-down onto the mounting medium. Imaging was done using the Zeiss LSM 710 inverted confocal microscope (Zeiss, Oberkochen, Germany) and the images were acquired using Zen Black software (Zeiss, Oberkochen, Germany).

3. Chapter 3: Generation of HuPrP 163X Knock-in mouse model

This chapter aims to describe the steps involved in generating the HuPrP knock-in mouse models. It will cover the targeting and genotyping strategy for these mice and provide details about the experiments that have been set up with these lines.

3.1 Construct design

Y163X-129V and WT-129V Knock-in mice were generated by Cyagen (*Cyagen* US Inc., Santa Clara, CA) on a C57BL/6N background.

To generate Y163X-129V knock-in mice, the endogenous mouse *Prnp* gene was replaced with the human *PRNP* gene that encodes valine at codon 129 and contains a stop codon mutation at residue 163. For a control, WT-129V knock-in mice were generated by replacing the endogenous mouse *Prnp* gene with the wild type human *PRNP* gene that encodes valine at codon 129.

The targeting vector (Figure 3.1) was electroporated into C57BL/6N embryonic stem cells (ES) and following drug selection the targeted clones were screened by PCR and Southern blot. The targeted ES cells were injected into C57BL/6N albino embryos and implanted into pseudo-pregnant surrogate mothers (CD-1 female mice). The resulting pups were scored for coat colour chimerism and germline transmission was confirmed by breeding male chimeric mice with C57BL/6N females (black). Offspring were genotyped by PCR to confirm transmission of the targeted allele.

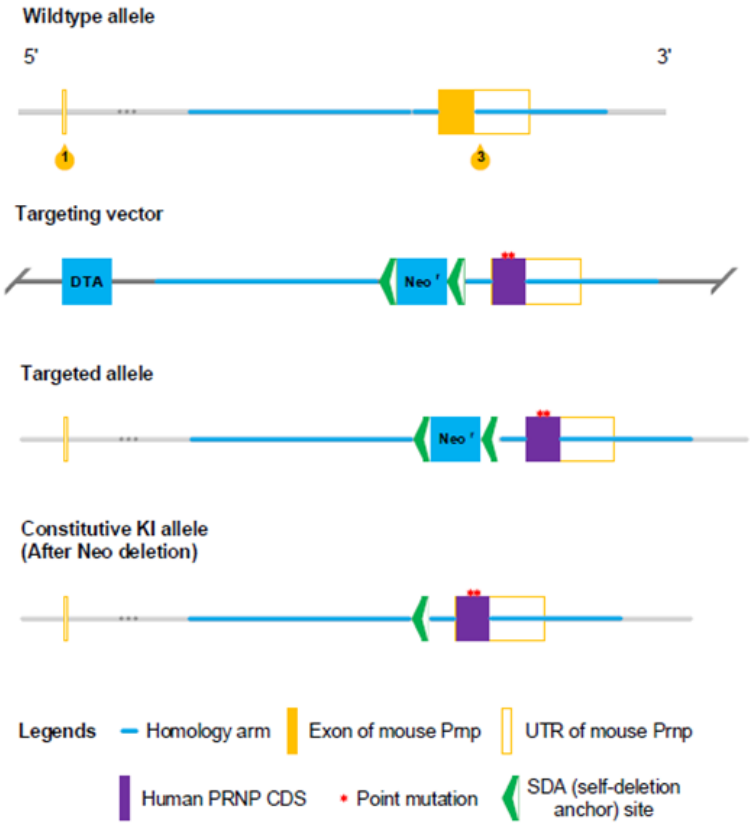

*UTR= Untranslated region, CDS= Coding sequence

Figure 3.1: Overview of targeting strategy for the generation of Y163-129V knock-in mice

The final targeting vector contains the HuPrP coding sequence, neomycin resistance coding sequence and diphtheria toxin A (DTA) negative selection gene. The positive selection marker, neomycin was flanked by self-deletion anchor sites to enable removal. The self-deletion anchor site recombination will occur after the founders have been crossed to wild-type C57BL/6N mice. The negative marker DTA was incorporated into the vector backbone for the identification of ES cells in which the DNA has randomly integrated. Image provided by Cyagen (Cyagen US Inc., Santa Clara, CA).

3.2 Genotyping strategy to identify knock-in founder mice and determine zygosity

Genomic DNA was obtained from ear biopsies for PCR analysis. KI PCR was used to identify mice with the knock-in HuPrP allele. Primers KI-F (F3): 5'-GGCTGGTAAGGGATATTTGCCTG-3'and KI-R (R3): 5'-CCAGCCTAGACCACGAGAATGCG-3' (Figure 3.2) were used to amplify a 447bp sequence within the human PrP coding sequence (Figure 3.3).

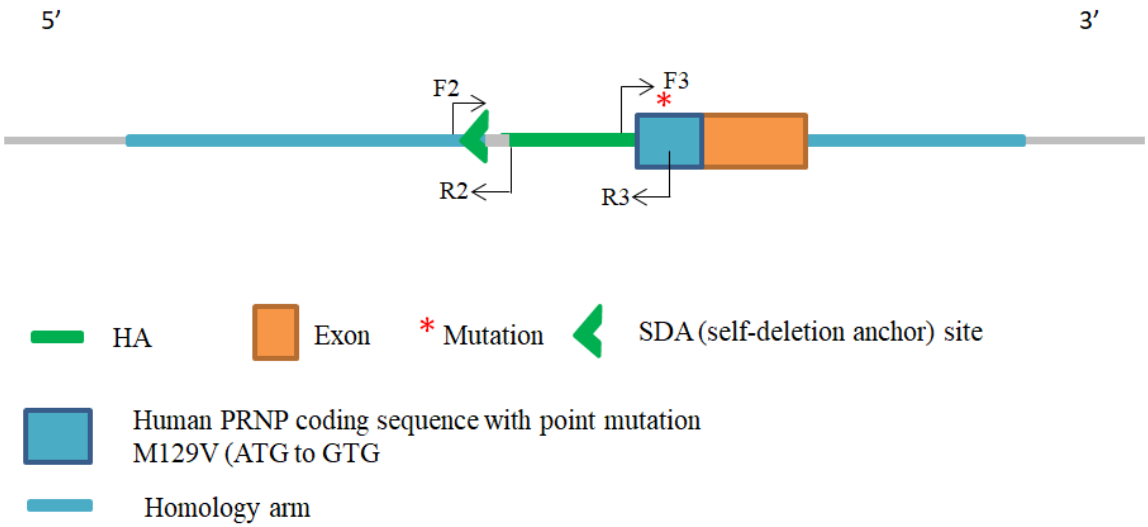

Figure 3.2: Map of primers used to identify knock-in founder mice and determine zygosity

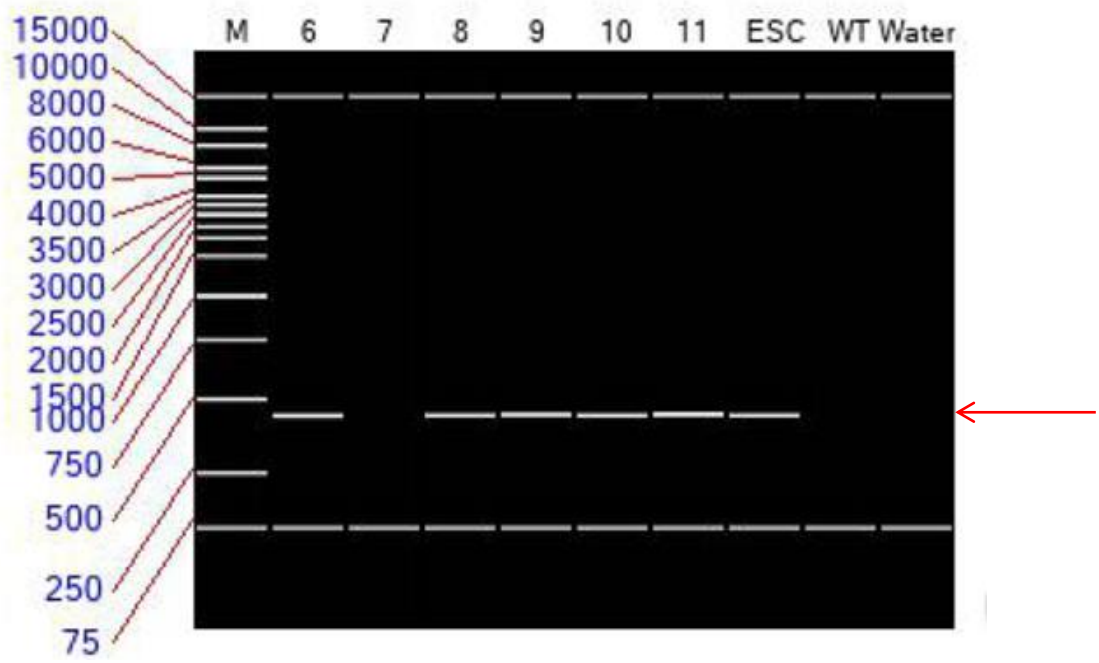

Figure 3 3: Identification of mice positive for the HuPrP Y163X KI allele using KI PCR

Five positives (#6, #8, #9, #10, #11) were identified positive by PCR screening for the knock-in allele (red arrow pointing to 447bp fragment). ESC= Embryonic stem cell, WT=Wildtype and M= Marker. Data provided by Cyagen (Cyagen US Inc., Santa Clara, CA).

Neo-deletion PCR was used to distinguish homozygous mice for the KI allele HuPrP_Y163X KI $^{(+/+)}$ from heterozygous HuPrP_Y163X KI $^{(+/-)}$ animals. Primers F2: 5'-AGGAGATTCTTGGCTTTGTGCTTA-3' and R2: 5'-TGTGAGTTCTAATACATCTGGGCT-3' were used to determine zygosity (Figure 3.2). This PCR amplifies the self-deletion anchor sequence on the 5' arm of the targeting vector. The wildtype allele produces a 179bp fragment and the mutant allele produces a 298bp fragment (Figure 3.4). Two fragments will be amplified in heterozygous mice (298bp and 179bp). In homozygous mice one fragment will be amplified (298bp).

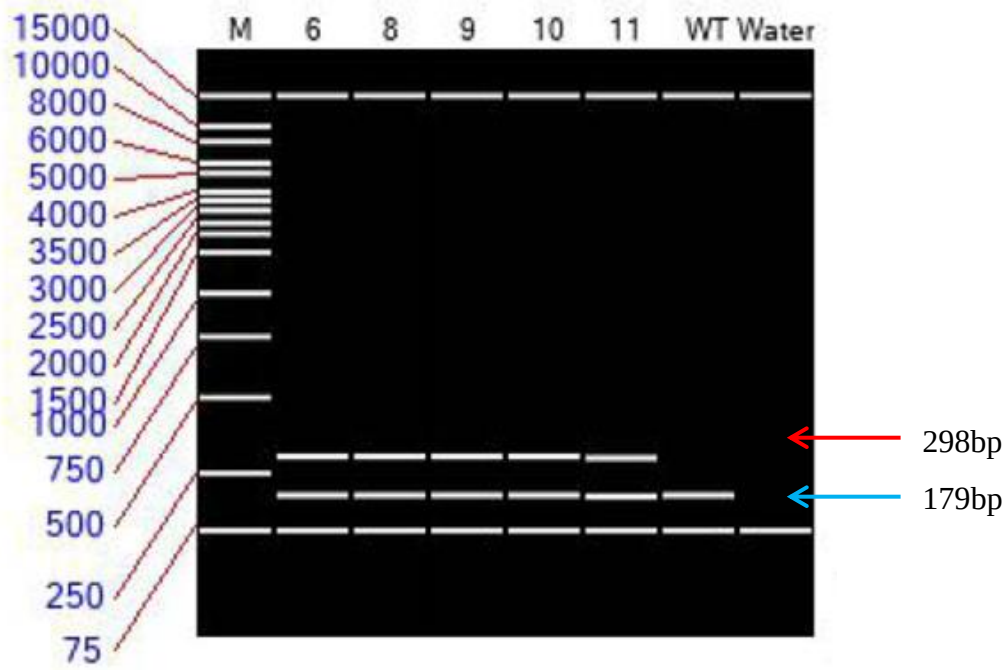

Figure 3.4: Identification of mice heterozygous for HuPrP Y163X KI allele using Neo-deletion PCR

Five positives (#6, #8, #9, #10, #11) were identified as heterozygotes by PCR screening using the neo deletion PCR (red arrow pointing to 298bp fragment (mutant) and blue arrow pointing to 179bp fragment (wild type). Data provided by Cyagen (Cyagen US Inc., Santa Clara, CA).

In total Cyagen (Cyagen US Inc., Santa Clara, CA) generated: Five mice (2 males and 3 females) heterozygous for the targeted allele containing the human *PRNP* gene encoding valine at codon 129 and a stop codon mutation at residue 163 and six mice (4 males and 2 females) heterozygous for the targeted allele containing the wild type human *PRNP* gene encoding valine at codon 129 were generated.

These mice were imported into the Biological Services Facility at the Institute of Prion Diseases and allowed to acclimatise before matings were set up to expand and breed the lines to homozygosity.

3.2.1 Establishment of homozygous Y163X and WT-129V knock-in lines for experimental use

The imported heterozygous offspring were then crossed with each other to obtain mice homozygous for the targeted allele. The pups resulting from these matings were screened by KI PCR and Neo-deletion PCR (Figure 3.5).

The knock-in lines were monitored by Cyagen prior to sending the heterozygous animals to the MRC Prion Unit where further breeding was carried to homozygosity. The mice were monitored carefully throughout the in-house breeding process, but no overt abnormal phenotype was observed.

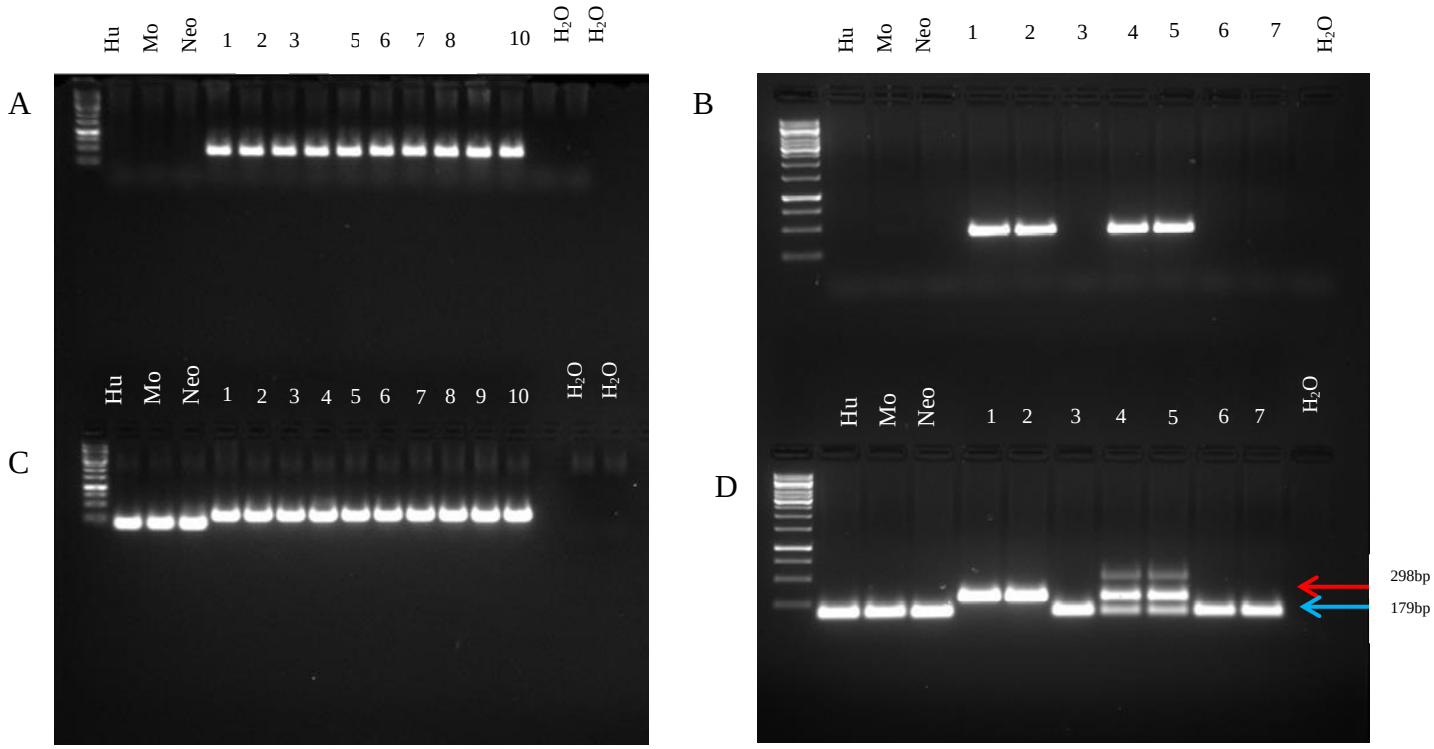

Figure 3.5: Screening of HuPrP Y163X-129V and WT-129V knock-in mice using KI and Neo deletion PCR

(A) KI PCR: 10 (#1-#10) HuPrP Y163X-129V KI identified positive by PCR screening for the knock-in allele. Genomic DNA from Tg28 (Hu), FVB (Mo) and F10_FVB/PrP null (Neo) mice were used as negative controls.

(B) KI PCR: 4 (#1, #2, #4 and #) Hu PrP WT-129V KI identified positive by PCR screening for the knock-in allele. Genomic DNA from Tg28 (Hu), FVB (Mo) and F10_FVB/PrP null (Neo) mice were used as negative controls.

(C) Neo deletion PCR: 10 (#1-#10) homozygous HuPrP Y163X KI-129V mice identified using the neo deletion PCR. Primers F2 and R2 amplified a sequence within wild-type mouse PrP in Tg28 (Hu), FVB (Mo) and F10_FVB/PrP null (Neo) mice to produce the 179bp fragment.

(D) Neo deletion PCR: 2 (#1 and #2) homozygous Hu PrP WT-129V KI mice, 2 (#4 and #5) heterozygous WT-129V KI mice and 3 (#3, #6 and #7) C57BL/6 mice identified using the neo deletion PCR. Primers F2 and R2 amplified a sequence within wild-type mouse PrP in Tg28 (Hu), FVB (Mo) and F10_FVB/PrP null (Neo) mice to produce the 179bp fragment.

3.3 Experiment 321: Long term observation of homozygous HuPrP Y163X-knock-in and HuPrP_129V-WT_knock-in mice

The aim of this experiment is to age homozygous Y163X-129V knock-in (HuPrP_Y163X_KI) and control WT-129V knock-in (HuPrP_129V-WT_KI) mice for the possible development of spontaneous PrP deposition. The long term plan is to investigate the possibility of preventing neuroinvasion with small molecules and monoclonal antibodies, once the earliest time point at which the deposition of PrP amyloid plaques occurs (if any) has been determined.

This experiment contains 28 groups, 14 groups for HuPrP_Y163X_KI (205 mice) and 14 groups for 129V-WT control line (205 mice). Groups of mice will be time-culled starting from 50 days of age, and subsequently at 50-day intervals until the 700-day endpoint. The number of mice to be culled from 50 to 250-day old groups will be 10 each, because inter-current illness is unlikely to deplete the experimental groups at these earlier time points. The number of mice to be time-culled from 300-500-day old group will be 15 each (as intermediate) and finally, for the 300 to 700-day old groups the number of mice per group will be 20.

These numbers and time intervals have been estimated based on our previous experience in ageing mice expressing mutant human PrP long term, to account for higher inter-current losses as the mice get older. Data collected from these long term studies will be used to calculate the sample sizes needed in follow up experiments. Time intervals for the LTO were also based on the design of a previous successful experiment involving ageing of mutant lines expressing the human PrP disease-associated A117V mutation.

The rationale was that spontaneous pathology associated with the human protein gene is highly unlikely to occur before 50 days of age, and changes thereafter are expected to be so slow and subtle if any, that any shorter intervals than 50 days would not be productive.

These uninoculated mice will be observed long term for the possible development of spontaneous neurological dysfunction, and criteria for termination will be either prion diagnostic clinical signs or planned time-culling of groups of mice. The main analytical procedure will be immunohistochemistry (IHC) (since from experience immunoblotting is not sensitive enough for LTO samples), in order to determine the earliest time point at which any spontaneous deposition of PrP amyloid plaques may occur.

Tissues to be fixed for IHC analyses will be taken from both the CNS and peripheral organs of each culled mouse, and will include: brain, spinal cord, spleen, lymph nodes, kidney, heart, lung, liver, gut (small intestine, colon and caecum). These tissues will then be fixed in 10% buffered formal saline and examined by standard PrP IHC using monoclonal antibodies ICSM35 and 3F4 (White et al., 2003).

The Y163X mutation is associated with peripheral and autonomic neuropathy. Peripheral symptoms of this condition, referred to as PrP systemic amyloidosis include weight loss. Therefore we need to monitor body weight of the LTO mice and correlate that data with the appearance of spontaneous plaques or neurological dysfunction.

For practical reasons the same mice in 1 group (700-day time cull group) for this experiment will be weighed once every 2 weeks from when they are 100 days old until they reach 300 days old. Then from 307 days (1 week after the last bi-weekly weighing), the weighing frequency will be weekly until they reach experimental endpoint of 700 days.

Weighing the same mice in the selected group that is planned to go to the terminal endpoint of the experiment means that enough body weight data would have been accumulated by the time any spontaneous disease phenotype develops, and can be correlated with the time point at which a phenotype is seen. It is hoped that at least 10 mice in the group of 20 will survive to 700 days to ensure acceptable statistical power.

3.4 Experiment 328: Long term observation of heterozygous HuPrP_Y163X_KI/ HuPrP_129V-WT_KI mice

The aim of this experiment is to age heterozygous HuPrP_Y163X_KI/ HuPrP_129V-WT_KI mice for the possible development of spontaneous PrP deposition.

The experimental design will be exactly the same as Experiment 321 and experimental groups have been populated.

In summary, two knock-in lines have been generated, the Y163X-129V and WT-129V(control) knock-in lines. Both lines have been bred to homozygosity and long-term observation experiments have been set up to monitor homozygous and heterozygous mice over a period of 700 days. These mice remain healthy in long-term observation experiments and CNS and peripheral tissues will be assessed for spontaneous PrP deposition.

4. Chapter 4: Generation of HuPrP 163X transgenic mouse models

This chapter aims to describe the construct design, assembly and genotyping strategy involved in the generation of transgenic mice overexpressing HuPrP 163X.

4.1 Construct design for the production of transgenic mice overexpressing HuPrP 163X in peripheral organs

The transgene was constructed in 3 separate parts which were assembled into the final construct used for microinjection.

Part I: Cloning oligonucleotide linker into pMG5.2 vector.

A modified version of pBluescriptSK(+) designated pMG5.2 (Figure 9A), was digested with restriction enzymes NotI and SaI sequentially to excise the promoter and intron and retain the HuPrP 3'UTR and SV40pA (Figure 4.1 C-D).

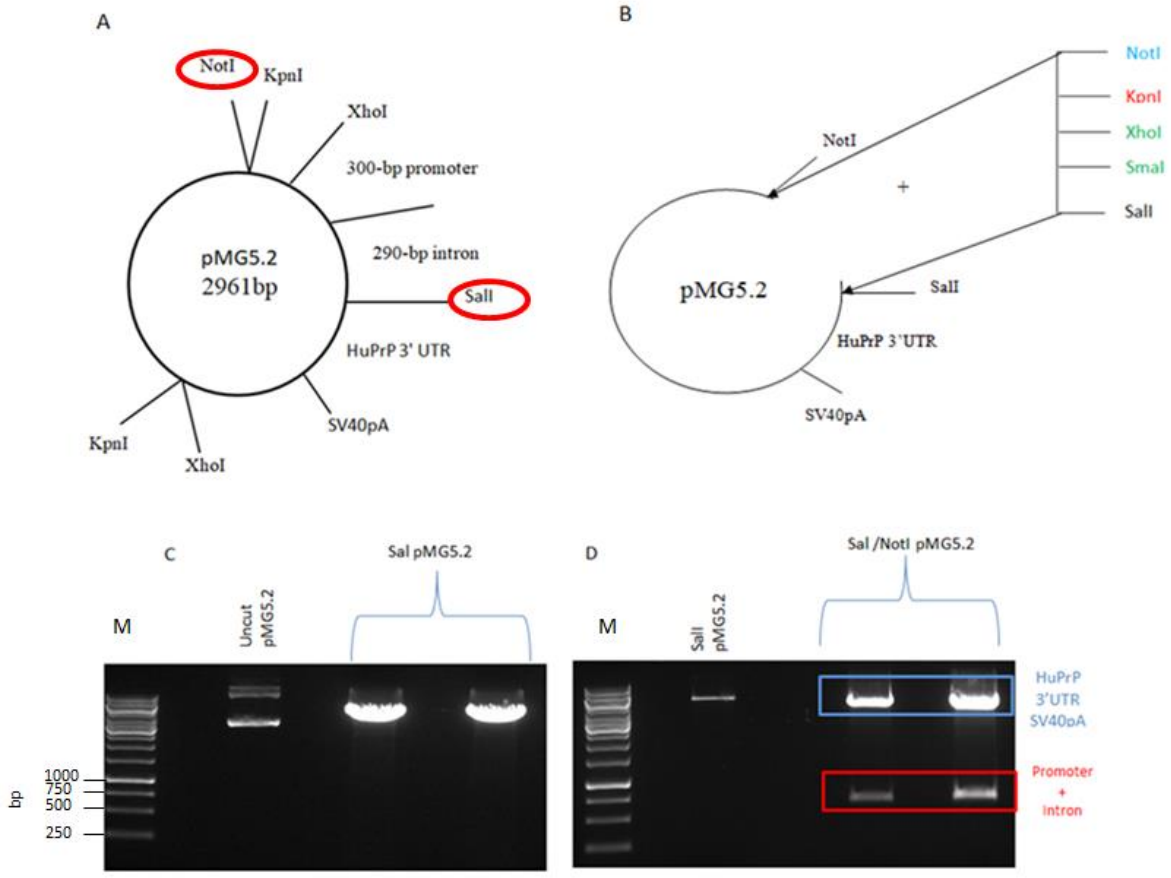

Figure 4.1: Cloning oligonucleotide linker into pMG5.2 vector.

(A) Schematic diagram of the pMG5.2 vector

(B) Ligation of pMG5.2 vector and NotI/SalI oligonucleotide linker

(C) SalI digestion of pMG5.2

(D) NotI digestion of SalI-digested pMG5.2 to excise the promoter and intron

M= GeneRuler 1 kb DNA Ladder (Catalogue number: SM0311, Thermo Fisher Scientific Ltd, Loughborough, UK

Then an oligonucleotide linker with the following sequences: forward primer 5'-GGCCGCGGTACCCTCGAGCCCGGGGTCGACC-3' (incorporating new enzyme sites NotI, KpnI, XhoI, SmaI and SalI) and its reverse-complement 5'-TCGAGGTCGACCCCGGGCTCGAGGGTACCGC-3' was annealed into a double strand, then ligated to the vector DNA containing the 3'UTR and SV40pA to introduce restriction sites needed for subsequent cloning (Figure 4.1B). The vector was then digested with SmaI and SalI to complete Part I which would enable ligation with the CAG promoter and β-actin intron being prepared in Part II.

Part II: Cloning the CAG promoter and β-actin intron into the pMG5.2 vector

The sequence for β-actin intron was appended to the CAG promoter sequence and sent for gene synthesis by GeneArt (Thermo Fisher Scientific Ltd, Loughborough, UK), who subcloned the synthesised gene into the pMKRQ vector (Figure 4.2).

The CAG plus β-actin intron composite was isolated from pMKRQ by first digesting with HindIII and blunting the cut sticky end. This was followed by SalI digestion to produce a fragment with one blunt end and a SalI sticky end (Figure 4.3A-B). This fragment was subsequently ligated to the pMG5.2 vector that had been previously digested with SmaI (producing a blunt end) and SalI from Part I.

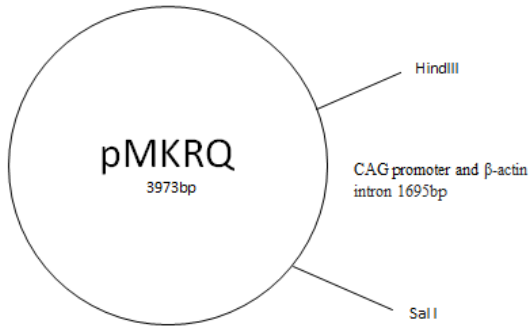

Figure 4.2: Schematic diagram of the pMKRQ vector containing the CAG promoter and β-actin intron

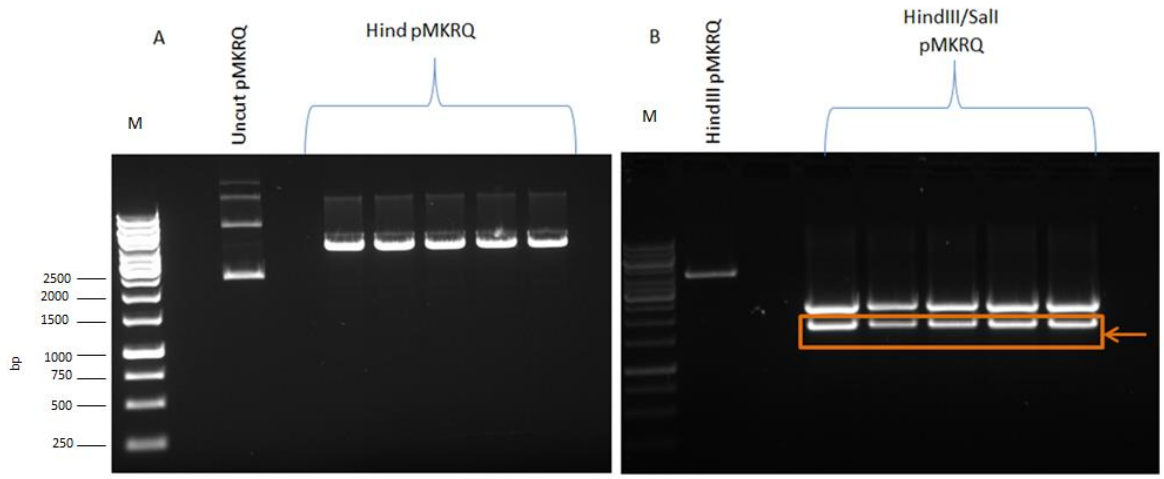

Figure 4.3: HindIII/ SalI digestion of pMKRQ

(A) HindIII digestion of pMKRQ, followed by blunting of the sticky end

(B) SalI digestion of pMKRO fragment previously cut with HindIII and blunted (orange arrow pointing to 1695bp fragment containing CAG promoter and β-actin intron)

M= GeneRuler 1 kb DNA Ladder (Catalogue number: SM0311, Thermo Fisher Scientific Ltd, Loughborough, UK

The ligation product was then used to transform competent *E. coli*, and plasmid DNA was purified from 5 clones using the QIAprep Spin Miniprep Kit (Qiagen, Hilden, Germany). After purifying the DNA, restriction digests with SalI and XhoI were used to identify recombinant plasmids containing the CAG promoter and β-actin intron (Figure 12). For positive clones, restriction digest with SalI produces one fragment of 6.6kb (pMG5.2 vector + CAG promoter and β-actin intron + HuPrP 3'UTR + SV40pA). Further digestion of positive clones with XhoI produces two fragments of 2961bp (pMG5.2 vector) and 3675bp (CAG promoter and β-actin intron + HuPrP 3'UTR + SV40pA).

Three positive clones were identified, #2, #5 and #6 (Figure 4.4). After full characterisation, glycerol stocks were made of clones #2 and #5, and miniprep plasmid DNA was prepared from clone #2 using the QIAprep Spin Miniprep Kit (Qiagen). This miniprep plasmid DNA was then digested with SalI in preparation for sub-cloning of the HuPrP ORF (with or without the Y163X mutation) prepared in Part III as described below.

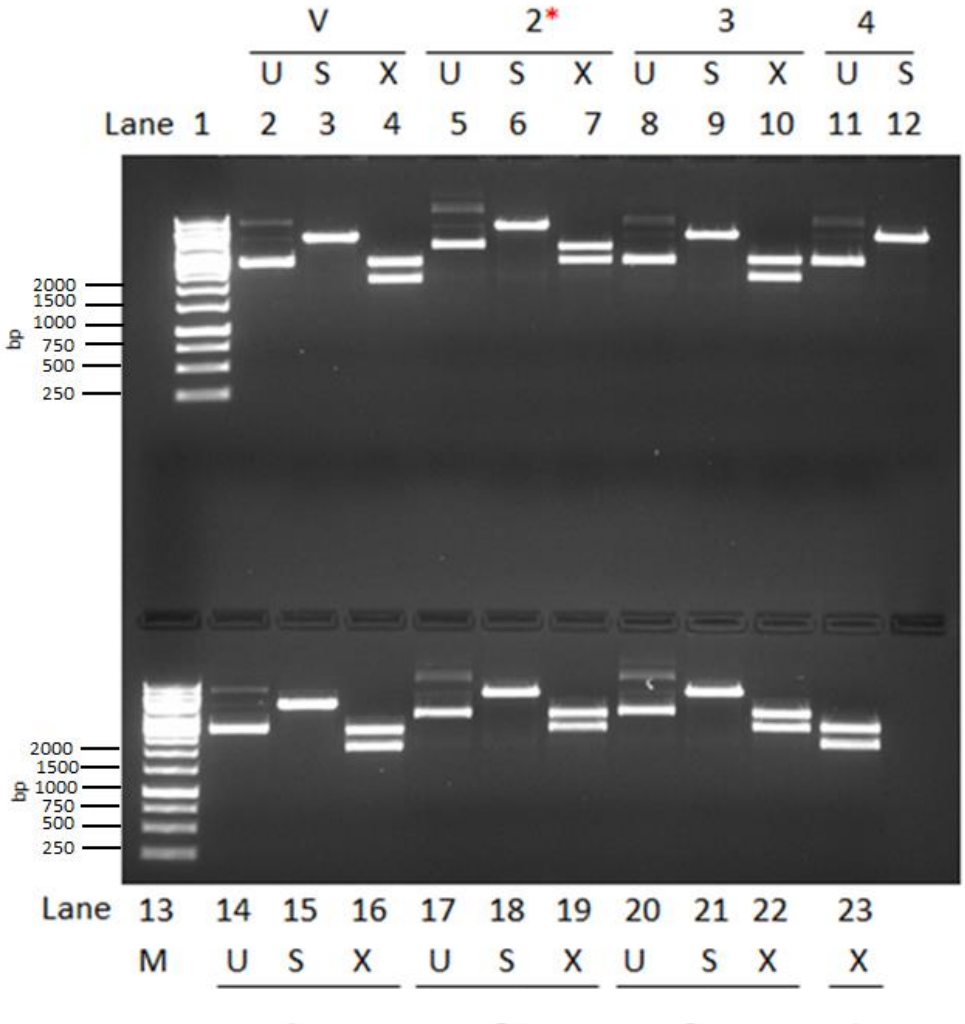

V=Vector, U= Undigested, S= SalI and X= XhoI

Figure 4.4: Positive clone selection for recombinants containing the CAG promoter and β-actin intron + HuPrP 3'UTR+SV40pA

SalI and XhoI enzyme digestion of selected clones. Lanes 1 and 13: GeneRuler 1 kb DNA Ladder (Catalogue number: SM0311, Thermo Fisher Scientific Ltd, Loughborough, UK. Lanes 2-4: Vector DNA undigested (U), SalI digested (S) and XhoI (X) digested respectively. Lanes 5-7: Clone #2 DNA undigested (U), SalI digested (S) and XhoI (X) digested. Lanes 8-10: Clone #3 DNA undigested (U), SalI digested (S) and XhoI (X) digested. Lanes 11, 12 and 23: Clone #4, DNA undigested (U), SalI digested (S) and XhoI (X) digested. Lanes 14-16: Vector DNA undigested (U), SalI digested (S) and XhoI (X) digested. Lanes 17-19: Clone #5, DNA undigested (U), SalI digested (S) and XhoI (X) digested. Lanes 20-22: Clone #6, DNA undigested (U), Sal I digested (S) and XhoI (X) digested. Clones #2 (Lanes 5-7), #5 (Lanes 17-19) and #6 (Lanes 20-22) were identified as positive (indicated with red asterisk).

Part III: Cloning the HuPrP ORF into the pMG5.2 vector containing the CAG promoter and β-actin intron

For the generation of transgenic mice overexpressing HuPrP 163X, the 762bp human PrP open reading frame (ORF) containing the Y163X mutation was amplified from the brain of a patient with the Y163X mutation by PCR with Taq polymerase from the pSP72 vector using forward primer 5'- CTGCAGGTCGAC**GCCACCATGG**CGAACCTTGGCTGCTGGA-3' (40bp) and reverse primer 5'-CCCGGGTCTAGATCATCCCACTATCAGGAAGATG-3' (34bp).

Restriction sites for SalI and XbaI (underlined) were added to the forward and reverse primers, respectively, as they were necessary for subsequent cloning steps. As the PrP gene does not conform to the consensus Kozak sequence (GCCRCCATGG, where R is a purine (A or G)), this was fixed by inserting the correct sequence into the forward primer (bold).

To confirm that the human PrP ORF contained the appropriate mutation, the PCR fragment was then cloned into a SalI-XbaI digested pSP72 vector for sequencing. Sequencing analysis confirmed that the human PrP ORF contained the expected stop codon TAG at position 163 and with valine at codon 129.

Additional restriction sites were inserted using a linker with the following sequence 5'-GATCGCTCGAGG-3' into the pSP72 vectors containing the HuPrP 163X-129V fragment. This was then digested with BamHI and treated with calf-intestinal alkaline phosphatase to remove 5' phosphates in order to prevent plasmid recircularization.

The digested vector was then ligated to the linker and used in a transformation reaction. Positive clones were selected, and clean DNA prepared for the next cloning step. The DNA was digested with SalI/Xho I to isolate the 762-bp HuPrP ORF (with or without) the Y163X mutation.

The SalI digested pMG5.2 vector from Part II (containing the CAG promoter and β-actin intron, HuPrP 3' UTR + SV40pA) was then ligated to the SalI/ XhoI HuPrP ORF fragment from Part III to produce the final vector pCAG-Y163X (Figure 4.5).

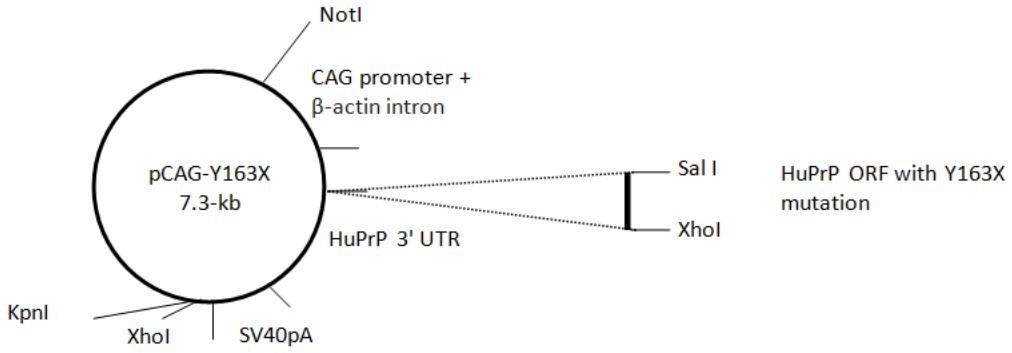

Figure 4.5: Schematic of pCAG-Y163X construct

The pCAG-Y163X construct containing the CAG promoter and β-actin intron + HuPrP 163X ORF+ HuPrP 3'UTR+ SV40pA.

The ligation product was then used to transform competent *E.coli* SCS110 cells and plasmid DNA was purified from 10 clones using the QIAprep Spin Miniprep Kit (Qiagen). After purifying the DNA, restriction digests with SalI and Xho I were used to identify recombinant plasmids containing the HuPrP ORF in the correct orientation. The restriction enzymes Sal I and Xho I have compatible sticky ends and therefore the SalI/ Xho I HuPrP ORF fragment could insert into the plasmid in two different orientations.

The purified plasmid DNA was therefore double digested with NotI and SalI then digested with Xho I only to determine the orientation of the insert. The digestion of positive clones in the right orientation should generate two fragments of 1695bp (CAG promoter and β-actin intron) and 5703bp (HuPrP ORF + HuPrP 3'UTR+SV40 pA+pMG5.2) with NotI and SalI. Clones inserted in reverse orientation should generate two fragments of 2457bp (CAG promoter and β-actin intron+ HuPrP ORF) and 4941bp (HuPrP 3'UTR+SV40 pA+pMG5.2).

Positive clones in the right orientation were further confirmed via digestion with Xho I which should generate two fragments of 4437bp (HuPrP ORF + HuPrP 3'UTR+SV40 pA+ CAG promoter and β-actin intron) and 2961bp (pMG5.2 vector).

Three confirmed positive clones were identified, #7, #8 and #9 (Figure 4.6). Glycerol stocks were made of clones #7 and #8 and plasmid DNA was prepared from clone #7 using the Hi Speed Plasmid Maxi Kit (Qiagen).

The plasmid DNA was then digested with Xho I to isolate the 4437-bp transgene construct (Figure 4.7A-B). The reaction was electrophoresed on a 1% agarose gel and the DNA fragment containing the construct was excised and recovered using the Zymoclean™ Gel DNA Recovery Kit (Zymo Research).

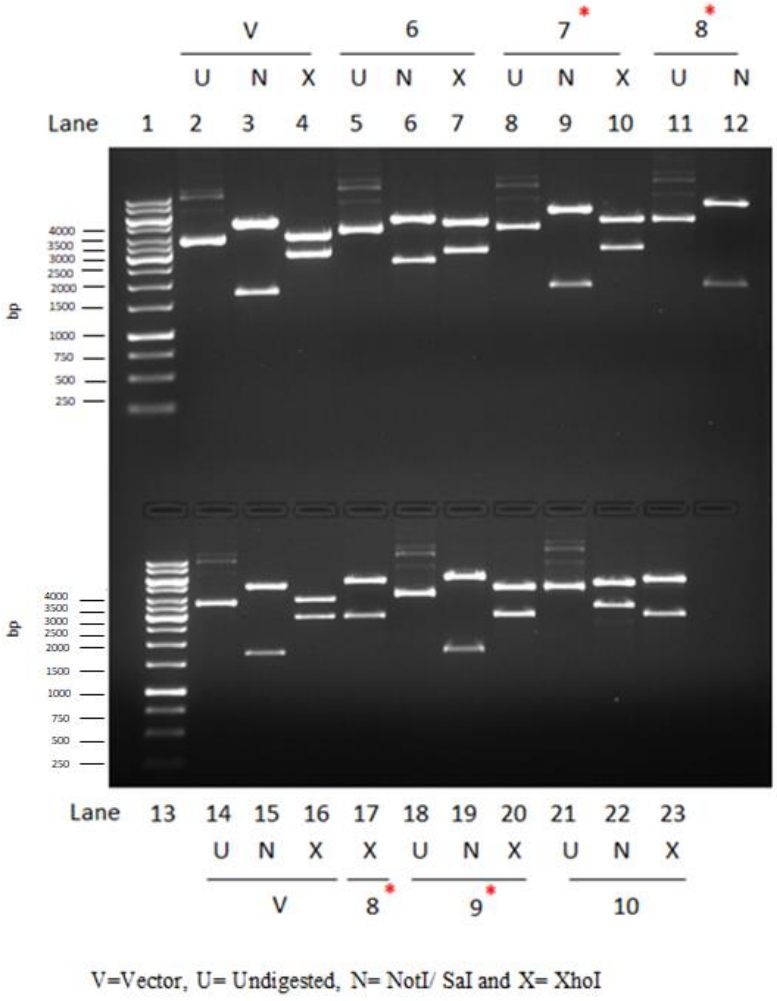

Figure 4.6: Positive clone selection for recombinants containing the CAG promoter and β-actin intron + HuPrP ORF+HuPrP 3'UTR+SV40 pA

NotI/SalI and XhoI enzyme digestion of selected clones. Lanes 1 and 13: GeneRuler 1 kb DNA Ladder (Catalogue number: SM0311, Thermo Fisher Scientific Ltd, Loughborough, UK. Lanes 2-4: Vector DNA undigested (U), NotI/SalI digested (N) and XhoI digested respectively. Lanes 5-7: Clone #6 DNA undigested (U), Not I/SalI digested (N) and XhoI digested (X). Lanes 8-10: Clone #7 DNA undigested (U), Not I/SalI digested (N) and XhoI digested. Lanes 11-12: Clone #8 DNA undigested (U), NotI/SalI digested (N) and XhoI digested. Lanes 14-16: Vector DNA undigested (U), NotI/SalI digested (N) and XhoI digested. Lane 18-20: Clone #9 DNA undigested (U), NotI/SalI digested (N) and XhoI digested. Lane 21-23: Clone #10 DNA undigested (U), NotI/SalI digested (N) and XhoI digested. Clones #7 (Lanes 8-10), #8 (Lanes 11, 12 and 17) and #9 (Lanes 18-20) were identified as positive (indicated with red asterisk).

A

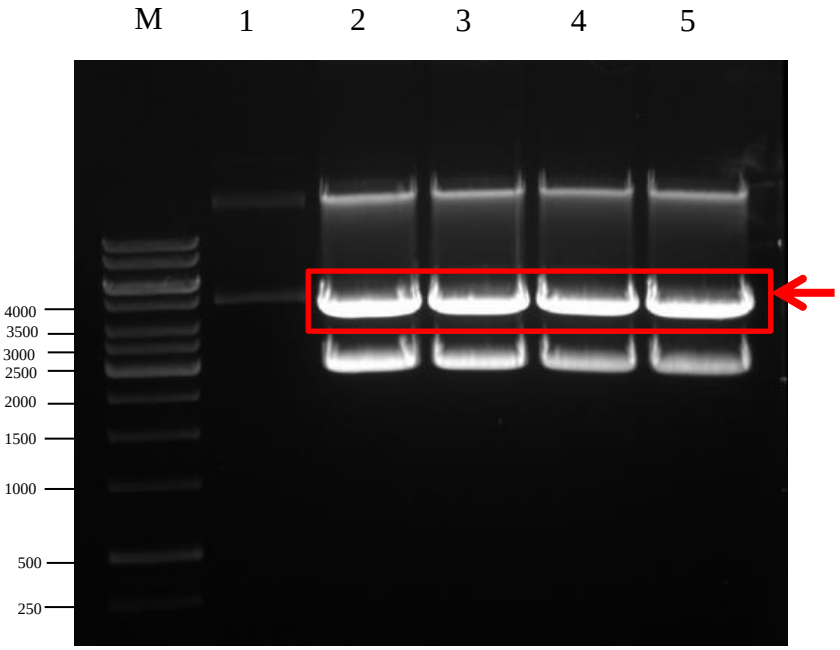

B

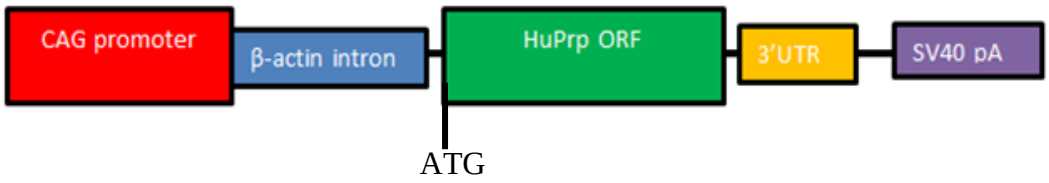

Figure 4.7: XhoI digestion of pCAG-Y163X to isolate 4437bp transgene construct

(A) Lane 1. Uncut pCAG-Y163X. Lanes 2-5 – Xho I pCAG-Y163X (red arrow pointing to 4437bp transgene construct).

(B) Schematic of the 4437bp transgene construct.

*M= GeneRuler 1 kb DNA Ladder (Catalogue number: SM0311, Thermo Fisher Scientific Ltd, Loughborough, UK.

Construct design for transgenic mice overexpressing HuPrP WT-129V

pCAG-WT129V (Figure 4.8) was constructed in exactly the same way as pCAG-Y163X.

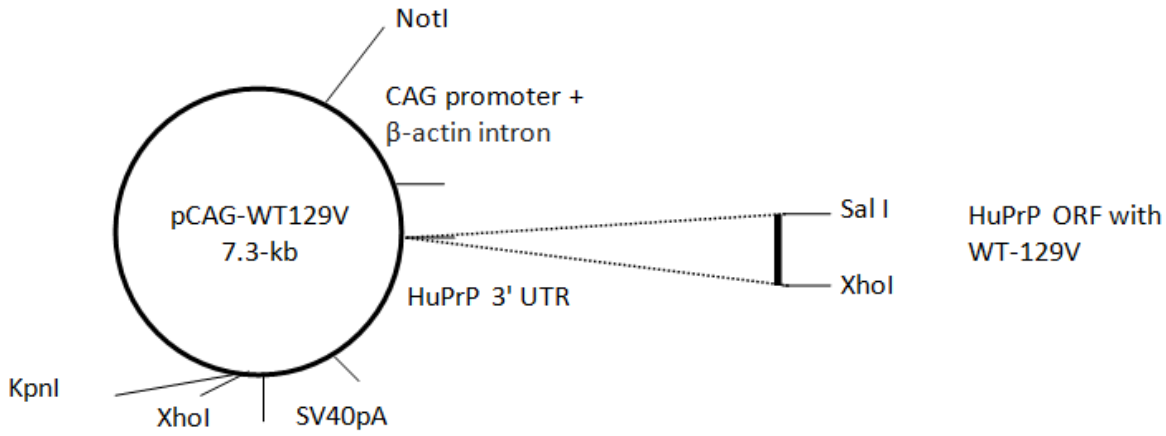

Figure 4.8: Schematic of pCAG-WT-129V construct

The pCAG-WT-129V construct containing the CAG promoter and β-actin intron + HuPrP 129V ORF+ HuPrP 3'UTR+ SV40pA.

4.2 Microinjection of transgene into mouse zygotes

The concentration of the transgene DNA was determined by a *NanoDrop* Spectrophotometer (Thermo Fisher Scientific Ltd, Loughborough, UK) and DNA quality and concentration was further assessed by running a 2ul aliquot of the transgene DNA on a 1% agarose gel. The purified transgene DNA was then diluted to 1ng/ µl in TE buffer ready for microinjection. The Y163X and WT-129V transgenes were microinjected into F10_FVB/PrP-null single cell embryos. F10_FVB/PrP-null single cell embryos were selected to ensure that mouse PrP was not present to interfere with the biology of human PrP. The embryos were cultured to the two-cell stage and surgically transferred into pseudo-pregnant recipient female mice. All microinjections were performed by Andrew Tomlinson (MRC Prion Unit, UCL, UK).

4.3 Genotyping of pCAG transgenic lines

Ear biopsies were collected and used to genotype the putative transgenic mice. Transgenic founders were identified using two separate sets of PCR conditions: Human_Mouse_Neo PCR and CAG specific PCR.

Human_Mouse_Neo PCR

The human, mouse, neo PCR is a multiplex PCR that uses 3 primer pairs to amplify 3 different target sequences. Primers Hu1 and Hu2 amplify a sequence in the HuPrP ORF to produce a 400bp PCR product (Figures 4.8 and 4.9).

Primers P10 and P315 amplify a WT mouse PrP sequence to produce a 500bp product and P3 and P315 amplify a junction fragment between the neo sequence and WT mouse PrP sequence found in F10_FVB/PrP null mice to produce a 270bp product (Figures 4.9 and 4.10).

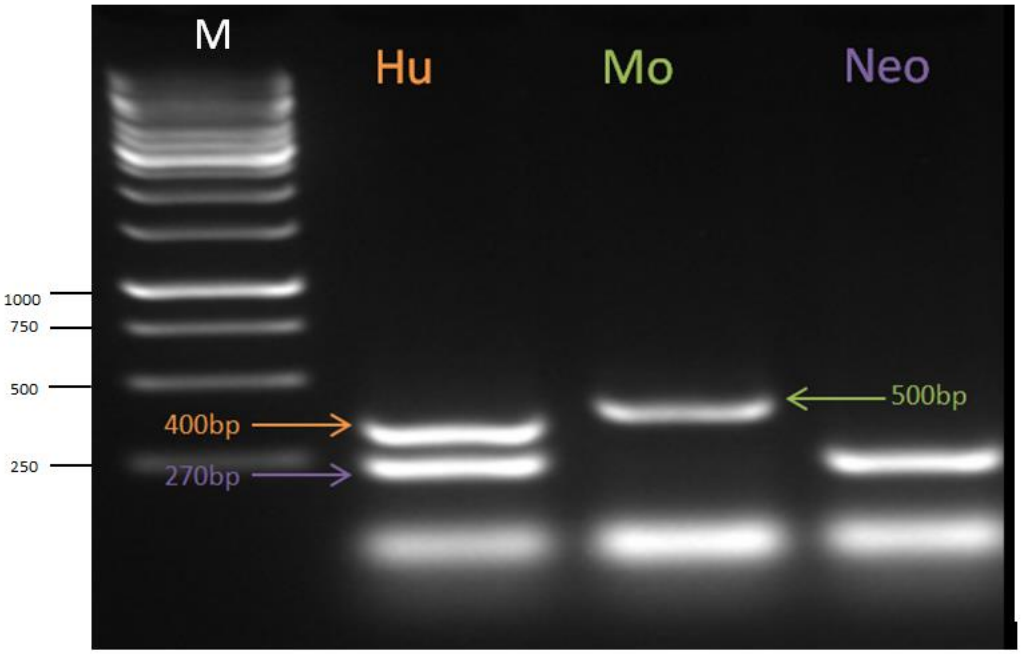

Figure 4.9: Human_Mouse_Neo PCR products

*M= GeneRuler 1 kb DNA Ladder (Catalogue number: SM0311, Thermo Fisher Scientific Ltd, Loughborough, UK.

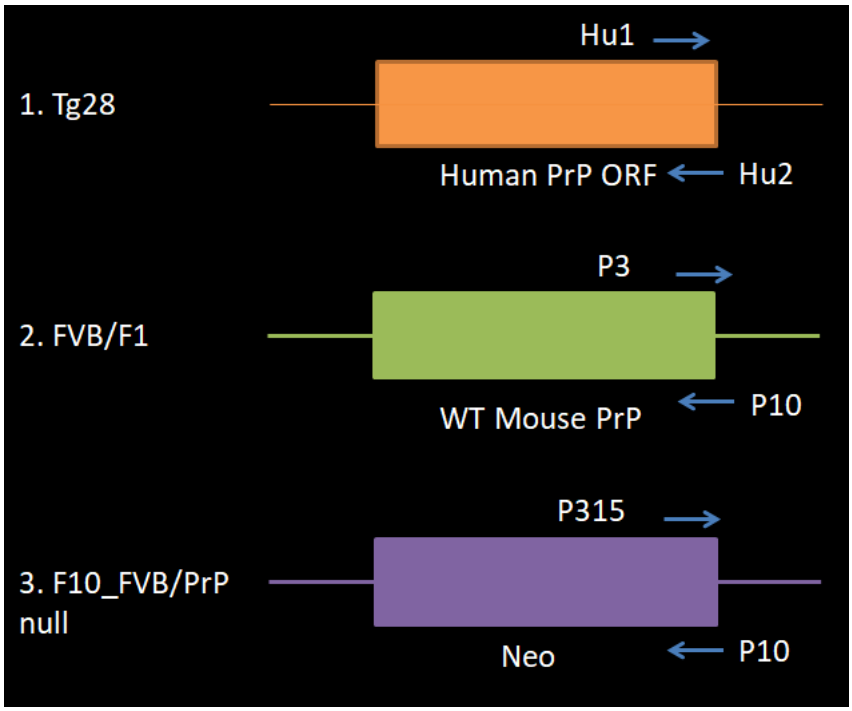

Figure 4.10: Controls used for Human_ Mouse_ Neo PCR

Controls for Human_Mouse_Neo PCR: 1. Genomic DNA from Tg (HuPrP-129MM)28 (Tg28) mice was used as a positive control for the human prion protein band as this line expresses HuPrP at endogenous level and was made on a F10_FVB/PrP null background. 2. Genomic DNA from FVB/N and C57xCBA (abbreviated to F1) mice was used as a positive control for the mouse band. 3. Genomic DNA from F10_FVB/PrP null mice was used as a positive control for this band for the presence of the null allele.

The two expected bands for mice positive for the transgene are the 400bp fragment that contains a sequence from the human PrP ORF and the 270bp fragment that contains a neo sequence (Figure 4.11).

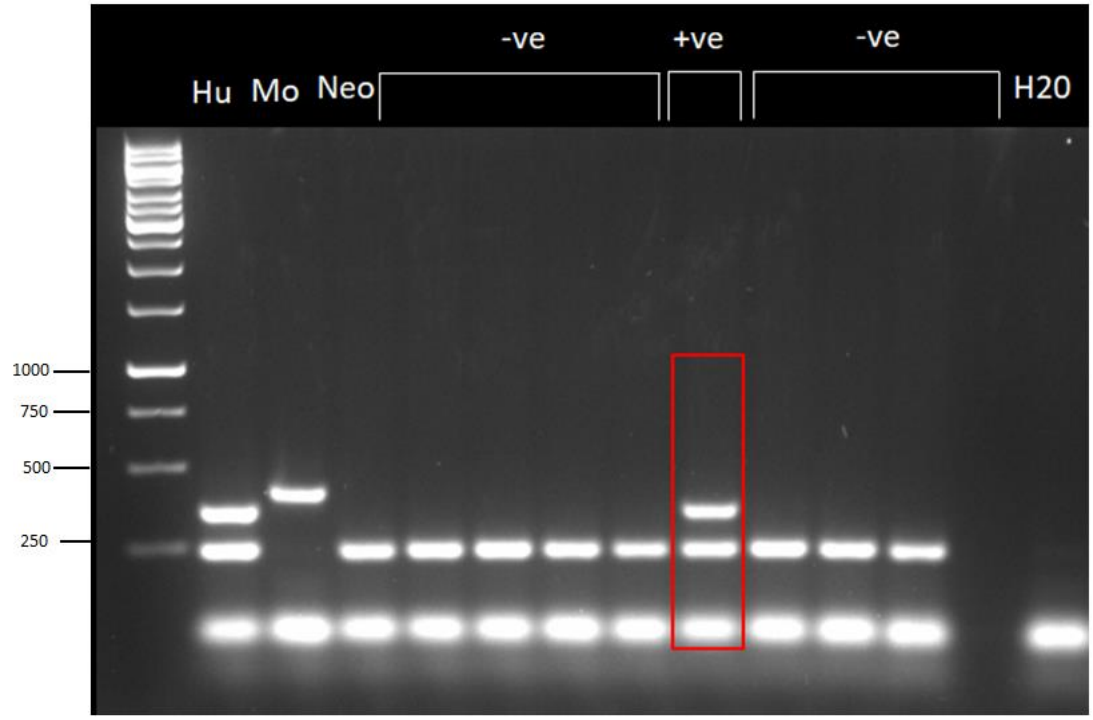

Figure 4.11: Identification of pCAG-WT-129V positive mouse using Hu_M_Neo PCR

The transgene positive founder (used to establish Tg374 line) was identified using the Hu_M_Neo PCR. This founder was distinguishable from the negative littermates by the presence of the 400bp and 270bp fragments, with the latter being the neomycin band that is common to all the mice because they were made on the *prnp*-null background.

CAG specific PCR

The CAG specific PCR primers amplify a junction fragment between the β-actin intron and the HuPrP ORF. Primers CAG_SN3 and CAG_ASN3 (Table 2.2) amplify a 167bp fragment (Figures 4.12 and 4.13).

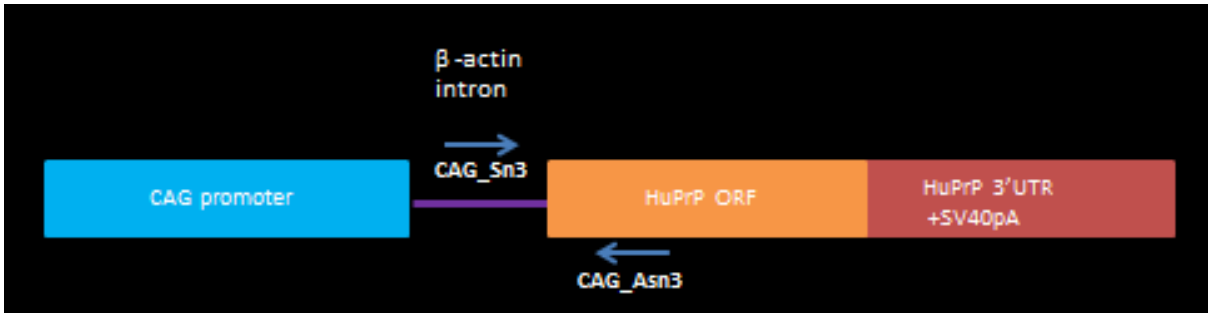

Figure 4.12: Map of CAG specific PCR primers

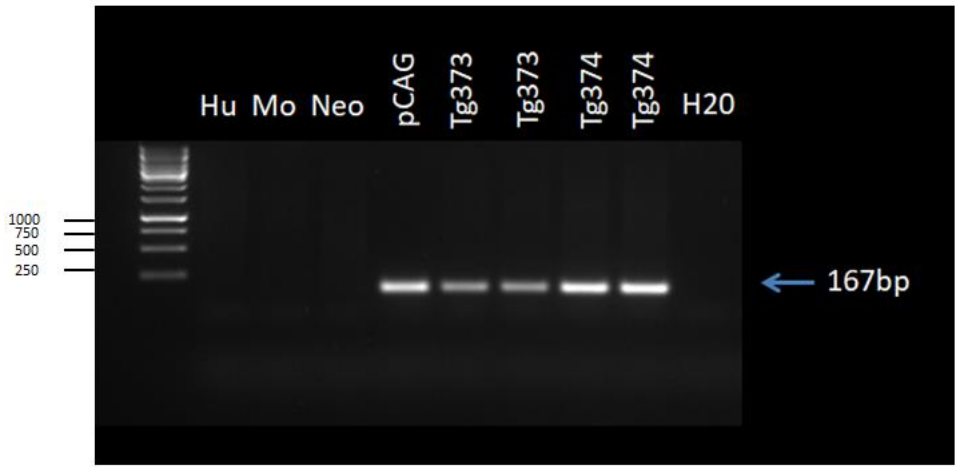

Figure 4.13: Identification of pCAG-WT-129V positive mouse using the CAG specific PCR.

pCAG-WT129V founders were identified by the presence of a 167bp fragment. Plasmid DNA (pCAG) was used as a positive control for this PCR assay. DNA extracted from the ear biopsies of Tg28 (Hu), F1 (Mo) and F10_FVB/PrP null (Neo) mice were used as negative controls.

Transgenic lines expressing human PrP 163X and WT-129V

Ten transgenic founders were produced following several rounds of successful microinjection sessions (Table 4.1), and the mice were bred to F10_FVB/PrP null mice to establish independent mouse lines.

Table 4.1 Established Y163X and WT-129V transgenic mouse lines

Tg Line	Construct
Tg373	WT-129V
Tg374	WT-129V
Tg379	WT-129V
Tg380	WT-129V
Tg375	Y163X-129V
Tg376	Y163X-129V
Tg377	Y163X-129V
Tg378	Y163X-129V
Tg381	Y163X-129V
Tg382	Y163X-129V

4.4 Establishment of homozygous pCAG transgenic lines for long-term observation

Heterozygous breeding pairs were set up to establish homozygous transgenic lines for long-term observation. It is the practice of the Transgenic Group to routinely keep one line that overexpresses at a high level and a second line that expresses the transgene at endogenous level. In prion biology overexpression can lead to shorter incubation periods, but in some cases artefacts of overexpression may be observed. However, in view of the fact that this study was adversely affected by the prolonged Covid-19 lockdown, we had to choose the lines that bred most efficiently and breed these to homozygosity. Therefore, expression of HuPrP mRNA was confirmed in the brain and spleen of all the transgenic lines that were generated (data not shown). Two pCAG-Y163X-129V (Tg375 and Tg377) and two pCAG-WT129V lines (Tg373 and Tg380) which were further advanced in the breeding process were selected for completing this study.

The practice of keeping at least two lines per transgene construct (high and low expressors) allows any potential effect of overexpression and/or position effects to be considered largely insignificant when the result are similar in both lines with different integration sites. Diverse results between any two lines expressing the same transgene construct may be ascribed to potential position effects.

Homozygous lines have been established for:

1) Tg375 and Tg377 (pCAG-Y163X-129V)

2) Tg373 and Tg380 (pCAG-WT-129V) controls

The litters were screened using TaqMan qPCR assays to identify homozygous mice and then breeding pairs were set up with homozygotes to establish lines for long-term observation experiments. Homozygous mating trios were set up for Tg380 and Tg377 and two homozygous pairs were set up for Tg375. The Tg373 could not be bred to homozygosity despite repeated attempts; therefore a decision has been made to maintain this line as a heterozygous line.

Long term observation experiments will be set up to age homozygous and heterozygous pCAG-Y163X-129V and control pCAG-WT-129V mice for the possible development of spontaneous PrP deposition, once homozygous lines have been established for the pCAG transgenics mentioned above. The experimental design will be exactly the same as experiments 321 and 328 (described in Chapters 3.4 and 3.5).

In summary, ten pCAG transgenic lines (Y163X-129V (6) and WT-129V (4) control lines have been successfully generated (described in Chapter 4.3).

These lines took slightly longer to breed to homozygosity therefore long-term observation experiments could not be set up within the duration of this project. However, colony expansion is ongoing in order to produce mouse cohorts for experiments.

5. Chapter 5: Generation of HuPrP 163X CRISPR/Cas9 mouse models

This chapter will address the methods used to generate and characterise HuPrP CRISPR/Cas9 knock-in mouse models.

Easi-CRISPR (Efficient additions with ssDNA inserts-CRISPR) was used to generate a HuPrP Y163X knock-in model. This method was chosen due to promising data that demonstrated the efficient generation of knock-in models using long ssDNA donors (Quadros et al., 2017) . The time to generate knock-in mice using this approach is also shorter as the EASI-CRISPR components (crRNA + tracrRNA + Cas9 ribonucleoprotein) can be microinjected directly into single-cell mouse embryos.

5.1 Subcloning of EcoRI/BamHI Mo-Hu-Mo PrP gene fragment into pSP72 vector

The dsDNA template containing the Human *PRNP* open reading frame with theY163X mutation was synthesised by Integrated DNA Technologies (IDT, Iowa, USA) (Figure 5.1).

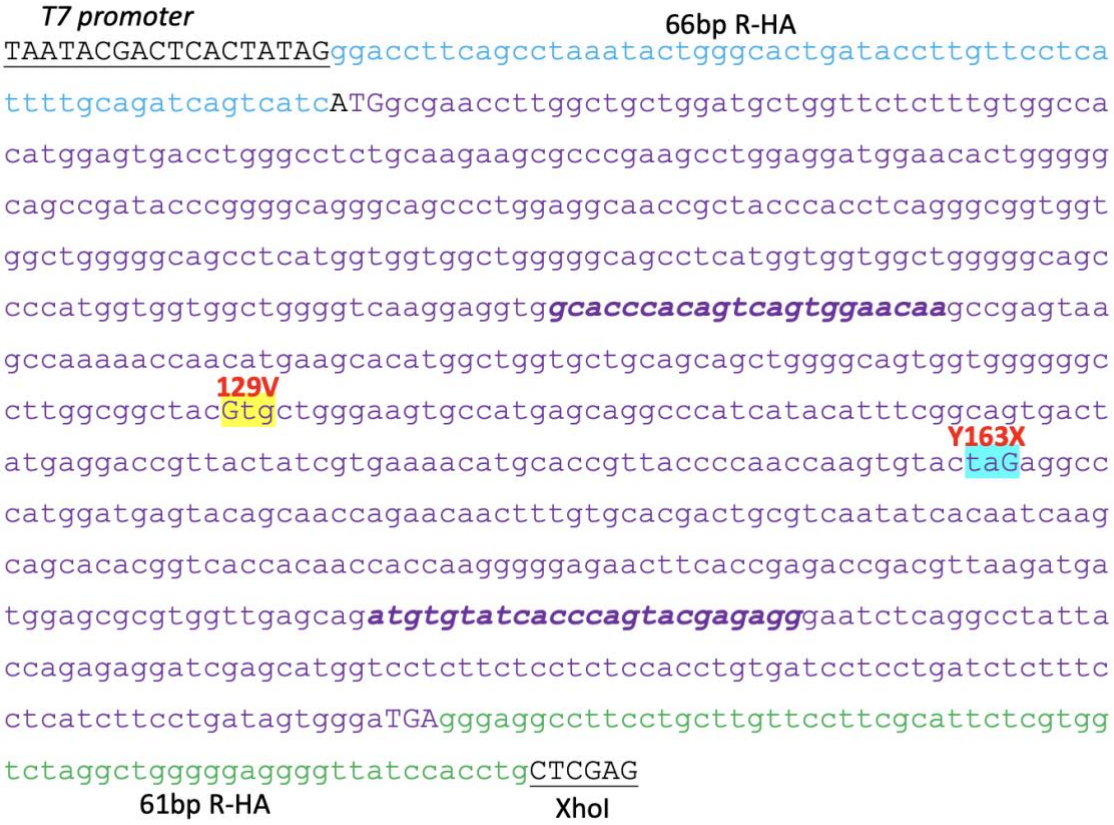

Figure 5.1: Synthesis of 889 bp Mo-Hu-Mo PrP dsDNA template by Integrated DNA Technologies

The dsDNA template, designated Mouse-Human-Mouse (Mo-Hu-Mo) consisted of the T7 promoter, the human *PRNP* open reading frame encoding valine at codon 129 and a stop codon at residue 163. The human *PRNP* open reading frame was flanked on the left and right respectively by 61-and 66- base pair homology arms directed to the mouse *Prnp* sequence. An additional Xho I restriction site was inserted for linearising the plasmid prior to *in vitro* transcription.

The T7 promoter was removed from the sequence prior to gene synthesis due to the manufacturer's concerns about the pathogenicity of the human prion protein gene. Therefore, the synthesised gene fragment had to be subcloned into a pSP72 vector as a BamHI/EcoRI fragment to allow the use of the T7 promoter in the pSP72 vector for RNA synthesis.

The gene fragment containing the wild-type human *PRNP* open reading frame encoding valine at codon 129 was prepared in exactly the same way as the Y163X fragment.

The pSP72 vector and Mouse-Human-Mouse PrP gene fragment containing the Y163X mutation were double digested with BamHI and EcoRI (Figure 5.2) and ligated together, following isolation and purification of the Mo-Hu_Mo fragment.

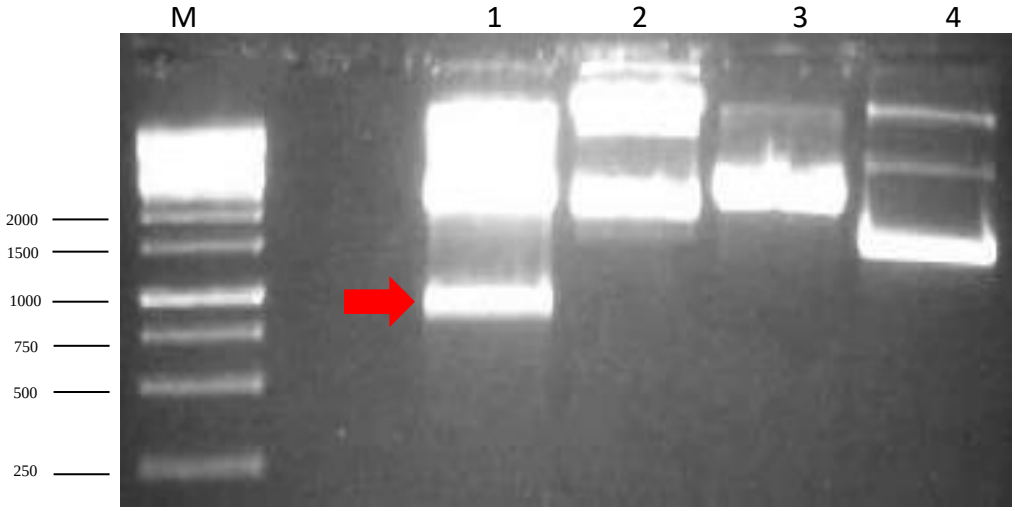

Figure 5.2: BamHI and EcoRI digestion of pSP72 vector and Y163X gene fragment

Lane M: 1 kb DNA Ladder. Lane 1: BamHI/ EcoRI digestion of Y163X construct showing isolation of the 889-bp Mo-Hu-Mo fragment (arrowed). Lane 2: Uncut Y163X construct. Lane 3: BamHI/ EcoRI digestion of pSP72 vector. Lane 4: Uncut pSP72 vector.

*M= GeneRuler 1 kb DNA Ladder (Catalogue number: SM0311, Thermo Fisher Scientific Ltd, Loughborough, UK.

Competent *E.coli* SCS110 cells were then transformed with the ligation mixture and plasmid DNA was purified from 6x Y163X-129V clones and 16x WT-129V clones. After purifying the DNA, restriction digests with EcoRI and BamHI were used to identify recombinant plasmids containing the HuPrP ORF. The double digestion of positive clones with EcoRI and BamHI should generate two fragments: 2462bp (pSP72 vector) and 889bp (HuPrP ORF containing either Y163X-129V or WT129V).

Two positive clones were identified for Y163X-129V (#1 and 2) and eleven positive clones were identified for WT-129V (#1-11). Glycerol stocks were made of clones #1 and 2 for Y163X-129V then clones # 6 and # 7 for WT-129V. Plasmid DNA was prepared from clones #1(Y163X) and # 6 (WT129V) using the Hi Speed Plasmid Maxi Kit (Qiagen, Hilden, Germany). The maxiprep DNA was then digested with EcoRI, BamHI, EcoRI/BamHI and XbaI to confirm that the clones contained the correct insert (Figure 5.3).

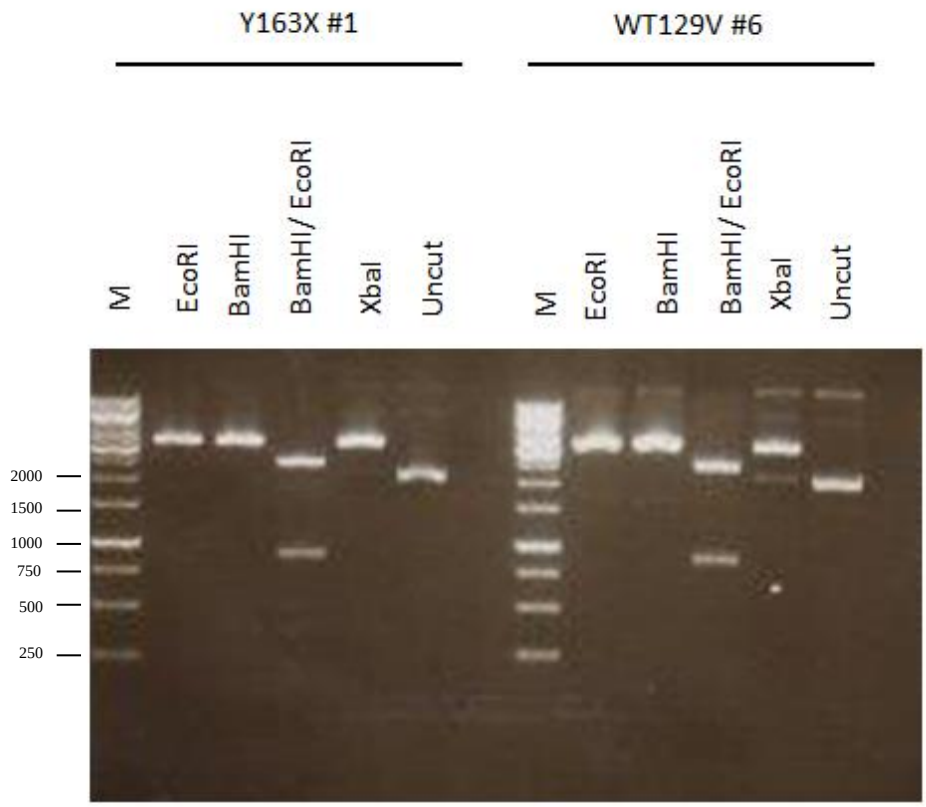

Figure 5.3: Restriction enzyme digestion of recombinant plasmids containing either the Y163X-129V or WT129V human PrP open reading frame

BamHI, EcoRI, EcoRI/BamHI and XbaI digestion of selected clones. Lane M: 1 kb DNA Ladder. Single digestion of the recombinant plasmids containing the either Y163X-129V or WT-129V human PrP ORF with EcoRI, BamHI or Xbal produced a 3351 bp fragment (pSP72+ Y163X-129V or WT-129V human PrP ORF). Whereas, double digestion generated two fragments: (1) 2462 bp (pSP72) (2) 889 bp (Y163X or WT129V human PrP ORF).

The plasmid DNA was then linearised with BamHI (Figure 5.4) prior to the *in vitro* transcription reaction.

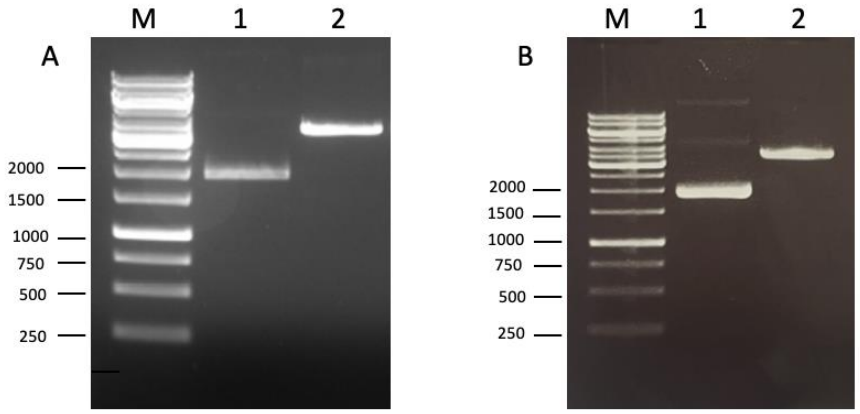

Figure 5.4: Linearisation of pSP72 vector containing Y163X-129V or WT-129V gene fragment

A: Linearisation of pSP72 vector containing Y163X-129V with BamHI. Lane M: 1 kb DNA Ladder. Lane 1: Uncut pSP72-Y163X. Lane 2: BamHI digested pSP72-Y163X.

B: Linearisation of pSP72 vector containing WT129V with BamHI. Lane M: 1 kb DNA Ladder. Lane 1: Uncut pSP72-WT-129V Lane 2: BamHI digested pSP72-WT-129V.

5.2 ssDNA synthesis by *iv*TRT

The linearised plasmid DNA was used as a template for the *in vitro* transcription reaction (Figure 5.5).

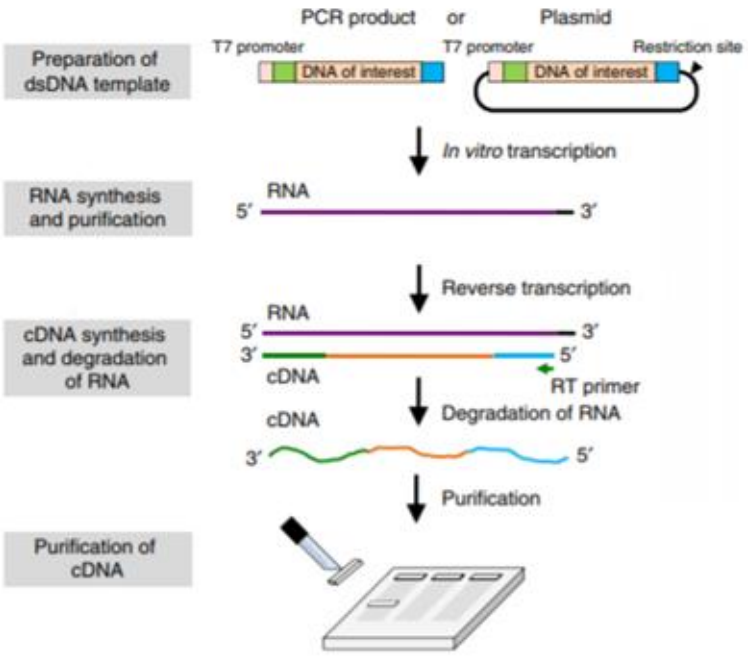

Figure 5.5: Overview of ivTRT reaction (Adapted from (Miura *et al.*, 2018)

A. A PCR product or plasmid digested with a suitable restriction enzyme can be used as a template for RNA synthesis.
B. The dsDNA template is then used to synthesise RNA by *in vitro* transcription.
C. The RNA is used as a template for cDNA synthesis using reverse transcription.
D. RNA in the hybrid is degraded with RNase-H, then the ssDNA is purified using a gel extraction kit or by ethanol precipitation before microinjection.

RNA was synthesised according to manufacturer's instructions using the mMESSAGE mMACHINE T7 Ultra Kit (Ambion, Texas, USA). The RNA was then purified using the MEGA clear Kit (Ambion, Texas, USA) and run on a 1% agarose gel to assess the quality of the RNA (Figure 5.6).

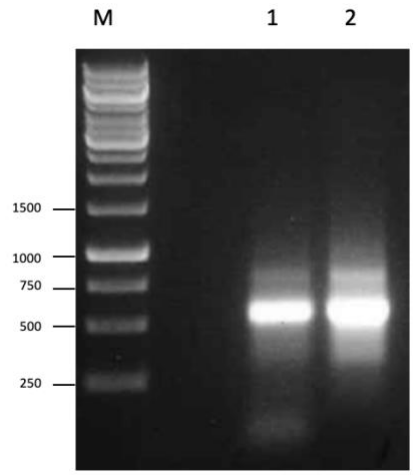

Figure 5.6: Y163X-129V or WT-129V RNA

Agarose gel electrophoresis of purified Y163X-129V or WT-129V RNA from *iv*TRT reaction. Lane M: 1 kb DNA Ladder. Lane 1: Y163X-129V RNA. Lane 2: WT-129V RNA

The purified RNA was used as a template for ssDNA synthesis with the SuperScript™ VILO™ cDNA Synthesis Kit (Invitrogen, Massachusetts, USA). The ssDNA was purified by ethanol precipitation following the reverse transcription reaction.

5.3 Preparation of Easi-CRISPR components for microinjection

The Alt-R CRISPR/Cas9 system from IDT (Iowa, USA) consists of two CRISPR RNA components, CRISPR RNA (crRNA) (medium modified) and trans-activating CRISPR RNA (tracrRNA). These two RNAs were annealed at a 1:1 molar concentration to generate active single guide RNA (sgRNA). The active sgRNA complex was then incubated with Alt-R *Streptococcus pyogenes* Cas9 Nuclease 3NLS (IDT, Iowa, USA) to generate the ctRNP (crRNA + tracrRNA + Cas9 Protein) complex. The ctRNP complex was then mixed with the ssDNA donor (at a final concentration of 20 ng) prior to microinjection of the CRISPR components. The Easi-CRISPR components (ctRNP+ ssDNA donor) were then filtered and microinjected into FVB/N single cell embryos (Figure 5.7). The Easi-CRISPR microinjection mix was run on a 1% agarose gel to check for degradation as ssDNA is less stable compared to dsDNA. All microinjections were performed by Andrew Tomlinson (MRC Prion Unit, UCL, UK).

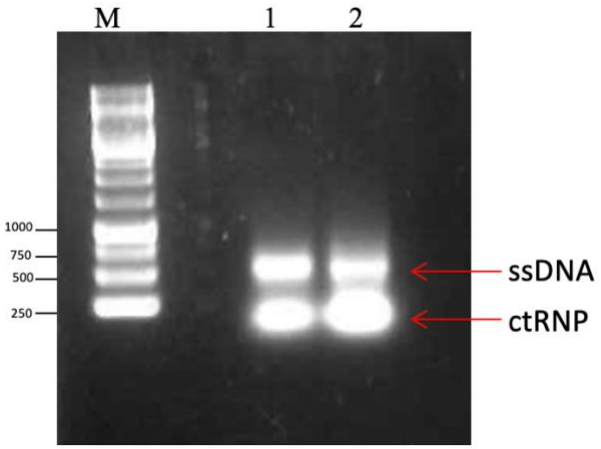

Figure 5.7 Agarose gel electrophoresis of Easi-CRISPR microinjection mix before and after microinjection showing no degradation of the CRISPR components.

Lane M: 1 kb DNA Ladder. Lane 1: ctRNP+Y163X-129V ssDNA donor before microinjection. Lane 2: ctRNP+Y163X-129V ssDNA donor after microinjection.

5.4 CRISPR/Cas9 knock-in lines expressing human PrP 163X and WT129V

Screening for CRISPR HuPrP knock-in positives using the Human PrP specific PCR assay

The human PrP specific PCR assay uses primers Hu1 and Hu2 to amplify a sequence in the HuPrP ORF to produce a 400bp PCR product.

Nine CRISPR/Cas9 knock-in positives were identified in total using the HuPrP ORF PCR assay (Figure 5.8)

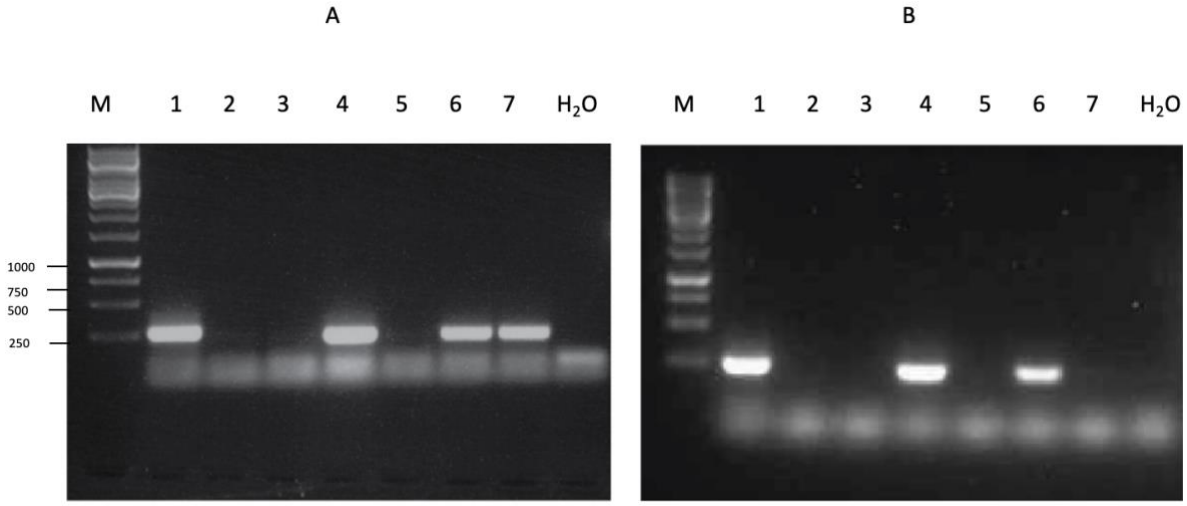

Figure 5.8: Identification of CRISPR/Cas9 knock-in positives using the Human PrP specific PCR assay

Figure A: 3/4 CRISPR -Y163X-129V positives (lanes #4, #6 & #7) identified by PCR screening for the human PrP ORF. Lane M: Marker. Lane 1: Genomic DNA from Tg(HuPrP-129MM) 28 (Tg28) mice was used as a positive control for the human prion DNA band. Lane 2: Genomic DNA from FVB/N mice was used as a negative control.

Figure B: 2/5 CRISPR –WT-129V positives (lanes #4 & #6) identified by PCR screening for the wild type human PrP ORF. Lane M: Marker. Lane 1: Genomic DNA from Tg (HuPrP-129MM) 28 (Tg28) mice was used as a positive control for the human prion DNA band. Lane 2: Genomic DNA from FVB/N mice was used as a negative control.

The CRISPR Knock-in founders were then crossed with F10_FVB/PrP-null mice to establish independent mouse lines (Table 5.1). The rationale for crossing with PrP-null mice was to avoid re-introduction of endogenous mouse PrP gene.

Table 5.1 CRISPR Y163X and WT129V Knock-in lines

KI Line	Construct
Tg354	Hu PrP Y163X-129V
Tg357	Hu PrP Y163X-129V
Tg361	Hu PrP WT-129V
Tg362	Hu PrP WT-129V

Most of the knock-in founders did not transmit the recombinant allele to their offspring when mated to F10_FVB/PrP-null mice. Only 2/4 CRIPSR-Y163X-129V (Tg354 and Tg357) and 2/5 CRISPR-WT-129V (Tg361 and Tg362) founders transmitted to their offspring. These four lines were selected for sequencing to determine if the desired genetic modification had been made. Mice with the correct genetic modification should be negative for the mouse prp gene and positive for the human PrP, as well as the neomycin resistance gene which derives from the crossing of founders to F10_FVB/PrP-null mice containing the neomycin resistance cassette.

Primers Sn2 and Asn3 were used to screen the offspring of the CRISPR knock-in founders (Figure 5.9A-C). This primer pair amplifies a 1114 bp fragment in FVB/N and Tg(HuPrP)28 controls, and in CRISPR knock-in founders with perfect genetic modifications. However, this primer pair may amplify different sized products in the CRISPR knock-in founders, in which genetic modifications such as deletions may have occurred. Once a knock-out mouse was found based on the failure of Sn2 and Asn3 to amplify the predicted 1114bp product, primers KO-Sn2 and KO-Asn6 were designed to specifically amplify a 1256-bp sequence in the CRISPR knockout line which was then designated as KO-1, with over 2400-bp of the MoPrP sequence deleted.

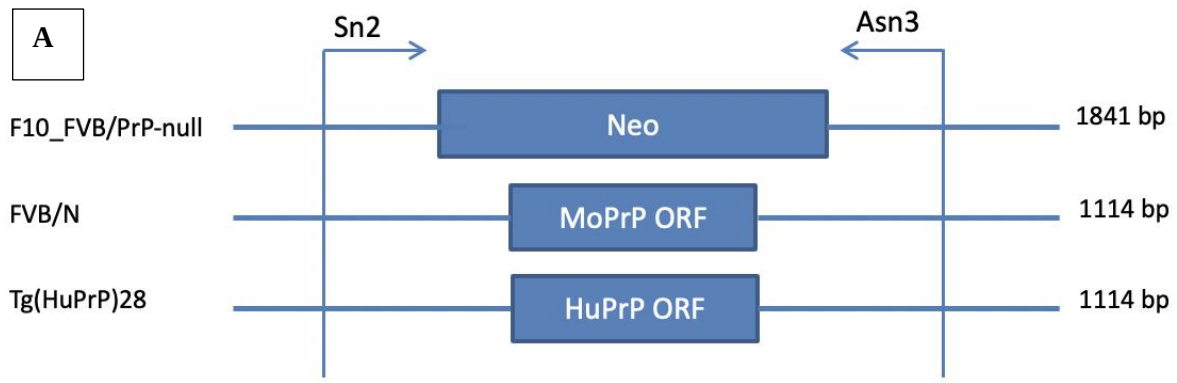

Figure 5.9: Screening of CRISPR offspring with Sn2 and Asn3

A) Primers Sn2 and Asn3 amplify a sequence in the neomycin cassette in F10_FVB/PrP-null mice to produce a 1841 bp band. Whereas, a 1114-bp sequence is amplified in the PrP ORF in FVB/N and Tg28 mice as the size of the PrP ORF is the same in mouse and human PrP.

B

MoPrP sequence

CCGTCCTGTTTCAGCCTCTACTTCCCAAGTGCTGGGGCACCAACGTGCACTTCCTCATGCCTGGCTCTGGAGACC

TACTGCTTGTCTCCAGGGCTCAAACACTGAGTCAGCTTTCTTCAAGTCCTTGCTCCTGCTGTAGCCACTCAGGAG

CCCTCCTGACTAGACCATGACTCAGGCCCTTGTGGTGTTACGGTTACTCAGGACCAGTGTACTCACAGCTACCCC

TGCAGGTGACTTTCTGCATTCTGGGGAATGAAGCCTACATCCGTGGATAAAGGTTCTCCTCTGTGTAGAGGCTCA

CACCCCACAGGACCCTGGGGCCATTATAGCAGCCTTATAGTACAGCTGCCAGGCTCCCCACAAGATCATGCCCAT

TTCCAAATTCCACTACATTGTTAAAGCTCAAAGCCATGGCGTAACAACCATGCAATATCACCTAGACCAGACGTG

Sn2

GTTTACCAGTTGGGGTAACTCTTGTCAAATCTGTCCTCAGAGGATGGGATGAGCTGTGTGTTTTTGATTTACTTT

TTTCCTGAAGGAAAAGCTACGGGGGGGGGGGGGGCGGGGGGGAGGGTTGACGCCATGACTTTCATACATTTGCTT

TGTAGATAGATGTCAAGGACCTTCAGCCTAAATACTGGGCACTGATACCTTGTTCCTCATTTTGCAGATCAGTCA

TCATGGCGAACCTTGGCTACTGGCTGCTGGCCCTCTTTGTGACTATGTGGACTGATGTCGGCCTCTGCAAAAAGC

GGCCAAAGCCTGGAGGGTGGAACACCGGTGGAAGCCGGTATCCCGGGCAGGGAAGCCCTGGAGGCAACCGTTACC

CACCTCAGGGTGGCACCTGGGGGCAGCCCCACGGTGGTGGCTGGGGACAACCCCATGGGGGCAGCTGGGGACAAC

CTCATGGTGGTAGTTGGGGTCAGCCCCATGGCGGTGGATGGGGCCAAGGAGGGGGTACCCATAATCAGTGGAACA

AGCCCAGCAAACCAAAAACCAACCTCAAGCATGTGGCAGGGGCTGCGGCAGCTGGGGCAGTAGTGGGGGGCCTTG

GTGGCTACATGCTGGGGAGCGCCATGAGCAGGCCCATGATCCATTTTGGCAACGACTGGGAGGACCGCTACTACC

GTGAAAACATGTACCGCTACCCTAACCAAGTGTACTACAGGCCAGTGGATCAGTACAGCAACCAGAACAACTTCG

TGCACGACTGCGTCAATATCACCATCAAGCAGCACACGGTCACCACCACCACCAAGGGGGAGAACTTCACCGAGA

CCGATGTGAAGATGATGGAGCGCGTGGTGGAGCAGATGTGCGTCACCCAGTACCAGAAGGAGTCCCAGGCCTATT

ACGACGGGAGAAGATCCAGCAGCACCGTGCTTTTCTCCTCCCCTCCTGTCATCCTCCTCATCTCCTTCCTCATCT

TCCTGATCGTGGGATGAGGGAGGCCTTCCTGCTTGTTCCTTCGCATTCTCGTGGTCTAGGCTGGGGGAGGGGTTA

TCCACCTGTAGCTCTTTCAATTGAGGTGGTTCTCATTCTTGCTTCTCTGTGTCCCCCATAGGCTAATACCCCTGG

Asn3

CACTGATGGGCCCTGGGAAATGTACAGTAGACCAGTTGCTCTTTGCTTCAGGTCCCTTTGATGGAGTCTGTCATC

AGCCAGTGCTAACACCGGGCCAATAAGAATATAACACCAAATAACTGCTGGCTAGTTGGGGCTTTGTTTTGGTCT

AGTGAATAAATACTGGTGTATCCCCTGACTTGTACCCAGAGTACAAGGTGACAGTGACACATGTAACTTAGCATA

GGCAAAGGGTTCTACAACCAAAGAAGCCACTGTTTGGGGATGGCGCCCTGGAAAACAGCCTCCCACCTGGGATAG

CTAGAGCATCCACACGTGGAATTCTTTCTTTACTAACAAACGATAGCTGATTGAAGGCAACAGGAAAAAAAAAAT

CAAATTGTCCTACTGACGTTGAAAGCAAACCTTTGTTCATTCCCAGGGCACTAGAATGATCTTTAGCCTTGCTTG

GATTGAACTAGGAGATCTTGACTCTGAGGAGAGCCAGCCCTGTAAAAAGCTTGGTCCTCCTGTGACGGGAGGGAT

GGTTAAGGTACAAAGGCTAGAAACTTGAGTTTCTTCATTTCTGTCTCACAATTATCAAAAGCTAGAATTAGCTTC

TGCCCTATGTTTCTGTACTTCTATTTGAACTGGATAACAGAGAGACAATCTAAACATTCTCTTAGGCTGCAGATA

AGAGAAGTAGGCTCCATTCCAAAGTGGGAAAGAAATTCTGCTAGCATTGTTTAAATCAGGCAAAATTTGTTCCTG

AAGTTGCTTTTTACCCCAGCAGACATAAACTGCGATAGCTTCAGCTTGCACTGTGGATTTTCTGTATAGAATATA

Figure 5.9: Screening of CRISPR offspring with Sn2 and Asn3.

B) MoPrP sequence with Sn2 and Asn3 primers highlighted in yellow and blue respectively. ATG and TGA of MoPrP are highlighted in red. The MoPrP ORF is highlighted in green.

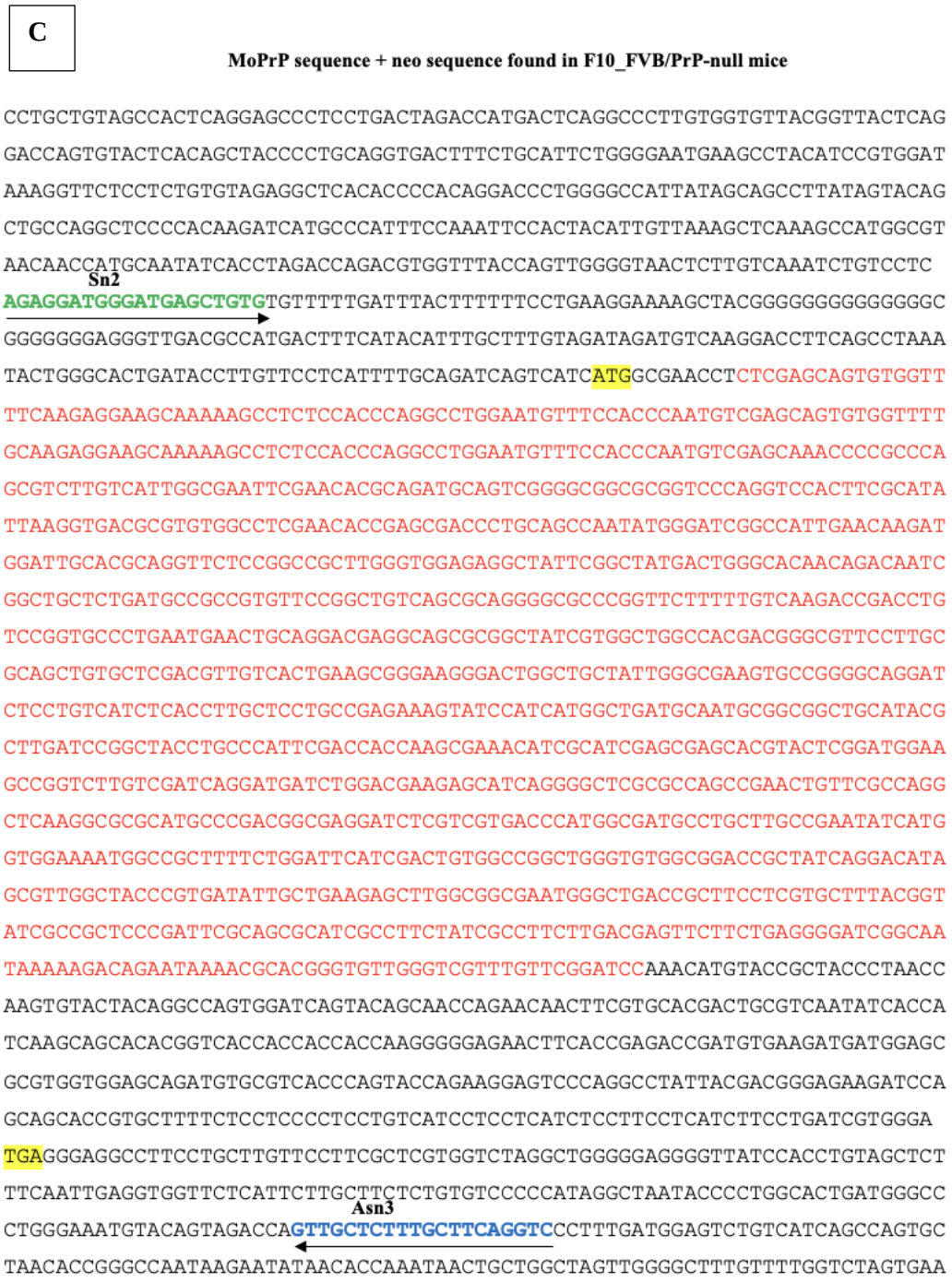

Figure 5.9: Screening of CRISPR offspring with Sn2 and Asn3

C) MoPrP sequence in F10_FVB/PrP-null mice with neomycin sequence highlighted in red. The remaining sequence in black is MoPrP. Sn2 and Asn3 primers are highlighted in green and blue respectively. ATG and TGA of MoPrP are highlighted in yellow.

.

PCR amplification of genomic DNA extracted from the offspring of Tg357 mice resulted in two bands (Figure 5.10) that were excised and the DNA was extracted for sequencing. The sequencing data revealed that the top band contained a sequence for the neomycin resistance gene and the bottom band contained the sequence for mouse or human PrP. However, none of the Tg354 had the correct genotype so only Tg357 was analysed further for the CRIPSR-Y163X-129V lines. The sequencing data revealed that the HuPrP ORF had been knocked-in, however it was truncated and the ATG start codon was missing (Figure 5.11). There were also errors found within the human PrP ORF (Figure 5.12).

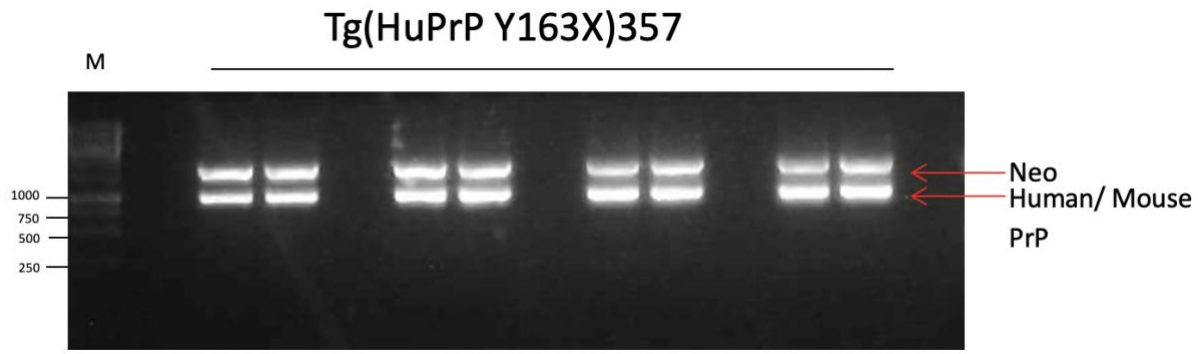

Figure 5.10: Screening offspring of Y163X-129V knock-in founders

Agarose gel electrophoresis showing results of PCR screen for Tg357 mice using primers Sn2 and Asn3. This PCR resulted in two bands that were extracted and sent for sequencing. The top band was confirmed as neo and the lower band represents mouse or human PrP.

*M= GeneRuler 1 kb DNA Ladder (Catalogue number: SM0311, Thermo Fisher Scientific Ltd, Loughborough, UK.

Figure 5.11: Truncated human PrP ORF in Tg357

Sequencing data from a Tg357 mouse with truncated human PrP ORF knocked into the endogenous mouse *Prnp* locus. Both sequencing primers 736For and Hu1 gave truncated sequence ending at the same point (end of red font with yellow highlight). Interestingly, the knocked-in truncated HuPrP ORF contained the expected gene modifications, namely valine at codon 129 and a TAG stop codon at residue 163 (highlighted in green). However, the TGA stop codon and additional sequences were missing from the human PrP ORF (blue font).

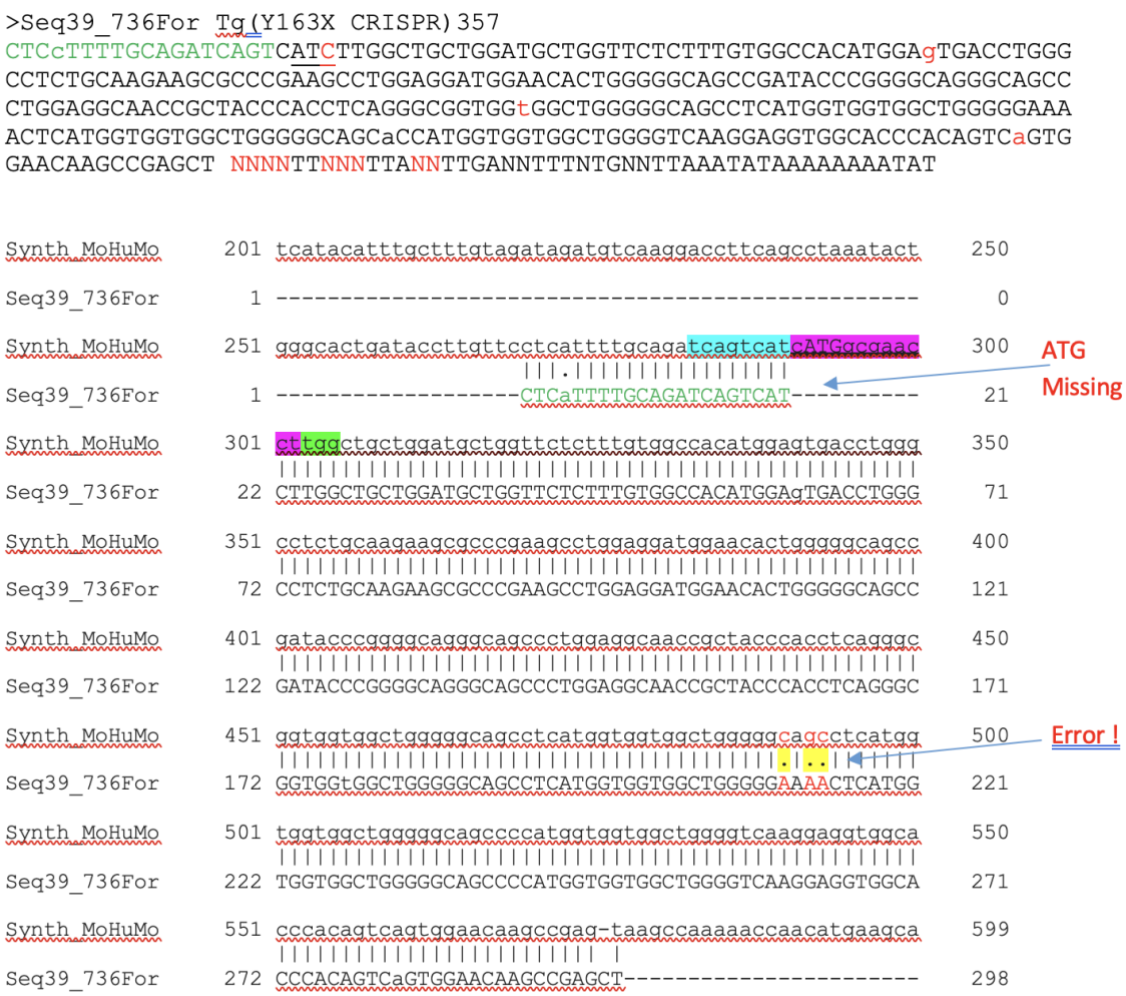

Figure 5.12: Errors in the HuPrP ORF knocked into Tg357 mouse

Although the HuPrP ORF containing the Y1633X mutation was knocked-into the mouse *Prnp* locus, the sequence was imprecise and contained errors (highlighted in yellow). The ATG start codon was also missing (highlighted in purple).

Although the HuPrP ORF was successfully knocked-in, the sequence was imprecise. Another issue that arose when sequencing the offspring of CRISPR-WT-129V founders, Tg361 and Tg362, was the presence of the neomycin resistance gene interfered with the sequencing of the HuPrP knock-in ORF (Figure 5.13). BLAST analysis revealed 91% identity with human PrP but 100% identity with mouse PrP. Therefore, the human PrP ORF was present but it was masked by the presence of the neo gene which hindered sequencing.

```
>Seq49_736For [Tg362; 129V-WT CRISPR]
TTTTGCAGATCAGTCATCATGGCGAACCCTCGAGCAGTGTGGTTTTCAAGAGGAAGCAAAAAGCCTCTCCA
CCCAGGCCTGGAATGTTTCCACCCAATGTCGAGCAGTGTGGTTTTGCAAGAGGAAGCAAAAAGCCTCTCCA
CCCAGGCCTGGAATGTTTCCACCCAATGTCGAGCAAACCCCGCCCAGCGTCTTGTCATTGGCGAATTCGAA
CACGCAGATGCAGTCGGGGCGGCGCGGTCCCAGGTCCACTTCGCATATTAAGGTGACGCGTGTGGCCTCGA
ACACCGAGCGACCCTGCAGCCAATATGGGATCGGCCATTGAACAAGATGGATTGCACGCAGGTTCTCCGGC
CGCTTGGGTGGAGAGGCTATTCGGCTATGACTGGGCACAACAGACAATCGGCTGCTCTGATGCCGCCGTGT
TCCGGCTGTCAGCGCAGGGGCGCCCGGTTCTTTTTGTCAAGACCGACCTGTCCGGTGCCCTGAATGAACTG
CAGGACGAGGCAGCGCGGCTATCGTGGCTGGCCACGACGGGCGTTCCTTGCGCAGCTGTGCTCGACGTTGT
CACTGAAGCGGGAAGGGACTGGCTGCTATTGNGCGAAGTGCCGGGGCAGGATCTCCTGTCATCTCACCTTG
CTCCTGCCGAGAAAGTATCNNT

pMC1neo          AGGGGGGATGTGCTGCAAGGCGATTAAGTTGGGTAACGCCAGGGTTTTCCCAGTCACGAC
Seq49_736For     ------------------------------------------------------TTT

pMC1neo          GTTGTAAAACGACGGCCAGTGAATTCTCGAGCAGTGTGGTTTTCAAGAGGAAGCAAAAAG
Seq49_736For     TGCAGATCAGTCATCATGGCGAACCCTCGAGCAGTGTGGTTTTCAAGAGGAAGCAAAAAG
                      *  *         * ***  **********************************

pMC1neo          CCTCTCCACCCAGGCCTGGAATGTTTCCACCCAATGTCGAGCAGTGTGGTTTTGCAAGAG
Seq49_736For     CCTCTCCACCCAGGCCTGGAATGTTTCCACCCAATGTCGAGCAGTGTGGTTTTGCAAGAG
                 ************************************************************

pMC1neo          GAAGCAAAAAGCCTCTCCACCCAGGCCTGGAATGTTTCCACCCAATGTCGAGCAAACCCC
Seq49_736For     GAAGCAAAAAGCCTCTCCACCCAGGCCTGGAATGTTTCCACCCAATGTCGAGCAAACCCC
                 ************************************************************

pMC1neo          GCCCAGCGTCTTGTCATTGGCGAATTCGAACACGCAGATGCAGTCGGGGCGGCGCGGTCC
Seq49_736For     GCCCAGCGTCTTGTCATTGGCGAATTCGAACACGCAGATGCAGTCGGGGCGGCGCGGTCC
                 ************************************************************

pMC1neo          CAGGTCCACTTCGCATATTAAGGTGACGCGTGTGGCCTCGAACACCGAGCGACCCTGCAG
Seq49_736For     CAGGTCCACTTCGCATATTAAGGTGACGCGTGTGGCCTCGAACACCGAGCGACCCTGCAG
                 ************************************************************

pMC1neo          CCAATATGGGATCGGCCATTGAACAAGATGGATTGCACGCAGGTTCTCCGGCCGCTTGGG
Seq49_736For     CCAATATGGGATCGGCCATTGAACAAGATGGATTGCACGCAGGTTCTCCGGCCGCTTGGG
                 ************************************************************

pMC1neo          TGGAGAGGCTATTCGGCTATGACTGGGCACAACAGACAATCGGCTGCTCTGATGCCGCCG
Seq49_736For     TGGAGAGGCTATTCGGCTATGACTGGGCACAACAGACAATCGGCTGCTCTGATGCCGCCG
                 ************************************************************
```

Figure 5.13: Presence of neomycin resistance gene interfering with sequencing of the HuPrP knock-in ORF

Comparison of the sequencing data obtained from Tg362 mouse with the neo resistance gene sequence. The sequence from the Tg362 mouse sequence (highlighted in yellow) was identical to the neo resistance gene sequence in the vector pMC1neo.

After screening all the offspring of the CRISPR knock-in founders through sequencing, there was not a single mouse with a perfect genetic modification. Incidentally, through this screening process, offspring of CRISPR knock-in founders in which over 2400 bp of the genomic sequence of MoPrP was knocked-out were identified (Figure 5.14). DNA repair was not possible in these mice due to the fact that such a large portion of the mouse genome has been cut by Cas9, thereby generating knock-outs. Western blot analysis of the CRISPR knock-out line, KO_1 revealed the absence of the mouse prion protein (Figure 5.15). This line amongst other CRISPR generated MoPrP knock-out lines are being maintained for future experimental use.

Figure 5.14: Sequencing data from CRISPR Knock-out mouse line KO_1

A large portion of the murine PrP genomic sequence (2494 bp) outside the mouse PrP ORF was cut by Cas-9 (sequence in blue font). This led to the generation of a CRISPR knock-out line (designated KO_1). The sequence in red was confirmed by sequencing to be present in the KO_1 knock-out line.

*The ATG start and TGA stop codons are highlighted in yellow. The positions of primers KO-Sn2 and KO-Asn6 are marked with arrows and also shown in yellow highlights.

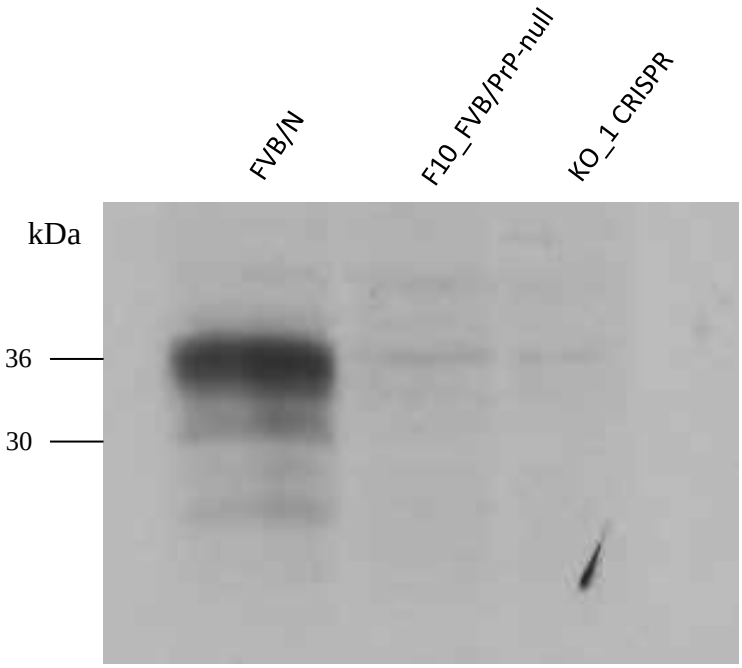

Figure 5.15: Immunoblot analysis of KO_1 CRISPR line

10% mouse brain homogenates analysed with monoclonal anti-PrP antibody ICSM35. No PrP^{C} was detected in the KO_1 CRISPR line. Positive control: FVB/N. Negative control: F10_FVB/PrP-null.

This chapter demonstrates that CRISPR knock-in mouse models could not be generated using EASI-CRISPR despite several attempts. The limitations of CRISPR/Cas technology are discussed further in the final discussion (Chapter 8).

6. Chapter 6: Results-Expression Studies in knock-in and transgenic models

This chapter will investigate the expression of HuPrP at mRNA and protein level in pCAG transgenics and knock-in mouse models.

6.1 Expression of HuPrP mRNA in transgenic and knock-in mouse models

PrP^C is expressed in a variety of organs, with high expression levels in the peripheral and central nervous systems (Wulf et al., 2017) . In the pCAG transgenic mice, the human PrP transgene is expressed under the control of the ubiquitous CAG promoter which is known to drive high levels of transgene expression (Fischer et al., 2020) . In contrast, the human PrP transgene constructs are under the control of endogenous PrP regulatory elements in the Y163X-129V and WT-129V knock-in lines. In keeping with the predominance of PrP amyloid deposition in peripheral organs of Y163X patients, expression of the human PrP was analysed in a variety of peripheral organs and the brain.

Brain, caecum, heart, kidney, large intestine, liver, lymph node, small intestine and spleen of selected pCAG and KI-lines were analysed for HuPrP mRNA expression via RT-PCR. RNA was extracted from these mouse tissues using the Direct-zol RNA purification kit (Zymo Research, USA). The RNA was then used as a template for cDNA synthesis using the QuantiTect ReverseTranscription Kit (Qiagen Ltd, Hilden, Germany) with the gene specific RT-primer MoPrP-20 (V2) (Table 2.2).

The cDNA obtained was amplified by PCR using human PrP specific primers Hu1 and Hu2 (Table 2.2), which amplify a 400-bp product within the human PrP ORF. HuPrP mRNA was detected in the brain, caecum, heart, kidney, large intestine, liver, lymph node, small intestine and spleen of Y163X-129V and WT-129V knock-in lines (Figure 6.1) and in the pCAG lines, Tg (Y163X-129V) 377 and Tg (WT-129V) 380 (Figure 6.2).

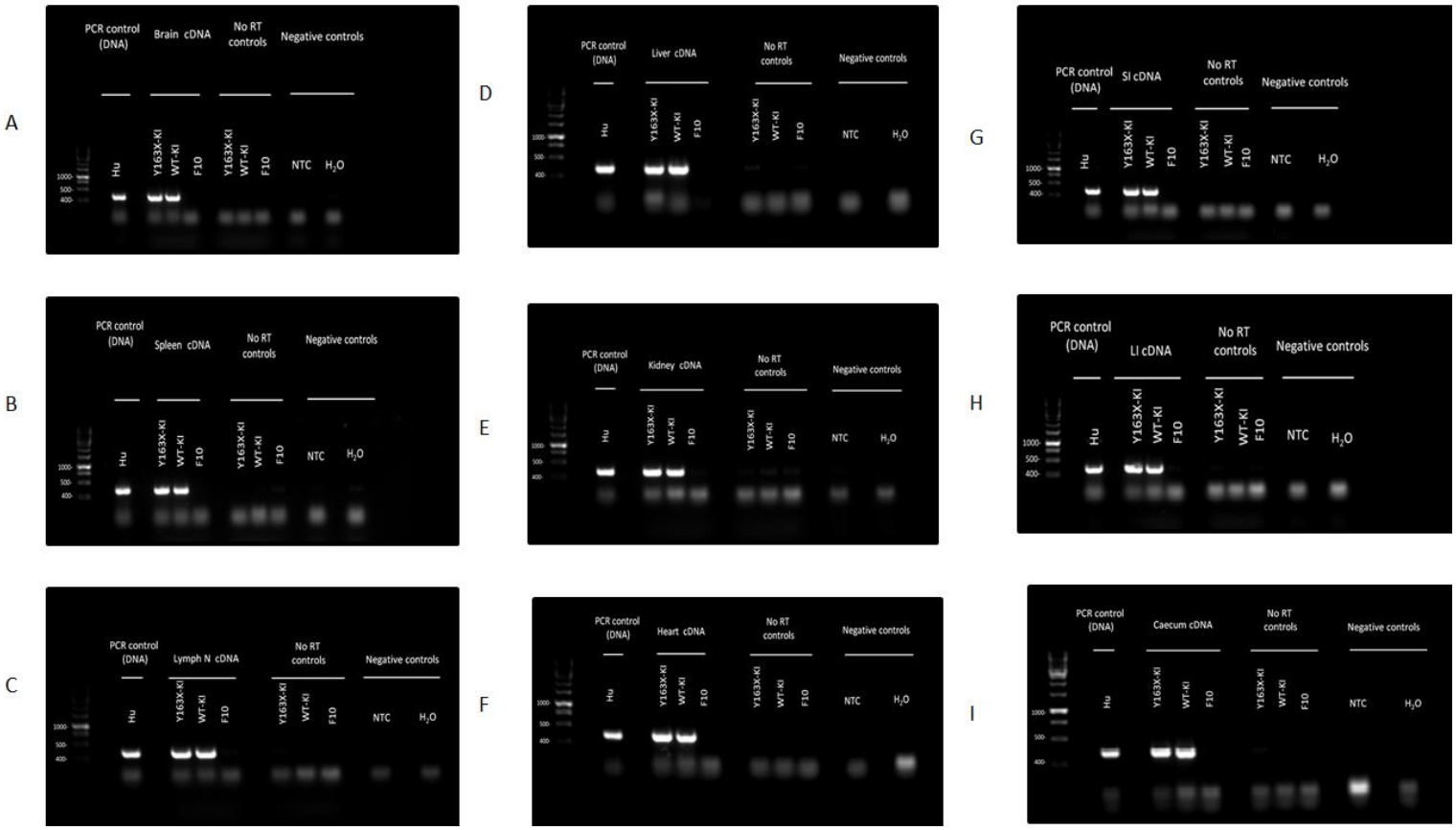

Figure 6.1: Expression of mRNA in Y163X-129V and WT-129V knock-in lines

The mRNA expression in (A) Brain (B) Spleen (C) Lymph Nodes (D) Kidney (E) Heart (F) Liver (G) Small Intestine (SI) (H) Large Intestine (LI) Caecum of Y163X-129V and WT-129V knock-in mice. RNA extracted from the brain, spleen, lymph nodes, kidney, heart, liver, small intestine, large intestine and caecum was used as a template for cDNA synthesis. The synthesised cDNA was then used as a template for the PCR amplification of the target sequence within the human PrP open reading frame. Primers Hu1 and Hu2 amplified a 400-bp fragment in all the tissues that were analysed.

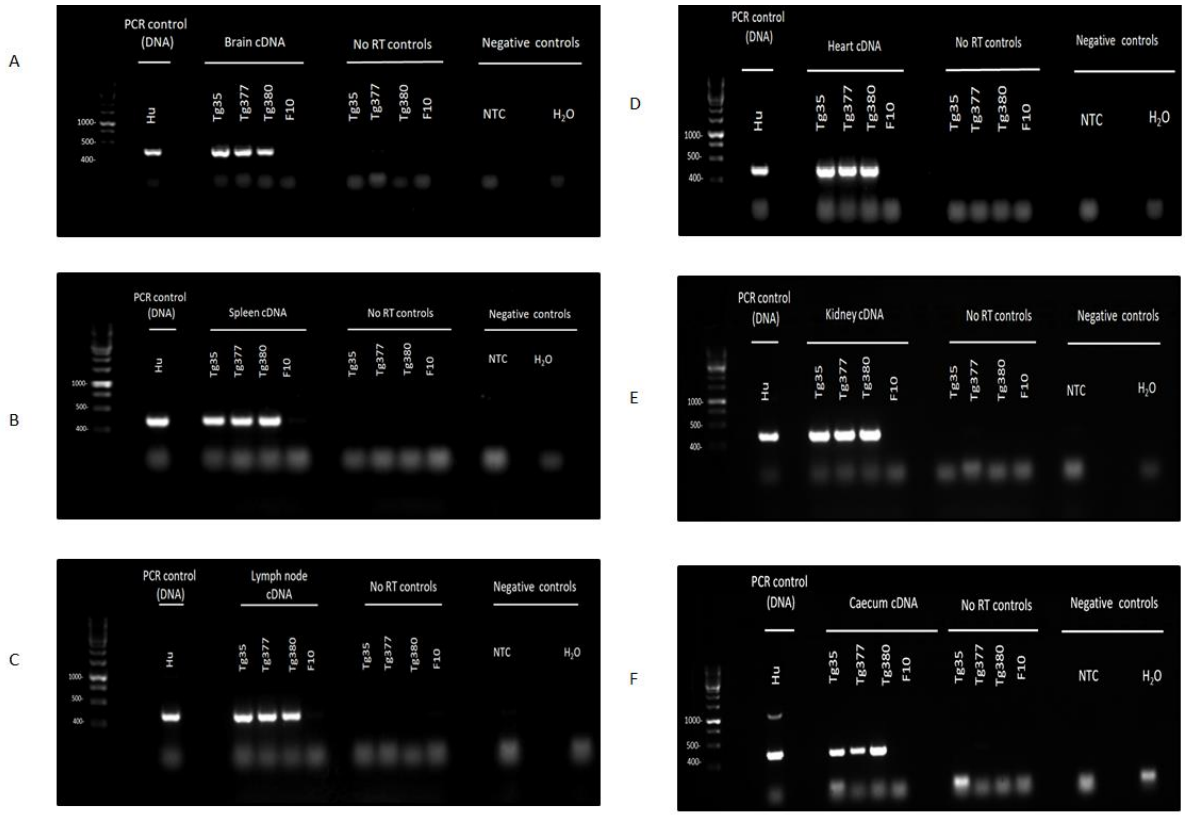

Figure 6.2: Expression of HuPrP mRNA in pCAG lines

The mRNA expression in (A) Brain (B) Spleen (C) Lymph Nodes (D) Kidney (E) Heart (F) Caecum of pCAG lines- Tg (Y163X-129V) 377 and Tg (WT-129V) 380. RNA extracted from the brain, spleen, lymph nodes, kidney, heart and caecum was used as a template for cDNA synthesis. The synthesised cDNA was then used as a template for the PCR amplification of the target sequence within the human PrP open reading frame. Primers Hu1 and Hu2 amplified a 400-bp fragment in all the tissues that were analysed.

To eliminate the possibility of a false positive signal by contamination with genomic DNA, control reactions without the reverse transcriptase enzyme (RT) were prepared alongside the experimental tissues. In the absence of RT, no PCR amplification was detected using Hu1 and Hu2 in any of the tissues analysed. This confirms that the amplification of HuPrP in the mouse tissues was specific to the RNA that was isolated from these tissues.

The specificity of the Hu1 and Hu2 primers was also confirmed by RT-PCR of mRNA obtained from the tissues of F10_ FVB/PrP null mice, in which there was no amplification of the target sequence in the human PrP ORF.

The homozygous Y163X-129V and WT-129V knock-in lines show similar levels of expression consistently in all the analysed tissue samples (Figure 6.1).
Overall, there are differences in HuPrP mRNA expression levels across the different organs in the heterozygous pCAG lines. However, the samples would need to be run with an appropriate housekeeping gene such as GAPH in order to compare the levels of expression in the different lines.

6.2 PrP^C detection in transgenic and knock-in mouse models by western blot

Monoclonal anti-PrP antibodies have differential affinities for glycosylated and truncated isoforms of PrP^C (Beringue et al., 2003). Previous work with the P102L humanised transgenic mouse model has also shown that mutations can influence antibody recognition of PrP (Wadsworth et al., 2006). The Y163X mutation leads to the formation of truncated PrP without a GPI anchor, therefore a panel of antibodies with different epitopes were used in order to assess the binding affinities for the truncated isoform (Table 6.1).

Table 6.1. Epitopes of the monoclonal anti-PrP antibodies used for screening the knock-in and transgenic lines.

Antibody	Epitope	Reference
SAF32	79-92	(Privat et al., 2008)
ICSM35	93–105	(Khalili-Shirazi et al., 2007)
6D11	95-110	(Sadowski et al., 2009)
ICSM61	96-105	(Khalili-Shirazi et al., 2007)
ICSM62	96-105	(Khalili-Shirazi et al., 2007)
3F4	109-112	(Privat et al., 2008)
ICSM37	96-105	(Khalili-Shirazi et al., 2007)
ICSM 17	140-159	(Khalili-Shirazi et al., 2007)
ICSM18	143-153	(Khalili-Shirazi et al., 2007)

Immunoblots were carried out on Tg373 (WT-129V), Tg375 (Y163X-129V), Tg376 (Y163X-129V) and knock-in mouse brains alongside controls (Figure 6.3). The pCAG lines were heterozygous and the knock-in lines were homozygous at the time of screening. All the antibodies tested showed the expected PrP profiles for Tg (WT-129V) 373 expressing wild type human PrP 129V. However, none of the antibodies tested were able to detect the truncated HuPrP 163X protein (predicted to be 14.6 kDa).

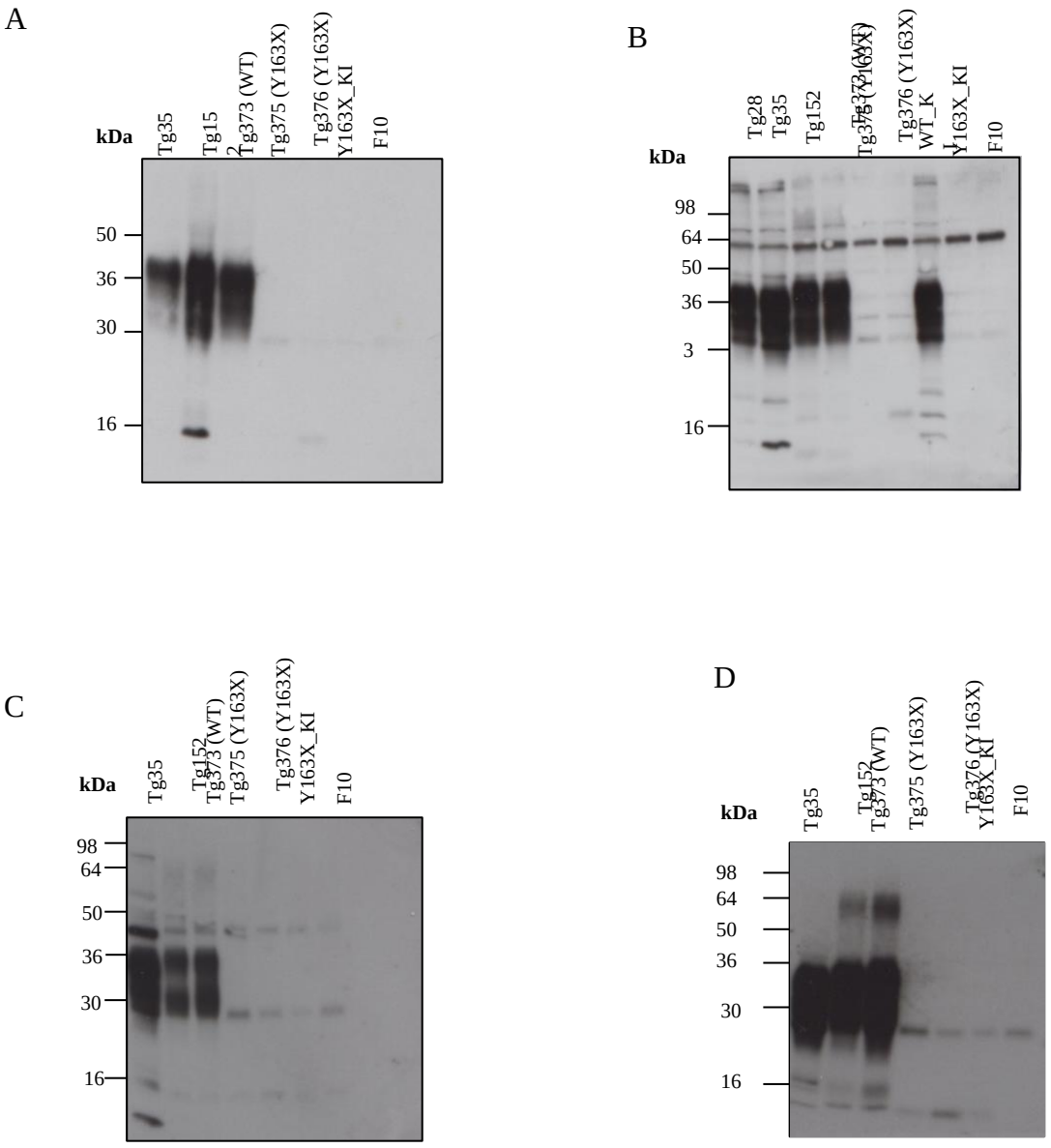

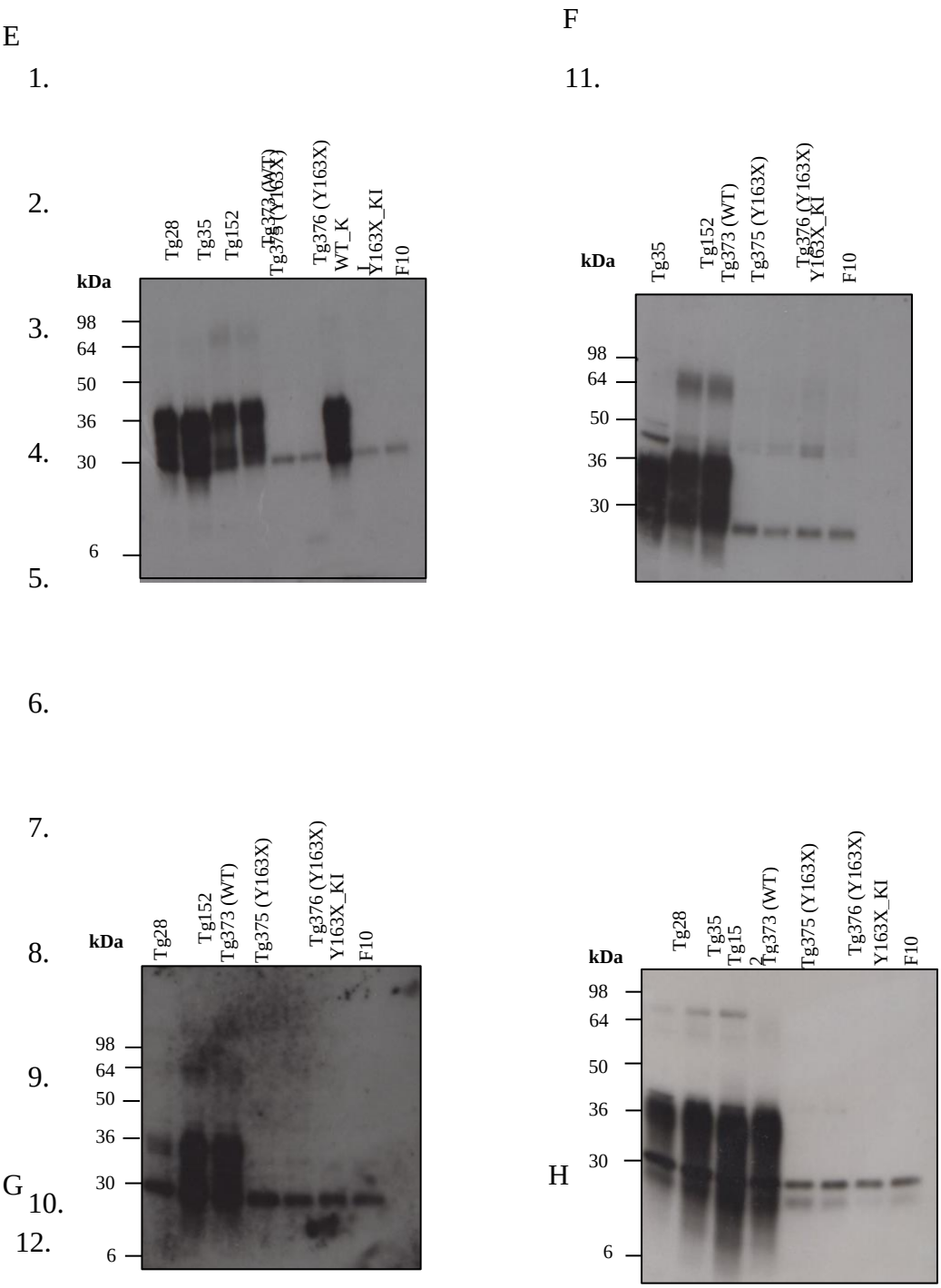

Figure 6.3: Immunoblot detection of PrP^{C} in transgenic and knock-in mouse brains

Mouse brain homogenates (2mg/ml) in RIPA buffer with a protease inhibitor cocktail (100ul/ml) analysed with anti-PrP monoclonal antibodies (A) SAF32 (B) ICSM35 (C) ICSM61 (D) ICSM62 (E) 3F4 (F) ICSM37 (G) ICSM17 and (H) ICSM18. Positive controls: 129MM Tg28, 129 MM Tg35, 129 VV Tg152. Negative control: F10_FVB/PrP-null.

6.3 PrP^C detection in transgenic and knock-in mouse models by ELISA

ELISA assays are one of the most sensitive methods used for the detection of disease-associated PrP(Tattum et al., 2010; Yam et al., 2010). Therefore this assay was used as an alternative method of detecting the mutant protein as it was undetectable by western blot. Human PrP 163X was successfully detected in the brain and peripheral tissues of pCAG transgenic and knock-in mice using a sandwich ELISA. The transgenic lines were heterozygous at the time of analysis therefore the PrP^C levels would be expected to double in homozygotes.

A higher immunoreactivity was observed in Tg373 (WT-129V) compared to the Tg35 control (expressing HuPrP ~2-fold above endogenous levels) in the brain (Figure 38A), spleen (Figure 6.4C), and caecum (Figure 38H). The trend in order of increasing immunoreactivity was Tg380 (WT) <Tg377 (Y163X) <Tg373 (WT) in the brain (Figure 6.4A), spleen (Figure 6.4C) and caecum (Figure 6.4H). However, in the heart immunoreactivity was higher in Tg377 and Tg380 compared to Tg35 (Figure 6.4F).

The immunoreactivity in WT-KI tissues was consistently higher in the brain (Figure 38B), spleen (Figure 6.4E) and caecum (Figure 6.4J) compared to Y163X-KI tissues. Lower immunoreactivity was also detected in the heart tissue obtained from the knock-in lines (Figure 6.4G).

AE Brai

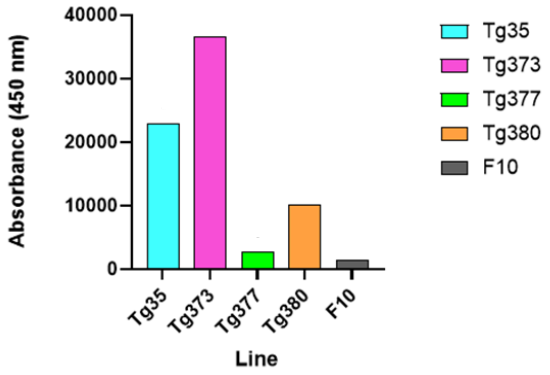

BF Brai

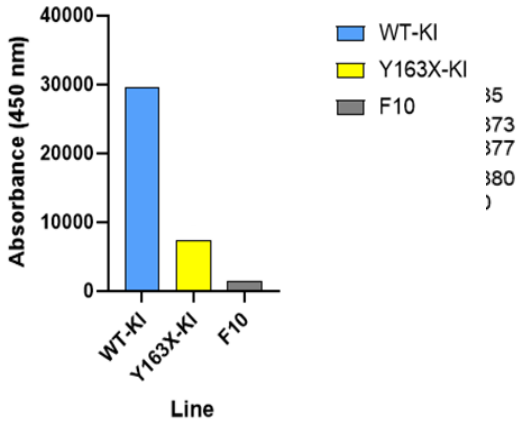

CG Spleen

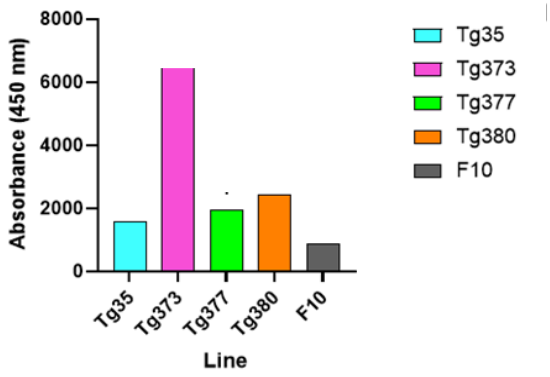

DH Spleen

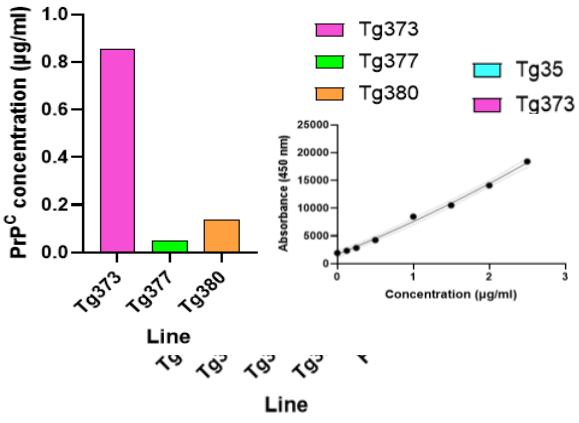

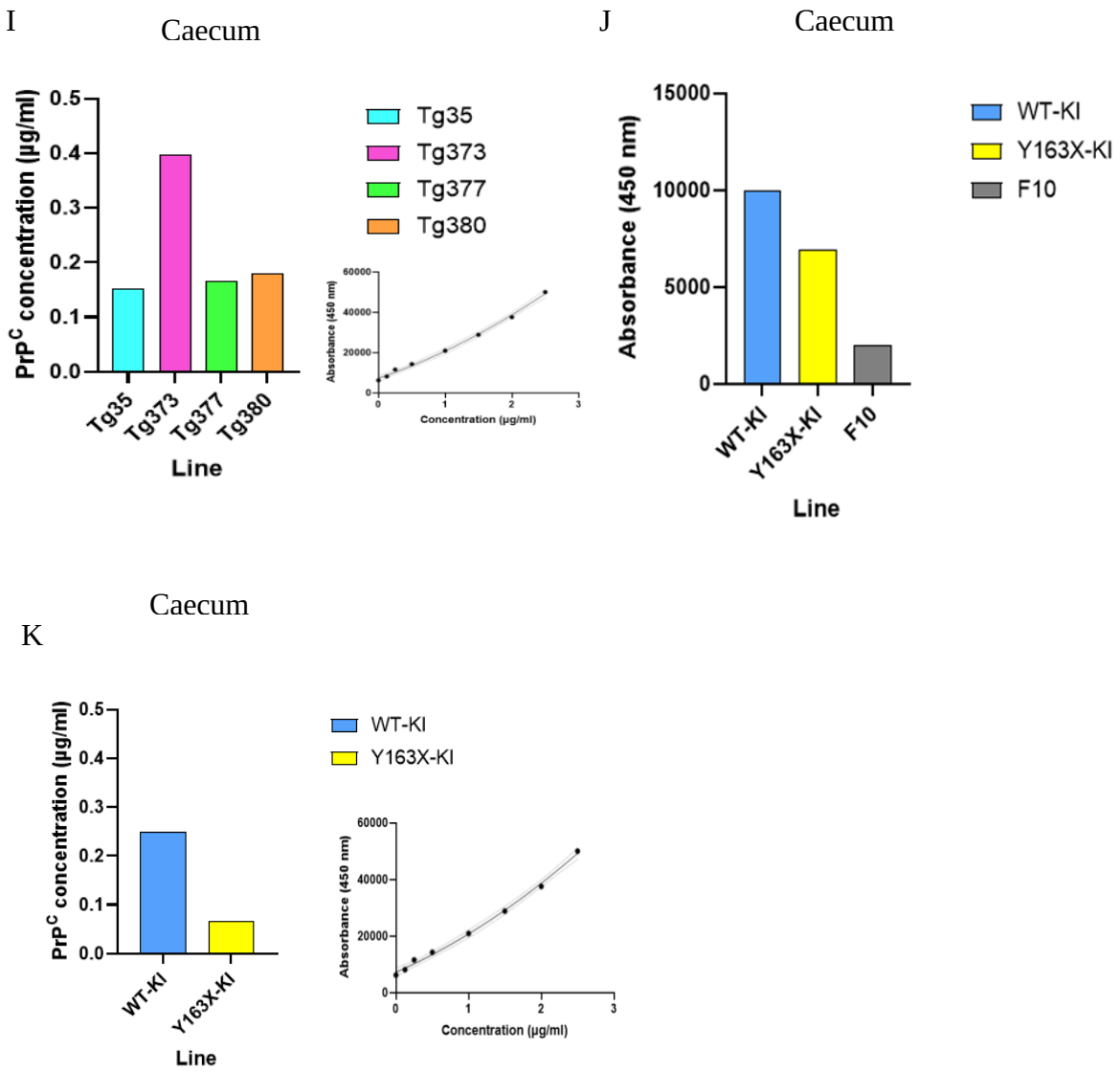

Figure 6.4: Detection of human PrP^C in pCAG transgenic and knock-in mice

Detection of human PrP^C by sandwich ELISA with 3F4 (capture) antibody and (biotinylated ICSM35) (ICSM35B) in the brain, spleen, heart and caecum of pCAG transgenic and knock-in mice. A-K, Quantitative results of PrP^C immunoreactivity in brain (A-B), spleen (C-E), heart (F-G) and caecum (H-K). Immunoreactivity was higher in Tg373 compared to Tg35 in (A) brain , (C) spleen and (H) caecum homogenates. A higher immunoreactivity was detected in (B) brain, (E) spleen and (J) caecum in WT-129V KI homogenates compared to Y163X-129V KI. PrP^C concentration was determined using standard curves (D, I and K) and the results shown were corrected for the background (F10). Positive control: 129 MM Tg35, 129 VV Tg152. Negative control: F10_FVB/PrP-null.

The results presented in this chapter have shown that HuPrP mRNA is expressed in the pCAG transgenics and the knock-in lines. However, HuPrP 163X could not be detected via western blot in the pCAG-Y163X or Y163X-KI lines despite testing several different anti-PrP antibodies. Researchers within the Prion Unit have also had difficulties trying to blot recombinant PrP. HuPrP 163X and recombinant PrP both lack post-translational modifications, such as the attachment of the GPI anchor which may be required for these proteins to be able to adhere to PVDF membranes (Nishina and Supattapone, 2007). HuPrP 163X was detected in the brains and peripheral organs of pCAG-Y163X-129V and Y163X-129V KI mice by ELISA which is a more sensitive technique. This suggests the absence of the mutant protein on the immunoblots was a technical issue.

7. Chapter 7: Generation of Y163X CAD5 cell line

A Y163X-129V CAD5 cell line was generated to investigate the trafficking properties of the mutant protein and to determine if HuPrP 163X could be detected by western blot in this new cell line. This chapter will describe the techniques and methods involved in generating the Y163X-129V CAD5 cell line.

7.1 Construct design

In contrast to full length PrP, previous studies demonstrate that truncated PrP molecules associated with stop codon mutations in *PRNP* are mainly localised intracellularly, so cell lines were generated to determine if human PrP 163X would have similar localisation properties (Petersen et al., 1996; Zanusso et al., 1999; Ivanova et al., 2001). CAD5 cells expressing HuPrP Y163X-129v driven by the CMV promoter were generated using CAD5KDB3 cells lacking endogenous mouse PrP expression. The pLNCX2 –Y163X construct was created by inserting the Y163X HuPrP ORF into the multiple cloning site of the pLNCX2 plasmid (Figure 7.1). Control cell lines expressing HuPrP WT-129V and pLNCX2 (vector only) were made alongside the mutant cell line in exactly the same way.

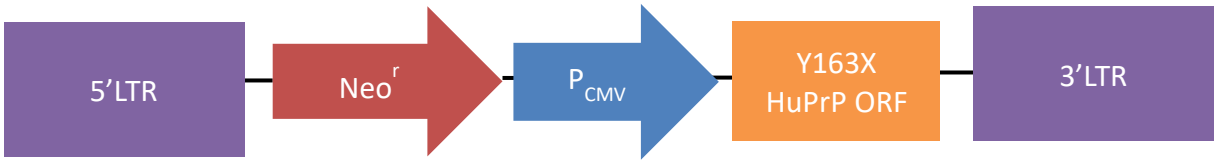

Figure 7.1: pLNCX2 –Y163X construct used to generate HuPrP 163X CADKDB3 cell line

The Human PrP ORF containing the Y163X mutation was synthesised by GeneArt (Thermo Fisher Scientific Ltd, Loughborough, UK) (Figure 7.2) and subcloned into the pMKRQ vector. The human signal peptide was replaced with the mouse signal peptide as evidence from previous experiments within the Prion Unit demonstrated that better expression of the transgene is achieved in mouse cell lines expressing the mouse signal peptide.

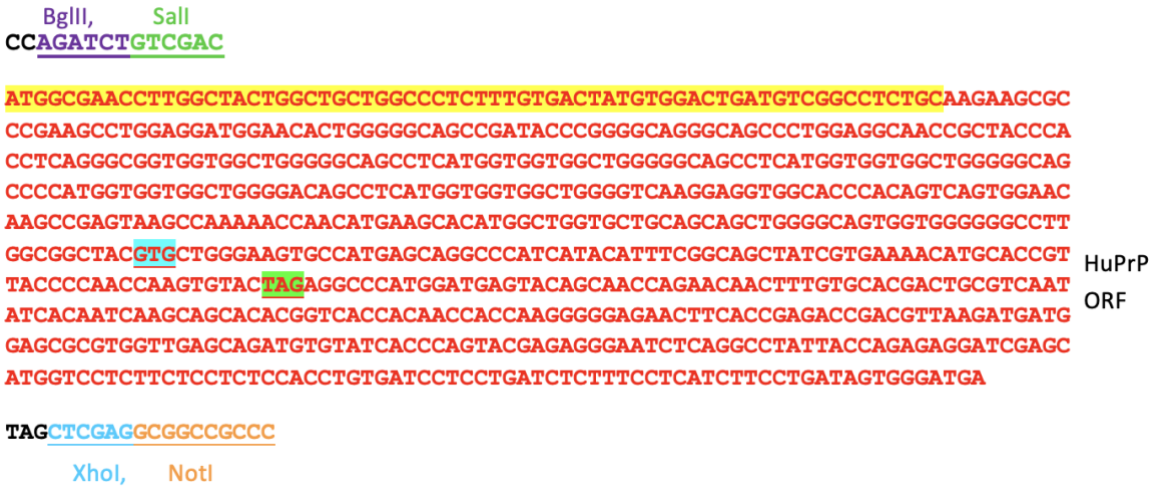

Figure 7.2 : Synthesis of 777 bp HuPrP ORF 163X by Gene Art

HuPrP ORF 163X sequence consisted of the mouse signal peptide (highlighted in yellow), the human *PRNP* open reading frame encoding valine at codon 129 (highlighted in blue) and a stop codon at residue 163 (highlighted in green). The sequence was flanked by restriction sites needed for cloning steps downstream (BglII, SalI, XhoI and NotI).

The human PrP ORF containing the Y163X mutation was isolated from the pMKRQ vector by digesting the vector with SalI and NotI sequentially (Figure 7.3). The pLNCX2 vector was also digested with SalI and NotI sequentially. Following this, the SalI/ NotI digested pLNCX2 vector was ligated to the SalI/NotI digested human PrP ORF fragment.

Then competent SCS110 *E. coli* cells were transformed with the ligation product and 5 clones were obtained after transformation of the bacteria with the ligation mixture. Plasmid DNA was purified from these clones using the QIAprep Spin Miniprep Kit (Qiagen, Hilden, Germany) and restriction digests with NotI and SalI were used to confirm positive clones containing the human PrP ORF.

For positive clones, double-digestion with NotI and SalI produces two bands: (1) pLNCX2-6133 bp (2) HuPrP ORF-777 bp. All five clones were identified as being positive (Figure 7.4).

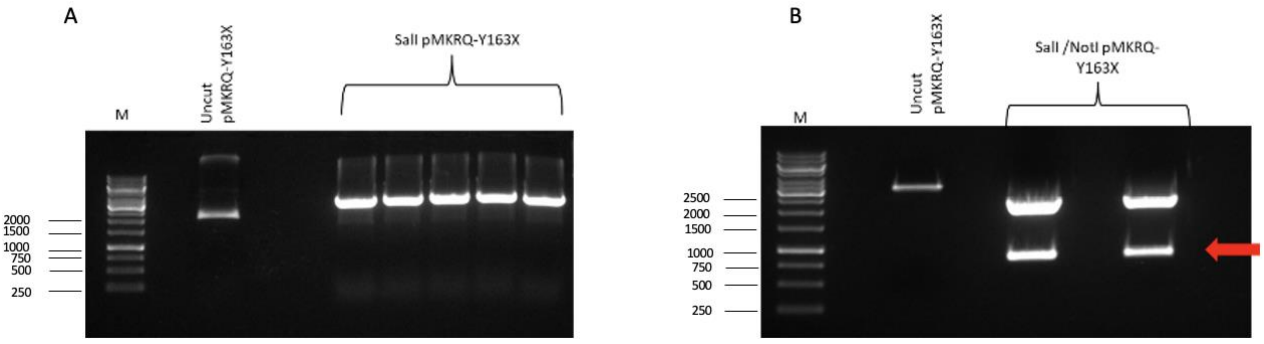

Figure 7.3 : SalI and NotI digestion of pMKRQ-Y163X to isolate the HuPrP ORF containing the Y163X mutation.

(A) SalI digestion of pMKRQ-Y163X

(B) NotI digestion of SalI digested pMKRQ-Y163X (red arrow pointing to 777bp HuPrP ORF containing the Y163X mutation)

*M= GeneRuler 1 kb DNA Ladder (Catalogue number: SM0311, Thermo Fisher Scientific Ltd, Loughborough, UK.

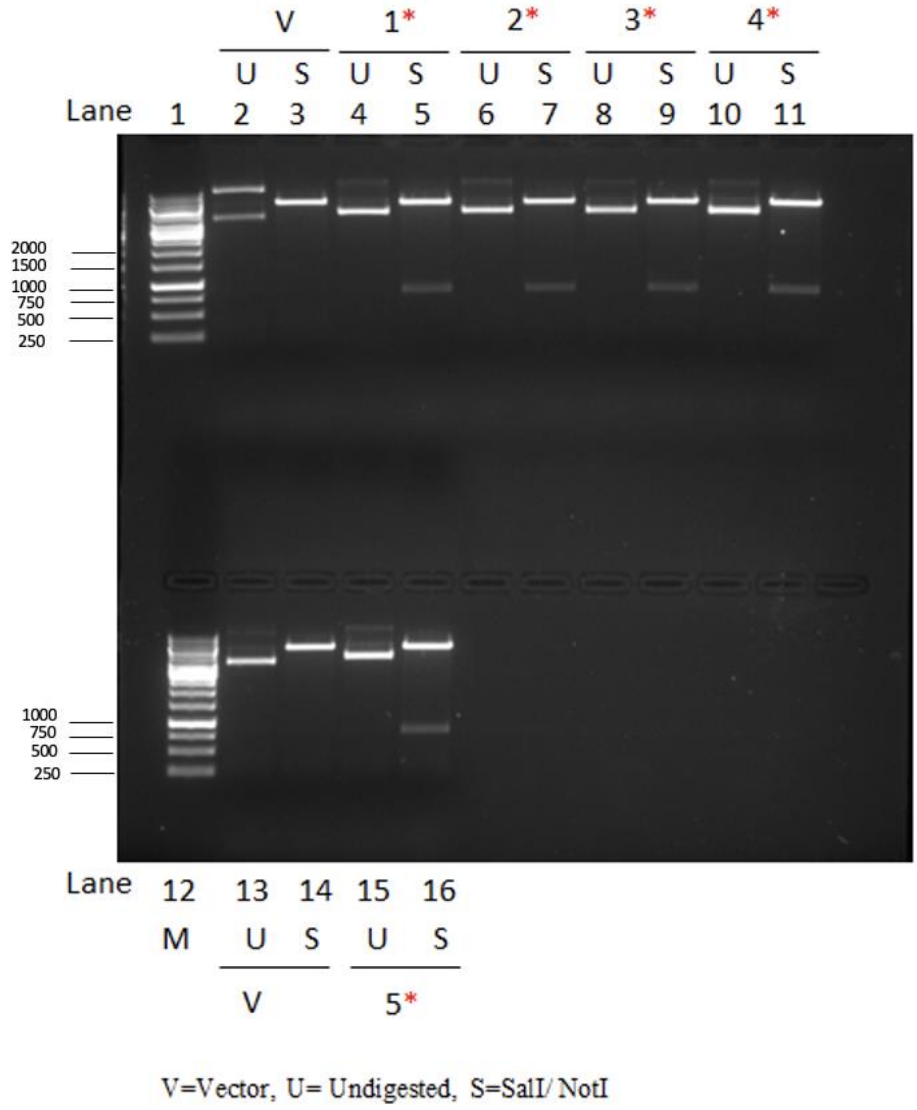

Figure 7.4: Positive clone selection for recombinants containing the HuPrP 163X ORF

NotI/SalI enzyme digestion of selected clones. Lanes 1 and 12: GeneRuler 1 kb DNA Ladder (Catalogue number: SM0311, Thermo Fisher Scientific Ltd, Loughborough, UK. Lanes 2-3: Vector DNA undigested (U) and Not I/Sal I digested (S) respectively. Lanes 4-5: Clone #1 DNA undigested (U), Not I/Sal I digested (S). Lanes 6-7: Clone #2 DNA undigested (U), Not I/Sal I digested (S). Lanes 8-9: Clone #3 DNA undigested (U), Not I/Sal I digested (S). Lanes 10-11: Clone #4 DNA undigested (U), Not I/Sal I digested (S). Lanes 13-14: Vector DNA undigested (U), Not I/Sal I digested (S). Lanes 15-16: Clone #5 DNA undigested (U), Not I/Sal I digested (S).

Glycerol stocks were made of clones #1 and #2 and plasmid DNA was prepared from clone #1 using the Hi Speed Plasmid Maxi Kit (Qiagen). CAD5KDB3 cells were transfected with maxiprep DNA prepared from clone #1 to generate the Y163X-129V CAD5 cell line (Figure 7.5).

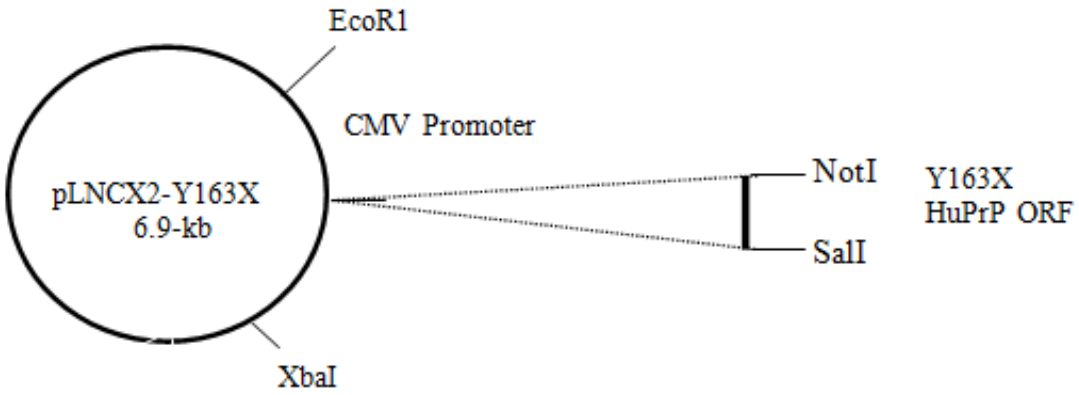

Figure 7.5 : pLNCX2-Y163X construct used to transfect CADKDB3 cells

7.2 Expression of HuPrP mRNA in Y163X-129V and WT-129V cell line

The expression of HuPrP mRNA in the Y163X-129V and control WT-129V CAD5 bulk cell lines was assessed by RT-PCR. RNA was extracted from the cell lines using the Direct-zol RNA purification kit (Zymo Research, USA). The extracted RNA was then used as a template for cDNA synthesis using the QuantiTect ReverseTranscription Kit (Qiagen Ltd, Hilden, Germany) with the HuPrP pLNCX2 forward and reverse primers (Table 2.2 and Figure 7.6). This primer pair amplifies a 248 bp PCR product within the HuPrP ORF. HuPrP mRNA was detected in the Y163X-129V and WT-129V CAD5 cell lines but not in the pLNCX2 (vector only) or CAD5 WT cell lines (Figure 7.7).

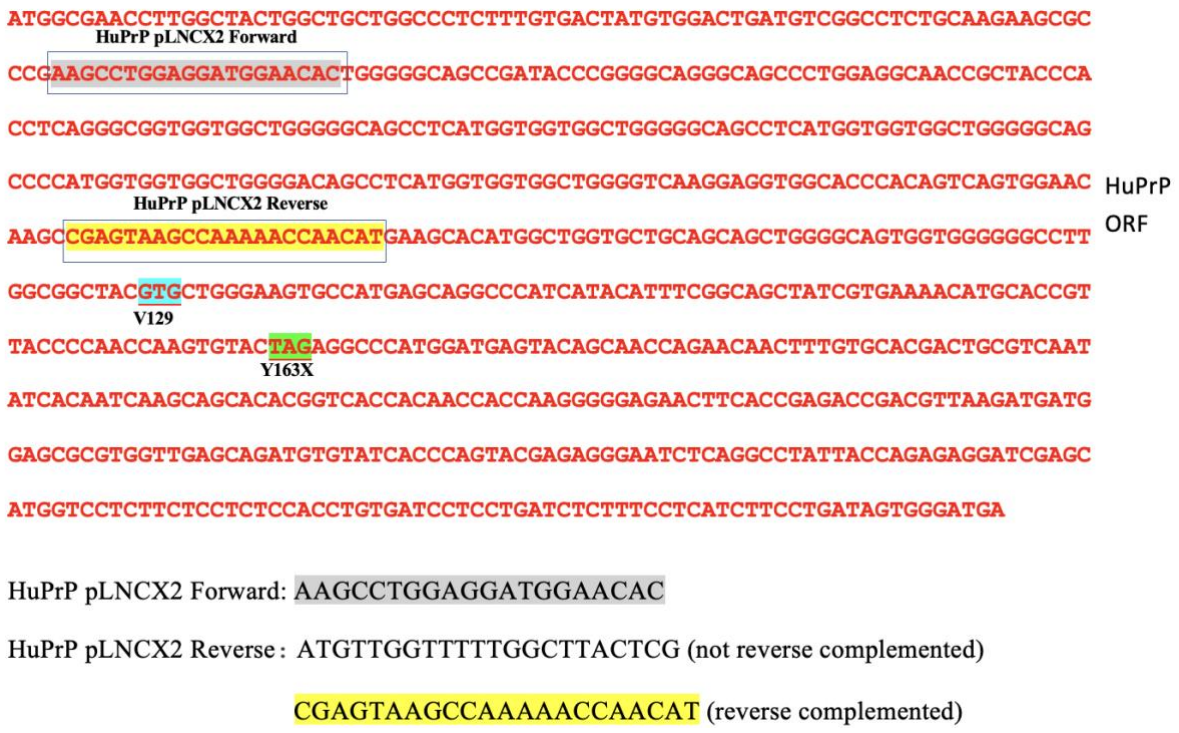

Figure 7.6: HuPrP ORF 163X sequence with HuPrP pLNCX2 primers highlighted

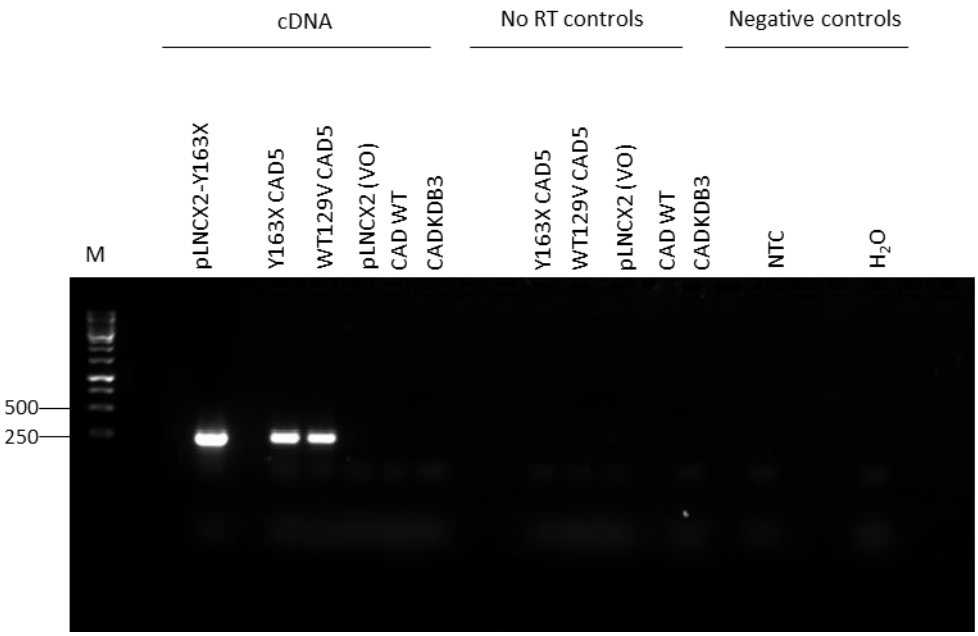

*M= GeneRuler 1 kb DNA Ladder (Catalogue number: SM0311, Thermo Fisher Scientific Ltd, Loughborough, UK.

Figure 7.7: HuPrP mRNA expression in Y163X-129V and WT-129V CAD5 cell lines

HuPrP mRNA was detected in the Y163X-129V and WT-129V CAD5 cell lines by RT-PCR. HuPrP pLNCX2 forward and reverse primers amplified a 248 bp PCR product in both of these cell lines. CADKDB3 cells and cell lines expressing pLNCX2 (vector only) and wild-type mouse PrP (CAD WT) were used as negative controls. HuPrP mRNA was not detected in pLNCX2 (vector only), CAD5 WT cell lines or the no RT controls. The specificity of the HuPrP pLNCX2 forward and reverse primers were confirmed by RT-PCR of cDNA synthesised from RNA extracted from CADKDB3 cell lines which lack the expression of endogenous mouse PrP. There was no amplification of HuPrP mRNA in CADKDB3 cell lines.

7.3 PrP^C detection in Y163X-129V CAD5 cell line by western blot

Anti-PrP monoclonal antibodies, ICSM35 and 3F4 were used to detect the expression of Human PrP in the cell lines. Human PrP was detected in the WT-129V CAD5 cell line but not in the mutant Y163X-129V line or negative control lines (pLNCX2 and CADKDB3) (Figure 7.8). The inability to detect the human PrP 163X protein was also observed in the western blot analysis of tissues extracted from pCAG-Y163X-129V and Y163X-129V KI mice. ICSM35 is cross-reactive to both human PrP and mouse PrP, therefore mouse PrP was detected in CAD5 WT cells using ICSM35 (Figure 45A), but no human PrP was detected in these cells using 3F4 (Figure 7.8B) as this antibody specifically recognises human PrP.

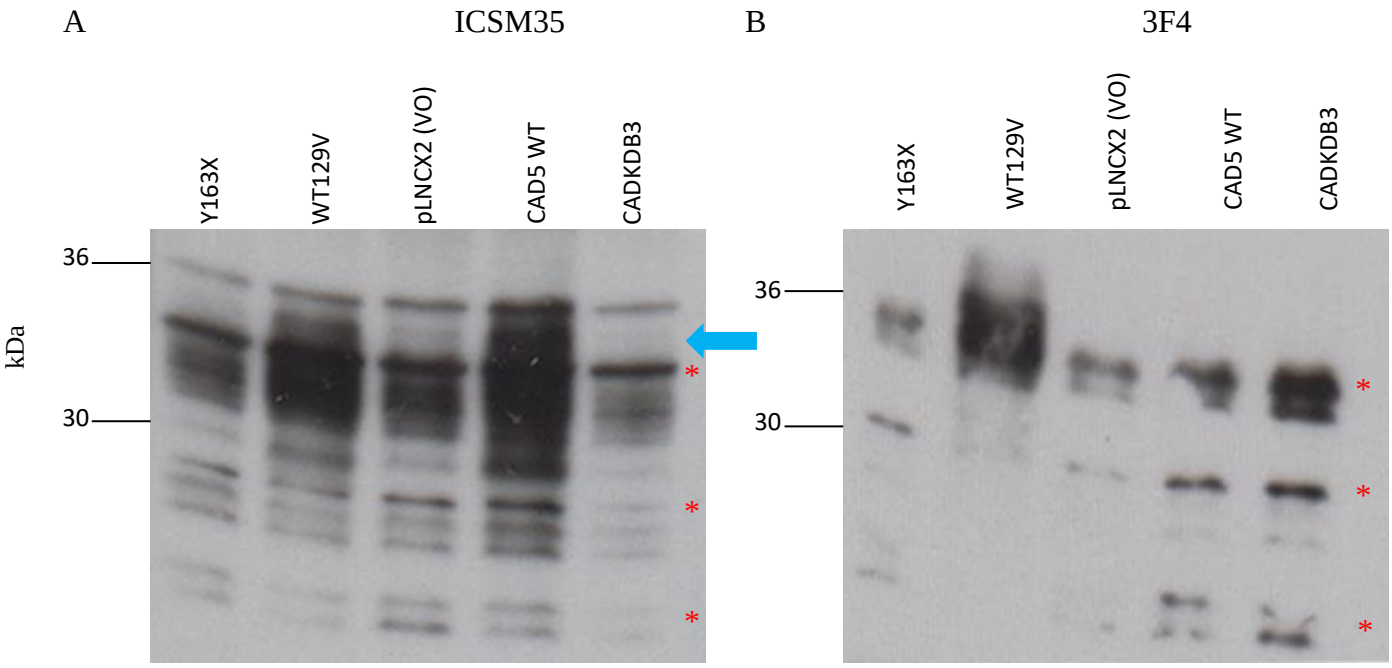

Figure 7.8: Western blot analysis of Y163X and WT129V CAD5 cell lines.

Cell lysates (2mg/ml) in RIPA analysed with anti-PrP monoclonal antibodies (A) ICSM35 and (B) 3F4 Positive control: WT-129V cell line. Negative controls: pLNCX2 and CADKDB3 cell lines. Human PrP expression was confirmed in WT-129V cell lines by western blot analysis. No Human PrP was detected in Y163X, pLNCX2 (vector only), CAD5 WT and CADKDB3 cell lines. The blots with ICSM35 and 3F4 gave rise to multiple non-specific bands; the red asterisks indicate the non-specific bands and the blue arrow indicates the band of intrest.

7.4 Immunohistochemical detection of PrP in Y163X CAD5 cell line

Previous studies suggest that truncated mutant PrP molecules associated with *PRNP* truncating mutations are trapped intracellularly rather than being transported to the cell surface (Petersen et al., 1996) (Zanusso et al., 1999) (Ivanova et al., 2001). Therefore, the trafficking of HuPrP 163X to the cell surface was investigated in the CAD5 cell line using fluorescent immunostaining.

The CAD5 cell lines were fixed and co-stained with anti-PrP antibody 6D11 and anti-mouse IgG2a Alexa Fluor® 488 (green) for cell surface PrP expression, the anti-alpha 1sodium potassium ATPase antibody and anti-mouse IgG1 Rhodamine Red™-X (red) as a marker for the plasma membrane and the nuclear marker DAPI (blue) (Figure 46).

Immunofluorescent analysis of the cell lines revealed that HuPrP 163X accumulated in the nucleus as HuPrP 163X staining co-localised with the nuclear marker DAPI (Figure 46M). Cell surface staining of HuPrP 163X was extremely weak and no clear co-localisation of the mutant protein and the cell membrane marker was observed (Figures 46A and 46M).

Wild-type human PrP appears to be predominantly localised to the cell membrane as there was co-localisation of WT HuPrP and the cell membrane marker (Figure 46N). No co-localisation of WT HuPrP and DAPI was observed (Figure 46N). The observations made in the CAD5WT cells were similar to the WT-129V line, but the staining of mouse PrP and the cell membrane was weaker compared to WT-129V cells (Figures 46C and 46G). CADKDB3 cells were stained as negative controls and PrP cell surface expression was barely detectable in these cells (Figure 46D).

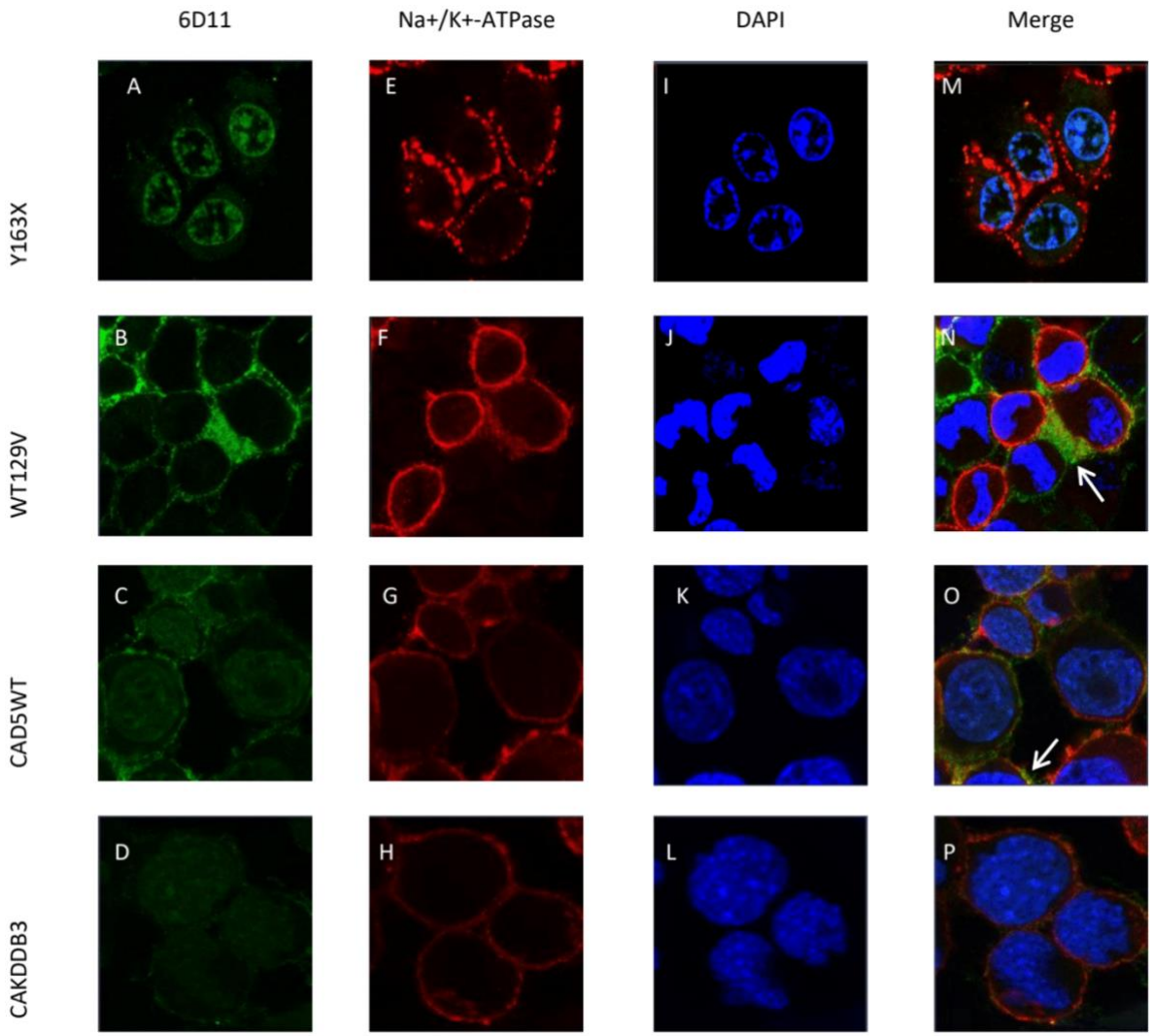

Figure 7.9: PrP trafficking in CAD5 cell lines.

PrP was detected in cell lines using the mouse monoclonal antibody 6D11 and anti-mouse IgG2a Alexa Fluor® 488 (green) (A-D). The cell membrane was detected using the anti-alpha 1 sodium potassium ATPase antibody and anti-mouse IgG1 Rhodamine Red™-X (red) (E-H). Co-localisation of the cell membrane marker and PrP was observed in the WT129V and CADWT lines (N and O; arrowed). DAPI was used as a marker of cell nuclei (blue) (I-L).

In summary, the cell membrane staining of the Y163X-129V CAD5 cells indicates abnormal trafficking of the mutant protein. HuPrP 163X was localised intracellularly, whereas wild-type PrP^{C} was expressed on the cell surface. This is in line with previous research which demonstrates that truncated PrP molecules arising from stop codon mutations are localised within subcellular compartments. These findings suggest that glycans and the GPI anchor facilitate correct trafficking of PrP.

8. Chapter 8: Discussion

The aims of this thesis were to generate and characterise mouse models expressing human PrP 163X to model this novel prion disease associated with chronic diarrhoea and peripheral neuropathy. Transgenic and knock-in mice expressing HuPrP 163X have been generated as new models of this inherited prion disease.

Transgenic and knock-in models of the Y163X mutation

The ubiquitous CAG promoter was selected to drive high levels of PrP expression in the CNS and peripheral tissues in order to more accurately model the peripheral pathogenesis associated with the Y163X mutation. Expression of the mutant protein was successfully driven by the CAG promoter in the transgenic lines and mRNA expression was confirmed in all analysed tissues. Ten transgenic lines were generated in total: 6 pCAG-Y163X-129V (Tg375, Tg376, Tg377, Tg378, Tg381 and Tg382) and 4 pCAG-WT-129V (Tg373, Tg374, Tg379 and Tg380).

Notably, protein expression was only detectable by western blotting in lines expressing wild type HuPrP despite testing different monoclonal anti-PrP antibodies covering the whole truncated protein position (79-153).

The difficulty encountered in detecting the truncated Y163X protein by western blotting in this study is consistent with reported observations working with Y163X patient brain. Nisha and Supattapone, 2007 reported that the amount of PrP^C detected by western blot decreased by approximately 95% following treatment with phosphatidylinositol-specific phospholipase C (PI-PLC) which cleaves the GPI anchor. The immunodetection of PrP^C following PI-PLC treatment on PVDF membranes was inefficient.

However, they were able to detect PrP^C following PI-PLC by slot blotting onto a nylon membrane or by using in-gel immunodetection (Nishina and Supattapone, 2007). Therefore the inability to detect HuPrP 163X may have been caused by the failure of the mutant protein to bind to the PVDF membrane in the absence of a GPI anchor and glycans that can facilitate the binding of PrP^C to the membrane. HuPrP 163X may be detectable by using alternative methods such as in-gel immunodetection and slot blotting using nylon membranes and this could be explored in future experiments.

High mRNA and protein expression levels of wild type HuPrP were observed particularly in pCAG-Tg373 (WT-129V) in the brain, spleen and caecum. The random insertion of transgenes into the host genome using transgenic technology can result in variations in the transgene copy number and the spatial expression pattern of the transgene (Kaczmarczyk and Jackson, 2015; Kaczmarczyk et al., 2016). The comparability between different transgenic lines can be confounded by variable PrP expression levels; this can be a limitation when using transgenic technology (Brandner and Jaunmuktane, 2017).

However, PrP overexpression models are useful for the purpose of testing therapeutics as the higher levels of PrP expression reduce the incubation time (Brandner and Jaunmuktane, 2017). This is particularly advantageous when modelling inherited prion diseases with slow disease progression in humans such as the Y163X mutation, because the faster rate of conversion ensures that disease is seen in the shorter lifespan of a mouse.

Knock-in mice expressing endogenous levels of mutant or wild-type PrP were also generated alongside the transgenics in order to address the limitations of overexpression models described above.

The mRNA expression levels were similar between the mutant Y163X-KI and control WT-129V line in all the tissues analysed, however, PrP^{C} immunoreactivity was consistently lower in the mutant line compared to the control.

The levels of mRNA expression in biological samples do not always necessarily correlate with protein levels (Vogel and Marcotte, 2012; Kosti et al., 2016; Perl et al., 2017). This is due to the fact that there are many different factors that either repress or enhance protein synthesis (Maier et al., 2009). Translational efficiency and mRNA stability can be influenced by RNA binding proteins (RBPs). RBPs can bind to sequences on the mRNA transcript to increase its stability or enhance translation (Abdelmohsen and Gorospe, 2010; Srikantan and Gorospe, 2012). Therefore it is important to quantify both mRNA and protein expression when characterising new mouse models.

At present, homozygous lines have been established for 4 transgenic lines: 1) Tg375 and Tg377 (pCAG-Y163X-129V) mutants and 2) Tg373 and Tg380 (pCAG-WT-129V) controls. The next step is to populate experimental groups for long-term observation experiments. Long term observation experiments are in progress for the knock-in lines and a panel of CNS and peripheral tissues are being collected at defined time points for immunohistochemical (IHC) analysis. The IHC analysis of tissues obtained from ageing cohorts of transgenic and knock-in mice will be essential in determining whether the low to undetectable levels of HuPrP 163X expression is sufficient to induce spontaneous formation of disease-associated PrP assemblies.

Up to date only one transgenic model expressing mutant human PrP has shown spontaneous formation of disease –related PrP. Asante *et al*. 2020 generated transgenic mice expressing HuPrP 117V (designated 117VV Tg30) and found PrP plaques in the anterior commissure of two mice at 476 ($117V^{Spont-A}$) and 734 ($117V^{SpontB}$) days of age. Brain homogenates from $117V^{Spont-A}$ and $117V^{SpontB}$ were passaged into groups of 117VV Tg30 mice and all the mice that had been inoculated with the spontaneous 117V prion isolates became infected.

Immunohistochemical analysis of brains from these mice revealed widespread deposition of PrP plaques and the pattern of plaque deposition seen in these mice was similar to that observed in A117V patient brains. This A117V transgenic model recapitulates the human disease and highlights the importance of generating animal models of IPDs that express the mutant human protein as opposed to superimposing the human PrP mutation onto mouse PrP (Wadsworth et al., 2010; Asante et al., 2020).

Modelling the Y163X mutation using CRISPR-Cas9 technology

Unfortunately, despite multiple attempts, Y163X knock-in mice could not be made using CRISPR-Cas9 technology due to CRISPR-induced off target deletions in the mouse genome. Incidentally, several different knock-out lines were generated. These CRISPR-generated knockout lines have been characterised and maintained for future experimental use.

The human PrP gene containing the Y163X was successfully inserted into the mouse genome using a variation of CRISPR methodology known as EASI-CRISPR; however sequencing analysis revealed that the inserted sequence was imprecise and contained errors. Screening offspring of CRISPR knock-in founders also revealed that large portions of the murine PrP genomic sequence (over 2000 bp) were deleted by CRISPR-Cas9, despite the fact that the guide RNA was designed to remove only 762-bp murine PrP open reading frame.

Other studies have also reported large deletions following CRISPR-Ca9 mediated gene editing (Parikh et al., 2015; Shin et al., 2017; Adikusuma et al., 2018). Parikh *et al.* 2015 targeted the tyrosinase gene in mice using CRISPR-Cas9 and they identified a mouse with an extremely large deletion of 42 kb. Initially, no PCR product was amplified for this allele but the deletion was later confirmed through sequencing (Parikh et al., 2015).

In another study by Shin *et al.* 2017, they reported that mice that were identified as homozygous founders were not actually genuine founders following sequencing analysis (Shin et al., 2017). The PCR strategy that was designed in this study used PCR primers to amplify short sequences (400-500 bp) around the target site. Small deletions were detected by PCR, however larger deletions were undetectable.

Therefore, these mice would appear to be homozygotes when in actual fact they were compound heterozygotes (Shin et al., 2017). Larger deletions were only detectable by using serial PCR primers that spanned the whole target site (Shin et al., 2017).

These findings highlight the importance of combining PCR-based screening methods with DNA sequencing when screening CRISPR founders and their offspring.

Another obstacle faced when using the CRISPR-Cas9 system to generate genetic animal models is mosaicism.

Mosaic mutants are made up of several cell types that carry different mutations (Hashimoto et al., 2016). These mutants can arise following CRISPR-Cas genome editing depending on the time window between the delivery of CRISPR components and the first DNA replication (Hashimoto et al., 2016; Lamas-Toranzo et al., 2019). It has been proposed that the continuous activity of the CRISPR-Cas complex at different stages of embryonic development can lead to the generation of mosaic mutants (Le et al., 2021). Mosaic mutations may also occur following DNA repair events in zygotes and divided embryonic cells (Mehravar et al., 2019).

Various different strategies have been proposed to reduce the occurrence of mosaicism using CRISPR-Cas9 technology. Mosaicism may be reduced by delivering the CRISPR-Cas reagents into early-stage zygotes as the timing of delivery relative to DNA replication contributes to the frequency of mosaicism (Kim et al., 2014; Hashimoto et al., 2016).

Hashimoto et al.2016 reported that they were able to generate non-mosaic mutant mouse embryos via electroporation of the CRISPR-Cas reagents into early pronuclear embryos that had been generated via IVF. The use of IVF enabled the researchers to control the timing of fertilisation. However, when the researchers electroporated zygotes that had been produced naturally, most of the embryos were mosaic (Hashimoto et al., 2016).

Another way in which mosaicism may be decreased is by using Cas9 protein as an alternative to Cas9 RNA (Singh et al., 2015).

The occurrence of genetic mosaicism can lead to different genotypes and phenotypes being observed in founder mice following CRISPR-Cas genome editing. This complicates the analysis of founder mice that have been generated using CRISPR/CAS technology (Yen et al., 2014; Mehravar et al., 2019) .

Mosaicism can lead to the generation of false-positive genotyping results. For example, the genome of a founder mouse may harbour the desired genetic modification based on genotyping assays using DNA extracted from the tail or ear punches (Oliver et al., 2015; Mehravar et al., 2019). However, this genetic modification may not be passed onto the offspring because it is not present in germline cells (Oliver et al., 2015)

It has been suggested that founders should be treated as chimeras which should be bred further to wild-type mice to achieve germline transmission and generate true homozygous or heterozygous mutants for experiments (Oliver et al., 2015; Mehravar et al., 2019).

In theory CRISPR-Cas genome editing is cheaper and faster compared to traditional recombinant DNA technology, but it was clear throughout this PhD investigations and from the literature that CRISPR technology presents its own unique challenges. There are still some technical hurdles that need to be overcome in order for researchers to make full use of this technology.

Y163X-129V CAD5 Cell line

The Y163X mutation causes protein synthesis to be prematurely terminated which produces truncated HuPrP 163X lacking both N-glycosylation sites and the GPI anchor. Previous research suggests that truncated PrP molecules resulting from *PRNP* stop codons mutations are abnormally trafficked due to the lack of PrP glycosylation and the GPI anchor *in vitro* (Petersen et al., 1996; Zanusso et al., 1999; Korth et al., 2000; Ivanova et al., 2001; Ma and Lindquist, 2001; Salamat et al., 2011) and *in vivo* (Cancellotti et al., 2005). Therefore, the Y163X-129V CAD5 cell line was generated in order to study the trafficking properties of HuPrP 163X. This cell line was also established to investigate whether the mutant protein could be detected by western blot using cell lines.

Immunohistochemical analysis demonstrated that the mutant protein accumulated in the nucleus whereas the wild-type protein was localised on the cell membranes. In line with this research, other studies have demonstrated that mutant PrP molecules lacking both glycosylation sites are less efficiently trafficked to the cell surface compared to wild-type PrP (Zanusso et al., 1999; Ma and Lindquist, 2001; Salamat et al., 2011).

Zanusso *et al*. 1999 generated a neuroblastoma cell model of the Y145X mutation and reported that blocking the proteasomal degradation pathway using proteasomal inhibitors lead to the intracellular accumulation of PrP^{145X} in membrane-bound organelles, including the nucleus, endoplasmic reticulum and the Golgi apparatus (Zanusso et al., 1999).

Another study by Ma and Lindquist. 2001 demonstrated that endogenous PrP from neuroblastoma cells accumulated in the cytoplasm following treatment with a proteasome inhibitor whereas in untreated cells, wild-type PrP was localised on the cell surface (Ma and Lindquist, 2001). They also observed that in COS (monkey kidney) cells expressing PrP^{D177N} (analagous to the human D178N mutation), the truncated mutant protein accumulated in the cytoplasm and co-localised with the heat shock protein Hsc70 in the absence of the proteasome inhibitor (Ma and Lindquist, 2001) .

The mechanisms that lead to the retention of truncated mutant PrP molecules remain unclear, however experimental evidence suggests that glycosylation plays a role in trafficking PrP to the cell surface (Salamat et al., 2011). Salamat *et al*. 2011 generated a variety of Rov (rabbit kidney) cells lines expressing different PrP glycosylation mutations. They observed that PrP was localised on the cell surface in cells expressing monoglycosylated mutant PrP, whereas PrP was mainly localised intracellulary in cell lines expressing double PrP mutants with both glycosylation sites abolished. Cell surface expression of mutant PrP was restored in the cell line expressing double mutant PrP by introducing an artificial glycosylation site into the sequence (Salamat et al., 2011). This demonstrates that one glycan chain is sufficient to enable trafficking of PrP to the cell surface.

Altogether, these studies suggest that the altered trafficking of truncated mutant PrP molecules could be due to lack of glycosylation and the GPI anchor.

Therefore, the intracellular localisation of HuPrP 163X observed in the Y163X-129V CAD5 cell line may be due to the fact that this mutant protein lacks both glycans and a GPI anchor in line with previous research. The intracellular accumulation of truncated mutant PrP in the Golgi apparatus, endoplasmic reticulum and nucleus may alter the trafficking of other proteins that are essential for neuronal function. Further experiments need to be carried out to investigate the impact of intracellular accumulation of truncated mutant PrP molecules in neurons and other cell types involved in the pathogenesis of inherited prion diseases.

Final Conclusions

This is the first time that the Y163X mutation has been modelled in mice. Two novel mouse models of the human Y163X mutation have been generated using the conventional transgenic approach and the gene targeted approach. This thesis also attempted to model the Y163X mutation using CRISPR/Cas9 technology but unfortunately despite extensive attempts, a knock-in model could not be generated using this method. CRISPR PrP knock-out mice were generated which will be useful in the generation of future mouse models of inherited prion diseases using CRISPR/Cas9. During the screening process of the Y163X CRISPR knock-in lines, the neo cassette present in the F10_FVB/PrP null mice interefered with sequencing. Therefore in the future CRISPR founders could be mated to these CRISPR knock-out mice instead of F10_FVB/PrP null mice.

The pCAG-Y163X-129V transgenic and Y163X-129V KI lines both express HuPrP 163X at mRNA level. The mutant protein could not be detected by western blot which is likely due to the absence of post-translational modifications such as the addition of glycans or the GPI anchor. HuPrP 163X was detected using sandwich ELISAs which are more sensitive than western blots and variable levels of PrP immunoreactivity were observed in the pCAG transgenic lines in the brain and peripheral tissues.

This thesis has also demonstrated using cell lines that the trafficking of HuPrP 163X to the cell surface is impeded which results in the intracellular accumulation of the mutant protein. These findings in line with previous studies suggest that glycosylation and the GPI anchor influence the trafficking of PrP^{C} to the cell surface. Further research needs to be carried out to investigate the impact of the intracellular accumulation of HuPrP 163X on the disease pathogenesis.

9. Chapter 9: Future Work

In this thesis, transgenic and knock-in mice expressing HuPrP 163X have been generated. The Y163X knock-in mice are currently in long-term observation studies and they remain healthy. The pCAG-Y163X-129V lines are currently being expanded in order to produce mice for long-term observation experiments.

Abnormal PrP is deposited as amyloid in the CNS, peripheral tissues and cerebral blood vessels of patients with the *PRNP* Y163X mutation. Therefore in order for these mouse models to resemble the human disease, PrP amyloid should be detected in the brain and peripheral organs of the pCAG transgenic and knock-in mice. Future experiments will investigate spontaneous and seeded deposition of PrP amyloid in the Y163X transgenic and knock-in lines (alongside controls).

The established transgenic and knock-in Y163X lines will be further investigated and used to:

- Study the unique molecular pathogenesis associated with this novel disease.
- Test the prevention of neuroinvasion with small molecules and monoclonal antibodies.
- Test the prevention of amyloid formation with compounds that inhibit amyloidosis.
- Determine the transmissibility of this disease.

Future experiments with Y163X pCAG transgenics and knock-in lines

- Immunohistochemical analysis of CNS and peripheral tissues* collected from long-term observation experiments at defined time points (*Brain, heart, liver, kidney, spleen, lymph nodes, small intestine, large intestine and cecum).
- Assessment of peripheral neuropathy- Nerve conduction velocity testing.
- Seeding experiments- Attempt to prime amyloid deposition by inoculating mice with homogenates prepared from Y163X patient brains.
- Assess protein expression levels using alternative methods such as slot blotting using nylon membranes in-gel immunodetection.
- Generate primary neuronal cultures to investigate trafficking of HuPrP Y163X and stain neurons with markers of the Golgi apparatus and endoplasmic reticulum to determine if the mutant protein accumulates in other subcellular compartments as described in the literature (Zanusso et al., 1999) (Ivanova et al., 2001) (Salamat et al., 2011).

In summary, two novel mouse models of the human Y163X mutation have been generated. The transgenic and knock-in models are both powerful tools that can be used to elucidate the cellular and molecular mechanisms involved in the pathogenesis of this disease. New therapies for inherited prion diseases could also be tested in these mice to assess their potential efficacy and safety before trialling in humans.

10. Chapter 10: References

Abdelmohsen K, Gorospe M (2010) Posttranscriptional regulation of cancer traits by HuR. Wiley Interdisciplinary Reviews: RNA 1:214–229.

Adikusuma F, Piltz S, Corbett MA, Turvey M, McColl SR, Helbig KJ, Beard MR, Hughes J, Pomerantz RT, Thomas PQ (2018) Large deletions induced by Cas9 cleavage. Nature 560:E8–E9.

Aird EJ, Lovendahl KN, St. Martin A, Harris RS, Gordon WR (2018) Increasing Cas9-mediated homology-directed repair efficiency through covalent tethering of DNA repair template. Communications Biology 1:1–6.

Apetri AC, Surewicz K, Surewicz WK (2004) The effect of disease-associated mutations on the folding pathway of human prion protein. The Journal of biological chemistry 279:18008–18014

Asante EA, Gowland I, Grimshaw A, Linehan JM, Smidak M, Houghton R, Osiguwa O, Tomlinson A, Joiner S, Brandner S, Wadsworth JDF, Collinge J (2009) Absence of spontaneous disease and comparative prion susceptibility of transgenic mice expressing mutant human prion proteins. Journal of General Virology 90:546–558.

Asante EA, Grimshaw A, Smidak M, Jakubcova T, Tomlinson A, Jeelani A, Hamdan S, Powell C, Joiner S, Linehan JM, Brandner S, Wadsworth JDF, Collinge J (2015) Transmission Properties of Human PrP 102L Prions Challenge the Relevance of Mouse Models of GSS. PLoS Pathogens 11 (7): e1004953. .

Asante EA, Linehan JM, Desbruslais M, Joiner S, Gowland I, Wood AL, Welch J, Hill AF, Lloyd SE, Wadsworth JDF, Collinge J (2002) BSE prions propagate as either variant CJD-like or sporadic CJD-like prion strains in transgenic mice expressing human prion protein. EMBO Journal 21:6358–6366.

Asante EA, Linehan JM, Smidak M, Tomlinson A, Grimshaw A, Jeelani A, Jakubcova T, Hamdan S, Powell C, Brandner S, Wadsworth JDF, Collinge J (2013) Inherited Prion Disease A117V Is Not Simply a Proteinopathy but Produces Prions Transmissible to Transgenic Mice Expressing Homologous Prion Protein. PLoS Pathogens 9 (9):e1003643 .

Asante EA, Linehan JM, Tomlinson A, Jakubcova T, Hamdan S, Grimshaw A, Smidak M, Jeelani A, Nihat A, Mead S, Brandner S, Wadsworth JDF, Collinge J (2020) Spontaneous generation of prions and transmissible PrP amyloid in a humanised transgenic mouse model of A117V GSS. PLoS Biology 18:e3000725.

Bagyinszky E, Van Giau V, Youn YC, An SSA, Kim S (2018) Characterization of mutations in prnp (PRION) gene and their possible roles in neurodegenerative diseases. Neuropsychiatric Disease and Treatment 14:2067–2085.

Beck JA, Mead S, Campbell TA, Dickinson A, Wientjens DPMW, Croes EA, Van Duijn CM, Collinge J (2001) Two-octapeptide repeat deletion of prion protein associated with rapidly progressive dementia. Neurology 57:354–356.

Belay ED (1999) Transmissible Spongiform Encephalopathies in Humans. Annual Review of Microbiology 53:283–314.

Béranger F, Mangé A, Goud B, Lehmann S (2002) Stimulation of PrPC retrograde transport toward the endoplasmic reticulum increases accumulation of PrPSc in prion-infected cells. Journal of Biological Chemistry 277:38972–38977.

Béringue V, Le Dur A, Tixador P, Reine F, Lepourry L, Perret-Llaudet A, Haik S, Vilotte JL, Fontés M, Laude H (2008) Prominent and persistent extraneural infection in human PrP transgenic mice infected with variant CJD. PLoS One 9;3 (1): e1419.

Beringue V, Mallinson G, Kaisar M, Tayebi M, Sattar Z, Jackson G, Anstee D, Collinge J, Hawke S (2003) Regional heterogeneity of cellular prion protein isoforms in the mouse brain. Brain 126:2065–2073.

Bian J et al. (2021) Adaptive selection of a prion strain conformer corresponding to established North American CWD during propagation of novel emergent Norwegian strains in mice expressing elk or deer prion protein. PLoS Pathogens 17:e1009748.

Bian J, Christiansen JR, Moreno JA, Kane SJ, Khaychuk V, Gallegos J, Kim S, Telling GC (2019) Primary structural differences at residue 226 of deer and elk PrP dictate selection of distinct CWD prion strains in gene-targeted mice. Proceedings of the National Academy of Sciences of the United States of America 116:12478–12487.

Bishop M, Hart P, Aitchison L, Baybutt H, Plinston C, Thomson V, Tuzi N, Head M, Ironside J, Will R, Manson J (2006) Predicting susceptibility and incubation time of human-to-human transmission of vCJD. Lancet Neurology 5:393–398.

Bollen Y, Post J, Koo BK, Snippert HJG (2018) How to create state-of-the-art genetic model systems: Strategies for optimal CRISPR-mediated genome editing. Nucleic Acids Research 46:6435–6454.

Bouabe H, Okkenhaug K (2013a) Gene targeting in mice: A review. In: Bailer S., Lieber D. (eds) Virus-Host Interactions. Methods in Molecular Biology (Methods and Protocols), (pp 315-316). Humana Press, Totowa, NJ.

Bouabe H, Okkenhaug K (2013b) A protocol for construction of gene targeting vectors and generation of homologous recombinant embryonic stem cells. In: Bailer S., Lieber D. (eds) Virus-Host Interactions. Methods in Molecular Biology (Methods and Protocols), (pp. 337-354). Humana Press, Totowa, NJ.

Bouybayoune I et al. (2015) Transgenic Fatal Familial Insomnia Mice Indicate Prion Infectivity-Independent Mechanisms of Pathogenesis and Phenotypic Expression of Disease. PLoS Pathogens 11 (4): e1004796.

Brandner S, Jaunmuktane Z (2017) Prion disease: experimental models and reality. Acta Neuropathologica 133:197–222.

Breitling J, Aebi M (2013) N-linked protein glycosylation in the endoplasmic reticulum. Cold Spring Harbor Perspectives in Biology 5:a013359.

Brown DR, Besinger A (1998) Prion protein expression and superoxide dismutase activity. Biochemical Journal 334 (Pt 2):423–429.

Brown DR, Qin K, Herms JW, Madlung A, Manson J, Strome R, Fraser PE, Kruck T, Von Bohlen A, Schulz-Schaeffer W, Giese A, Westaway D, Kretzschmar H (1997a) The cellular prion protein binds copperin vivo. Nature 390:684–687.

Brown DR, Schulz-Schaeffer WJ, Schmidt B, Kretzschmar HA (1997b) Prion protein-deficient cells show altered response to oxidative stress due to decreased SOD-1 activity. Experimental Neurology 146:104–112.

Bryda EC, Pearson M, Agca Y, Bauer BA (2006) Method for detection and identification of multiple chromosomal integration sites in transgenic animals created with lentivirus. BioTechniques 41:715–719.

Büeler H, Aguzzi A, Sailer A, Greiner R-A, Autenried P, Aguet M, Weissmann C (1993) Mice devoid of PrP are resistant to scrapie. Cell 73:1339–1347.

Büeler H, Fischer M, Lang Y, Bluethmann H, Lipp HP, Dearmond SJ, Prusiner SB, Aguet M, Weissmann C (1992) Normal development and behaviour of mice lacking the neuronal cell-surface PrP protein. Nature 356:577–582.

Cancellotti E, Wiseman F, Tuzi NL, Baybutt H, Monaghan P, Aitchison L, Simpson J, Manson JC (2005) Altered glycosylated PrP proteins can have different neuronal trafficking in brain but do not acquire scrapie-like properties. Journal of Biological Chemistry 280:42909–42918.

Capellari S, Strammiello R, Saverioni D, Kretzschmar H, Parchi P (2011) Genetic Creutzfeldt-Jakob disease and fatal familial insomnia: Insights into phenotypic variability and disease pathogenesis. Acta Neuropathologica 121:21–37.

Carlson GA, Kingsbury DT, Goodman PA, Coleman S, Marshall ST, DeArmond S, Westaway D, Prusiner SB (1986) Linkage of prion protein and scrapie incubation time genes. Cell 46:503–511.

Chandler R (1961) Encephalopathy in mice produced by inoculation with scrapie brain material. The Lancet 277:1378–1379.

Charpentier E, Richter H, van der Oost J, White MF (2015) Biogenesis pathways of RNA guides in archaeal and bacterial CRISPR-Cas adaptive immunity. FEMS Microbiology Reviews 39:428–441.

Chen SG, Parchi P, Brown P, Capellari S, Zou W, Cochran EJ, Vnencak-Jones CL, Julien J, Vital C, Mikol J, Lugaresi E, Autilio-Gambetti L, Gambetti P (1997) Allelic origin of the abnormal prion protein isoform in familial prion diseases. Nature Medicine 3:1009–1015.

Chen SG, Teplow DB, Parchi P, Teller JK, Gambetti P, Autilio-Gambetti L (1995) Truncated forms of the human prion protein in normal brain and in prion diseases. Journal of Biological Chemistry 270:19173–19180.

Chesebro B, Race B, Meade-White K, LaCasse R, Race R, Klingeborn M, Striebel J, Dorward D, McGovern G, Jeffrey M (2010) Fatal transmissible amyloid encephalopathy: a new type of prion disease associated with lack of prion protein membrane anchoring. PLoS Pathogens 6:e1000800.

Chesebro B, Trifilo M, Race R, Meade-White K, Teng C, LaCasse R, Raymond L, Favara C, Baron G, Priola S, Caughey B, Masliah E, Oldstone M (2005) Medicine: Anchorless prion protein results in infectious amyloid disease without clinical scrapie. Science 3;308 (5727): 1435-1439.

Cho A, Haruyama N, Kulkarni AB (2009) Generation of transgenic mice. Current protocols in cell biology 42:11–19.

Codner GF et al. (2018) Application of long single-stranded DNA donors in genome editing: Generation and validation of mouse mutants. BMC Biology 16:1–16.

Colling SB, Collinge J, Jefferys JGR (1996) Hippocampal slices from prion protein null mice: Disrupted Ca2+-activated K+ currents. Neuroscience Letters 209:49–52.

Collinge J (2001) Prion diseases of humans and animals: Their causes and molecular basis. Annual Review of Neuroscience 24:519–550.

Collinge J (2005) Molecular neurology of prion disease. Journal of Neurology, Neurosurgery and Psychiatry 76 (7): 906-919.

Collinge J (2016) Mammalian prions and their wider relevance in neurodegenerative diseases. Nature 539:217–226.

Collinge J, Clarke AR (2007) A general model of prion strains and their pathogenicity. Science 318:930–936.

Collinge J, Palmer MS, Sidle KCL, Hill AF, Gowland I, Meads J, Asante E, Bradley R, Doey LJ, Lantos PL (1995) Unaltered susceptibility to BSE in transgenic mice expressing human prion protein. Nature 378:779–783.

Collinge J, Sidle KCL, Meads J, Ironside J, Hill AF (1996) Molecular analysis of prion strain variation and the aetiology of "new variant" CJD. Nature 383:685–690.

Collinge J, Whittington MA, Sidle KC, Smith CJ, Palmer MS, Clarke AR, Jefferys JG (1994) Prion protein is necessary for normal synaptic function. Nature 370:295–297.

Croes EA, Theuns J, Houwing-Duistermaat JJ, Dermaut B, Sleegers K, Roks G, Van Den Broeck M, Van Harten B, Van Swieten JC, Cruts M, Van Broeckhoven C, Van Duijn CM (2004) Octapeptide repeat insertions in the prion protein gene and early onset dementia. Journal of Neurology, Neurosurgery and Psychiatry 75:1166–1170.

Cronier S, Gros N, Tattum MH, Jackson GS, Clarke AR, Collinge J, Wadsworth JDF (2008) Detection and characterization of proteinase K-sensitive disease-related prion protein with thermolysin. Biochemical Journal 416:297–305.

Curtis J, Errington M, Bliss T, Voss K, MacLeod N (2003) Age-dependent loss of PTP and LTP in the hippocampus of PrP-null mice. Neurobiology of Disease 13:55–62.

D'Aignaux JH, Cousens SN, Delasnerie-Lauprêtre N, Brandel JP, Salomon D, Laplanche JL, Hauw JJ, Alpérovitch A (2002) Analysis of the geographical distribution of sporadic Creutzfeldt-Jakob disease in France between 1992 and 1998. International Journal of Epidemiology 31:490–495.

Dickinson AG, Fraser H, Outram GW (1975) Scrapie incubation time can exceed natural lifespan. Nature 256 (5520):732-733.

Dossena S et al. (2008) Mutant Prion Protein Expression Causes Motor and Memory Deficits and Abnormal Sleep Patterns in a Transgenic Mouse Model. Neuron 60:598–609.

Duffy P (1974) Possible person-to-person transmission of Creutzfeld-Jakob disease. N Engl J Med 290:692–693.

Erwood S, Gu B (2020) Embryo-based large fragment knock-in in mammals: Why, how and what's next. Genes 11:140.

Feng Y-Q, Lorincz MC, Fiering S, Greally JM, Bouhassira EE (2001) Position Effects Are Influenced by the Orientation of a Transgene with Respect to Flanking Chromatin. Molecular and Cellular Biology 1;21 (1): 298-309.

Fischer A, Manske K, Seissler J, Wohlleber D, Simm N, Wolf-van Buerck L, Knolle P, Schnieke A, Fischer K (2020) Cytokine-inducible promoters to drive dynamic transgene expression: The "Smart Graft" strategy. Xenotransplantation 27:e12634.

Flechsig E, Shmerling D, Hegyi I, Raeber AJ, Fischer M, Cozzio A, Von Mering C, Aguzzi A, Weissmann C (2000) Prion protein devoid of the octapeptide repeat region restores susceptibility to scrapie in PrP knockout mice. Neuron 27:399–408.

Fong JC, Rojas JC, Bang J, Legati A, Rankin KP, Forner S, Miller ZA, Karydas AM, Coppola G, Grouse CK, Ralph J, Miller BL, Geschwind MD (2016) Genetic prion disease caused by PRNP Q160X mutation presenting with an orbitofrontal syndrome, cyclic diarrhea, and peripheral neuropathy. Journal of Alzheimer's Disease 55:249–258.

Gajdusek DC, Zigas V (1959) Kuru: clinical, pathological and epidemiological study of an acute progressive degenerative disease of the central nervous system among natives of the Eastern Highlands of New Guinea. The American journal of medicine 26:442–469.

Gelpi E, Kovacs GG, Ströbel T, Koperek O, Voigtländer T, Liberski PP, Budka H (2005) Prion disease with a 144 base pair insertion: Unusual cerebellar prion protein immunoreactivity. Acta Neuropathologica 110:513–519.

Gerstmann J, Sträussler E, Scheinker I (1936) Über eine eigenartige hereditär- familiäre Erkrankung des Zentralnervensystems. Zeitschrift für die gesamte Neurologie und Psychiatrie 154:736–762.

Ghetti B, Piccardo P, Spillantini MG, Ichimiya Y, Porro M, Perini F, Kitamoto T, Tateishi J, Seiler C, Frangione B, Bugiani O, Giaccone G, Prelli F, Goedert M, Dlouhy SR, Tagliavini F (1996) Vascular variant of prion protein cerebral amyloidosis with τ-positive neurofibrillary tangles: The phenotype of the stop codon 145 mutation in PRNP. Proceedings of the National Academy of Sciences of the United States of America 93:744–748.

Gleditzsch D, Pausch P, Müller-Esparza H, Özcan A, Guo X, Bange G, Randau L (2019) PAM identification by CRISPR-Cas effector complexes: diversified mechanisms and structures. RNA Biology 16:504–517.

Goldfarb LG et al. (1992) Fatal familial insomnia and familial Creutzfeldt-Jakob disease: Disease phenotype determined by a DNA polymorphism. Science 258:806–808.

Goldgaber D, Goldfarb LG, Brown P, Asher DM, Brown WT, Lin S, Teener JW, Feinstone SM, Rubenstein R, Kascsak RJ, Boellaard JW, Gajdusek DC (1989) Mutations in familial Creutzfeldt-Jakob disease and Gerstmann-Sträussler-Scheinker's syndrome. Experimental Neurology 106:204–206.

Goold R, McKinnon C, Rabbanian S, Collinge J, Schiavo G, Tabrizi SJ (2013) Alternative fates of newly formed PrPSc upon prion conversion on the plasma membrane. Journal of Cell Science 126:3552–3562.

Goold R, Rabbanian S, Sutton L, Andre R, Arora P, Moonga J, Clarke AR, Schiavo G, Jat P, Collinge J, Tabrizi SJ (2011) Rapid cell-surface prion protein conversion revealed using a novel cell system. Nature Communications 2:1–11.

Graner E, Mercadante AF, Zanata SM, Forlenza O V, Cabral ALB, Veiga SS, Juliano MA, Roesler R, Walz R, Minetti A, Izquierdo I, Martins VR, Brentani RR (2000a) Cellular prion protein binds laminin and mediates neuritogenesis. Molecular Brain Research 76:85–92.

Graner E, Mercadante AF, Zanata SM, Martins VR, Jay DG, Brentani RR (2000b) Laminin-induced PC-12 cell differentiation is inhibited following laser inactivation of cellular prion protein. FEBS Letters 482:257–260.

Griffith JS (1967) Self-replication and scrapie. Nature 215:1043–1044.

Hainfellner JA, Brantner-Inthaler S, Cervenáková L, Brown P, Kitamoto T, Tateishi J, Diringer H, Liberski PP, Regele H, Feucht M, Mayr N, Wessely P, Summer K, Seitelberger F, Budka H (1995) The Original Gerstmann-Sträussler-Scheinker Family of Austria: Divergent Clinicopathological Phenotypes but Constant PrP Genotype. Brain Pathology 5:201–211.

Hall B, Cho A, Limaye A, Cho K, Khillan J, Kulkarni AB (2018) Genome Editing in Mice Using CRISPR/Cas9 Technology. Current Protocols in Cell Biology 81:e57.

Hartsough GR, Burger D (1965) Encephalopathy of mink: I. epizootiologic and clinical observations. Journal of Infectious Diseases 115:387–392.

Hashimoto M, Yamashita Y, Takemoto T (2016) Electroporation of Cas9 protein/sgRNA into early pronuclear zygotes generates non-mosaic mutants in the mouse. Developmental biology 418:1–9.

Herms J, Tings T, Gall S, Madlung A, Giese A, Siebert H, Peter Schürmann O, Windl T, Brose N, Kretzschmar H (1999) Evidence of presynaptic location and function of the prion protein. Journal of Neuroscience 19:8866–8875.

Hill AF, Joiner S, Beck JA, Campbell TA, Dickinson A, Poulter M, Wadsworth JDF, Collinge J (2006) Distinct glycoform ratios of protease resistant prion protein associated with PRNP point mutations. Brain 129:676–685.

Hill AF, Joiner S, Wadsworth JDF, Sidle KCL, Bell JE, Budka H, Ironside JW, Collinge J (2003) Molecular classification of sporadic Creutzfeldt-Jakob disease. Brain 126:1333–1346.

Horii T, Hatada I (2016) Challenges to increasing targeting efficiency in genome engineering. Journal of Reproduction and Development 62:7–9.

Hsiao KK, Scott M, Foster D, Groth DF, Dearmond SJ, Prusiner SB (1990) Spontaneous neurodegeneration in transgenic mice with mutant prion protein. Science 14;250 (4987): 1587-1590.

Hsu PD, Lander ES, Zhang F (2014) Development and applications of CRISPR-Cas9 for genome engineering. Cell 157:1262–1278.

Hudson AJ, Farrell MA, Kalnins R, Kaufmann JCE (1983) Gerstmann-Sträussler-Scheinker disease with coincidental familial onset. Annals of Neurology 14:670–678.

Imran M, Mahmood S (2011) An overview of animal prion diseases. Virology journal 8:493.

Ivanova L, Barmada S, Kummer T, Harris DA (2001) Mutant Prion Proteins Are Partially Retained in the Endoplasmic Reticulum. Journal of Biological Chemistry 276:42409–42421.

Jackson WS, Borkowski AW, Faas H, Steele AD, King OD, Watson N, Jasanoff A, Lindquist S (2009) Spontaneous Generation of Prion Infectivity in Fatal Familial Insomnia Knockin Mice. Neuron 63 (4): 438-450.

Jackson WS, Borkowski AW, Watson NE, King OD, Faas H, Jasanoff A, Lindquist S (2013) Profoundly different prion diseases in knock-in mice carrying single PrP codon substitutions associated with human diseases. Proceedings of the National Academy of Sciences 110 (36): 14759-14764

Jackson WS, Krost C (2014) Peculiarities of Prion Diseases. PLoS Pathogens 10 (11):e1004451.

Jakob A (1921) Über eigenartige erkrankungen des zentralnervensystems mit bemerkenswertem anatomischen befunde. Zeitschrift für die gesamte Neurologie und Psychiatrie 64:147–228.

Jansen C, Parchi P, Capellari S, Vermeij AJ, Corrado P, Baas F, Strammiello R, Van Gool WA, Van Swieten JC, Rozemuller AJM (2010) Prion protein amyloidosis with divergent phenotype associated with two novel nonsense mutations in PRNP. Acta Neuropathologica 119:189–197.

Jeffrey M, González L (2007) Classical sheep transmissible spongiform encephalopathies: Pathogenesis, pathological phenotypes and clinical disease. Neuropathology and Applied Neurobiology 33:373–394.

Jinek M, Chylinski K, Fonfara I, Hauer M, Doudna JA, Charpentier E (2012) A programmable dual-RNA-guided DNA endonuclease in adaptive bacterial immunity. Science 337:816–821.

Kaczmarczyk L, Jackson WS (2015) Astonishing advances in mouse genetic tools for biomedical research. Swiss Medical Weekly 18 (43).

Kaczmarczyk L, Mende Y, Zevnik B, Jackson WS (2016) Manipulating the prion protein gene sequence and expression levels with CRISPR/Cas9. PloS one 11:e0154604.

Khalili-Shirazi A, Kaisar M, Mallinson G, Jones S, Bhelt D, Fraser C, Clarke AR, Hawke SH, Jackson GS, Collinge J (2007) β-PrP form of human prion protein stimulates production of monoclonal antibodies to epitope 91-110 that recognise native PrPSc. Biochimica et Biophysica Acta - Proteins and Proteomics 1774:1438–1450.

Khalili-Shirazi A, Summers L, Linehan J, Mallinson G, Anstee D, Hawke S, Jackson GS, Collinge J (2005) PrP glycoforms are associated in a strain-specific ratio in native PrPSc. Journal of General Virology 86:2635–2644.

Kim MO, Takada LT, Wong K, Forner SA, Geschwind MD (2018) Genetic PrP prion diseases. Cold Spring Harbor Perspectives in Biology 10:a033134.

Kim S, Kim D, Cho SW, Kim J, Kim J-S (2014) Highly efficient RNA-guided genome editing in human cells via delivery of purified Cas9 ribonucleoproteins. Genome research 24:1012–1019.

King A, Doey L, Rossort M, Mead S, Collinge J, Lantos P (2003) Phenotypic variability in the brains of a family with a prion disease characterized by a 144-base pair insertion in the prion protein gene. Neuropathology and Applied Neurobiology 29:98–105.

Korth C, Kaneko K, Prusiner SB (2000) Expression of unglycosylated mutated prion protein facilitates PrP(Sc) formation in neuroblastoma cells infected with different prion strains. Journal of General Virology 81:2555–2563.

Kosti I, Jain N, Aran D, Butte AJ, Sirota M (2016) Cross-tissue Analysis of Gene and Protein Expression in Normal and Cancer Tissues. Scientific Reports 6:1–16.

Kovács GG, Trabattoni G, Hainfellner JA, Ironside JW, Knight RSG, Budka H (2002) Mutations of the prion protein gene: Phenotypic spectrum. Journal of Neurology 249:1567–1582.

Kuang E, Wan Q, Li X, Xu H, Zou T, Qi Y (2006) ER stress triggers apoptosis induced by Nogo-B/ASY overexpression. Experimental Cell Research 312:1983–1988.

Lahiri D, Pattnaik S, Bhat A, Dubey S, Biswas A, Roy BK (2019) Young-onset sporadic Creutzfeldt-Jakob disease with atypical phenotypic features: A case report. Journal of Medical Case Reports 13:163.

Lamas-Toranzo I, Galiano-Cogolludo B, Cornudella-Ardiaca F, Cobos-Figueroa J, Ousinde O, Bermejo-Álvarez P (2019) Strategies to reduce genetic mosaicism following CRISPR-mediated genome edition in bovine embryos. Scientific reports 9:1–8.

Lawson VA, Collins SJ, Masters CL, Hill AF (2005) Prion protein glycosylation. Journal of Neurochemistry 93:793–801.

Le QA, Tanihara F, Wittayarat M, Namula Z, Sato Y, Lin Q, Takebayashi K, Hirata M, Otoi T (2021) Comparison of the effects of introducing the CRISPR/Cas9 system by microinjection and electroporation into porcine embryos at different stages. BMC research notes 14:1–7.

Lee HS, Qi Y, Im W (2015) Effects of N-glycosylation on protein conformation and dynamics: Protein Data Bank analysis and molecular dynamics simulation study. Scientific Reports 5:8926.

Lee SH, Kim S, Hur JK (2018) CRISPR and target-specific DNA endonucleases for efficient DNA knock-in in eukaryotic genomes. Molecules and Cells 41:943–952.

Lugaresi E, Medori R, Montagna P, Baruzzi A, Cortelli P, Lugaresi A, Tinuper P, Zucconi M, Gambetti P (1986) Fatal Familial Insomnia and Dysautonomia with Selective Degeneration of Thalamic Nuclei. New England Journal of Medicine 315:997–1003 .

Ma J, Lindquist S (2001) Wild-type PrP and a mutant associated with prion disease are subject to retrograde transport and proteasome degradation. Proceedings of the National Academy of Sciences of the United States of America 98:14955–14960.

Mahal SP, Baker CA, Demczyk CA, Smith EW, Julius C, Weissmann C (2007) Prion strain discrimination in cell culture: The cell panel assay. Proceedings of the National Academy of Sciences of the United States of America 104:20908–20913.

Maier T, Güell M, Serrano L (2009) Correlation of mRNA and protein in complex biological samples. FEBS Letters 583:3966–3973.

Makrinou E, Collinge J, Antoniou M (2002) Genomic characterization of the human prion protein (PrP) gene locus. Mammalian Genome 13:696–703.

Manson JC, Jamieson E, Baybutt H, Tuzi NL, Barron R, McConnell I, Somerville R, Ironside J, Will R, Sy MS, Melton DW, Hope J, Bostock C (1999) A single amino acid alteration (101L) introduced into murine PrP dramatically alters incubation time of transmissible spongiform encephalopathy. EMBO Journal 18:6855–6864.

Marín-Moreno A, Espinosa JC, Torres JM (2020) Transgenic mouse models for the study of prion diseases. In: Progress in Molecular Biology and Translational Science 1;175: 147-177.

Masters CL, Gajdusek DC, Gibbs CJ (1981) Creutzfeldt-jakob disease virus isolations from the gerstmann-sträussler syndrome: With an analysis of the various forms of amyloid plaque deposition in the virus-induced spongiform encephalopathies. Brain 104:559–588.

McGowan JP (1922) Scrapie in sheep. Scott J Agric 5:365–375.

Mead S (2006) Prion disease genetics. European journal of human genetics : EJHG 14:273–281.

Mead S et al. (2013) A novel prion disease associated with diarrhea and autonomic neuropathy. The New England journal of medicine 369:1904–1914.

Mead S, Reilly MM (2015) A new prion disease: Relationship with central and peripheral amyloidoses. Nature Reviews Neurology 11:90–97.

Medori R, Montagna P, Tritschler HJ, LeBlanc A, Cortelli P, Tinuper P, Lugaresi E, Gambetti P (1992) Fatal familial insomnia: A second kindred with mutation of prion protein gene at codon 178. Neurology 42:669–670.

Meggendorfer F (1930) Klinische und genealogische Beobachtungen bei einem Fall von spastischer Pseudosklerose Jakobs. Zeitschrift für die gesamte Neurologie und Psychiatrie 128:337–341.

Mehravar M, Shirazi A, Nazari M, Banan M (2019) Mosaicism in CRISPR/Cas9-mediated genome editing. Developmental Biology 445:156–162.

Miura H, Gurumurthy CB, Sato T, Sato M, Ohtsuka M (2015) CRISPR/Cas9-based generation of knockdown mice by intronic insertion of artificial microRNA using longer single-stranded DNA. Scientific Reports 5:1–11.

Miura H, Quadros RM, Gurumurthy CB, Ohtsuka M (2018) Easi-CRISPR for creating knock-in and conditional knockout mouse models using long ssDNA donors. Nature Protocols 13:195–215.

Miura T, Sasaki S, Toyama A, Takeuchi H (2005) Copper reduction by the octapeptide repeat region of prion protein: pH dependence and implications in cellular copper uptake. Biochemistry 44:8712–8720.

Mizuno S, Dinh TTH, Kato K, Mizuno-Iijima S, Tanimoto Y, Daitoku Y, Hoshino Y, Ikawa M, Takahashi S, Sugiyama F, Yagami KI (2014) Simple generation of albino C57BL/6J mice with G291T mutation in the tyrosinase gene by the CRISPR/Cas9 system. Mammalian Genome 25:327–334.

Modrzejewski D, Hartung F, Lehnert H, Sprink T, Kohl C, Keilwagen J, Wilhelm R (2020) Which Factors Affect the Occurrence of Off-Target Effects Caused by the Use of CRISPR/Cas: A Systematic Review in Plants. Frontiers in Plant Science 11:1838.

Modrzejewski D, Hartung F, Sprink T, Krause D, Kohl C, Wilhelm R (2019) What is the available evidence for the range of applications of genome-editing as a new tool for plant trait modification and the potential occurrence of associated off-target effects: A systematic map. Environmental Evidence 8:1–33.

Morales R (2017) Prion strains in mammals: Different conformations leading to disease. PLoS Pathogens 13(7):e1006323.

Mou H, Kennedy Z, Anderson DG, Yin H, Xue W (2015) Precision cancer mouse models through genome editing with CRISPR-Cas9. Genome Medicine 7(1):1-11.

Nishina KA, Supattapone S (2007) Immunodetection of glycophosphatidylinositol-anchored proteins following treatment with phospholipase C. Analytical biochemistry 363:318–320.

Noguchi A, Takekawa N, Einarsdottir T, Koura M, Noguchi Y, Takano K, Yamamoto Y, Matsuda J, Suzuki O (2004) Chromosomal mapping and zygosity check of transgenes based on flanking genome sequences determined by genomic walking. Experimental Animals 53:103–111.

Okamoto S, Amaishi Y, Maki I, Enoki T, Mineno J (2019) Highly efficient genome editing for single-base substitutions using optimized ssODNs with Cas9-RNPs. Scientific Reports 9:1–11.

Oliver D, Yuan S, McSwiggin H, Yan W (2015) Pervasive genotypic mosaicism in founder mice derived from genome editing through pronuclear injection. PloS one 10:e0129457.

Owen F, Poulter M, Shah T, Collinge J, Lofthouse R, Baker H, Ridley R, McVey J, Crow TJ (1990) An in-frame insertion in the prion protein gene in familial Creutzfeldt-Jakob disease. Molecular Brain Research 7:273–276.

Pal A, Levy Y (2019) Structure, stability and specificity of the binding of ssDNA and ssRNA with proteins. PLoS Computational Biology 15:1–32.

Parchi P, Castellani R, Capellari S, Ghetti B, Young K, Chen SG, Farlow M, Dickson DW, Sima AAF, Trojanowski JQ (1996) Molecular basis of phenotypic variability in sporadc creudeldt-jakob disease. Annals of neurology 39:767–778.

Parchi P, Castellani R, Cortelli P, Montagna P, Chen SG, Petersen RB, Manetto V, Vnencak-Jones CL, McLean MJ, Sheller JR, Lugaresi E, Autilio-Gambetti L, Gambetti P (1995) Regional distribution of protease-resistant prion protein in fatal familial insomnia. Annals of Neurology 38:21–29.

Parchi P, Giese A, Capellari S, Brown P, Schulz-Schaeffer W, Windl O, Zerr I, Budka H, Kopp N, Piccardo P (1999) Classification of sporadic Creutzfeldt-Jakob disease based on molecular and phenotypic analysis of 300 subjects. Annals of neurology 46:224–233.

Parchi P, Strammiello R, Notari S, Giese A, Langeveld JPM, Ladogana A, Zerr I, Roncaroli F, Cras P, Ghetti B (2009) Incidence and spectrum of sporadic Creutzfeldt–Jakob disease variants with mixed phenotype and co-occurrence of PrP Sc types: an updated classification. Acta neuropathologica 118:659–671.

Parikh BA, Beckman DL, Patel SJ, White JM, Yokoyama WM (2015) Detailed phenotypic and molecular analyses of genetically modified mice generated by CRISPR-Cas9-mediated editing. PLoS ONE 10:e0116484.

Pastrana MA, Sajnani G, Onisko B, Castilla J, Morales R, Soto C, Requena JR (2006) Isolation and characterization of a proteinase K-sensitive PrPSc fraction. Biochemistry 45:15710–15717.

Pear WS, Nolan GP, Scott ML, Baltimore D (1993) Production of high-titer helper-free retroviruses by transient transfection. Proceedings of the National Academy of Sciences of the United States of America 90:8392–8396.

Perl K, Ushakov K, Pozniak Y, Yizhar-Barnea O, Bhonker Y, Shivatzki S, Geiger T, Avraham KB, Shamir R (2017) Reduced changes in protein compared to mRNA levels across non-proliferating tissues. BMC genomics 18:1–14.

Petersen RB, Parchi P, Richardson SL, Urig CB, Gambetti P (1996) Effect of the D178N mutation and the codon 129 polymorphism on the metabolism of the prion protein. Journal of Biological Chemistry 271:12661–12668.

Piccardo P et al. (1998) Phenotypic variability of Gerstmann-Straussler-Scheinker disease is associated with prion protein heterogeneity. Journal of Neuropathology and Experimental Neurology 57:979–988.

Piccardo P, Liepnieks JJ, William A, Dlouhy SR, Farlow MR, Young K, Nochlin D, Bird TD, Nixon RR, Ball MJ, DeCarli C, Bugiani O, Tagliavini F, Benson MD, Ghetti B (2001) Prion proteins with different conformations accumulate in Gerstmann-Sträussler-Scheinker disease caused by A117V and F198S mutations. American Journal of Pathology 158:2201–2207.

Poggiolini I, Saverioni D, Parchi P (2013) Prion protein misfolding, strains, and neurotoxicity: An update from studies on mammalian prions. International Journal of Cell Biology 2013:910314-910234.

Poulter M, Baker HF, Frith CD, Leach M, Lofthouse R, Ridley RM, Shah T, Owen F, Collinge J, Brown J, Hardy J, Mullan MJ, Harding AE, Bennett C, Doshi R, Crow TJ (1992) Inherited prion disease with 144 base pair gene insertion: 1. Genealogical and molecular studies. Brain 115:675–685.

Privat N, Laffont-Proust I, Faucheux BA, Sazdovitch V, Frobert Y, Laplanche J-L, Grassi J, Hauw J-J, Haïk S (2008) Human prion diseases: from antibody screening to a standardized fast immunodiagnosis using automation. Modern Pathology 21:140–149.

Prusiner SB (1982) Novel proteinaceous infectious particles cause scrapie. Science 216:136–144.

Prusiner SB (1998) Prions. Proceedings of the National Academy of Sciences 95:13363–13383.

Prusiner SB, Cochran SP, Downey DE, Groth DF (1981) Determination of scrapie agent titer from incubation period measurements in hamsters. Advanced Experimental Biology 1981;134:385-399

Prusiner SB, Cochran SP, Groth DF, Downey DE, Bowman KA, Martinez HM (1982) Measurement of the scrapie agent using an incubation time interval assay. Annals of Neurology 11(4): 253-358.

Prusiner SB, Scott M, Foster D, Pan KM, Groth D, Mirenda C, Torchia M, Yang SL, Serban D, Carlson GA, Hoppe PC, Westaway D, DeArmond SJ (1990) Transgenetic studies implicate interactions between homologous PrP isoforms in scrapie prion replication. Cell 63:673–686.

Puig B, Altmeppen HC, Linsenmeier L, Chakroun K, Wegwitz F, Piontek UK, Tatzelt J, Bate C, Magnus T, Glatzel M (2019) GPI-anchor signal sequence influences PrP C sorting, shedding and signalling, and impacts on different pathomechanistic aspects of prion disease in mice. PLoS Pathogens 15:e1007520.

Quadros RM et al. (2017) Easi-CRISPR: A robust method for one-step generation of mice carrying conditional and insertion alleles using long ssDNA donors and CRISPR ribonucleoproteins. Genome Biology 18:1–15.

Ranawakage DC, Okada K, Sugio K, Kawaguchi Y, Kuninobu-Bonkohara Y, Takada T, Kamachi Y (2021) Efficient CRISPR-Cas9-Mediated Knock-In of Composite Tags in Zebrafish Using Long ssDNA as a Donor. Frontiers in Cell and Developmental Biology 2021:1926.

Rao RSP, Wollenweber B (2010) Do N-glycoproteins have preference for specific sequons? Bioinformation 5:208–212.

Reily C, Stewart TJ, Renfrow MB, Novak J (2019) Glycosylation in health and disease. Nature Reviews Nephrology 15:346–366.

Renner C, Fiori S, Fiorino F, Landgraf D, Deluca D, Mentler M, Grantner K, Parak FG, Kretzschmar H, Moroder L (2004) Micellar Environments Induce Structuring of the N-Terminal Tail of the Prion Protein. Biopolymers 73:421–433.

Roth TL et al. (2018) Reprogramming human T cell function and specificity with non-viral genome targeting. Nature 559:405–409.

Roth Z, Yehezkel G, Khalaila I (2012) Identification and Quantification of Protein Glycosylation. International Journal of Carbohydrate Chemistry 2012:1–10.

Saayman S, Ali SA, Morris K V, Weinberg MS (2015) The therapeutic application of CRISPR/Cas9 technologies for HIV. Expert Opinion on Biological Therapy 15:819–830.

Sadowski MJ, Pankiewicz J, Prelli F, Scholtzova H, Spinner DS, Kascsak RB, Kascsak RJ, Wisniewski T (2009) Anti-PrP Mab 6D11 suppresses PrPSc replication in prion infected myeloid precursor line FDC-P1/22L and in the lymphoreticular system in vivo. Neurobiology of Disease 34:267–278.

Safar J, Wille H, Itri V, Groth D, Serban H, Torchia M, Cohen FE, Prusiner SB (1998) Eight prion strains have PrPSc molecules with different conformations. Nature medicine 4:1157–1165.

Salamat MK, Dron M, Chapuis J, Langevin C, Laude H (2011) Prion Propagation in Cells Expressing PrP Glycosylation Mutants. Journal of Virology 85:3077–3085.

Salsman J, Masson J-Y, Orthwein A, Dellaire G (2017) CRISPR/Cas9 Gene Editing: From Basic Mechanisms to Improved Strategies for Enhanced Genome Engineering In Vivo. Current Gene Therapy 17:263–274.

Sandberg MK, Al-Doujaily H, Sharps B, Clarke AR, Collinge J (2011) Prion propagation and toxicity in vivo occur in two distinct mechanistic phases. Nature 470:540–542.

Sandberg MK, Al-Doujaily H, Sharps B, De Oliveira MW, Schmidt C, Richard-Londt A, Lyall S, Linehan JM, Brandner S, Wadsworth JDF (2014) Prion neuropathology follows the

accumulation of alternate prion protein isoforms after infective titre has peaked. Nature communications 5 (1):1-7.

Santuccione A, Sytnyk V, Leshchyns'ka I, Schachner M (2005) Prion protein recruits its neuronal receptor NCAM to lipid rafts to activate p59fyn and to enhance neurite outgrowth. Journal of Cell Biology 169:341–354.

Schmitz M, Dittmar K, Llorens F, Gelpi E, Ferrer I, Schulz-Schaeffer WJ, Zerr I (2017) Hereditary Human Prion Diseases: an Update. Molecular Neurobiology 54:4138–4149.

Scott M, Foster D, Mirenda C, Serban D, Coufal F, Wälchli M, Torchia M, Groth D, Carlson G, DeArmond SJ, Westaway D, Prusiner SB (1989) Transgenic mice expressing hamster prion protein produce species-specific scrapie infectivity and amyloid plaques. Cell 59:847–857.

Shin HY, Wang C, Lee HK, Yoo KH, Zeng X, Kuhns T, Yang CM, Mohr T, Liu C, Hennighausen L (2017) CRISPR/Cas9 targeting events cause complex deletions and insertions at 17 sites in the mouse genome. Nature Communications 8:1–10.

Singh P, Schimenti JC, Bolcun-Filas E (2015) A mouse geneticist's practical guide to CRISPR applications. Genetics 199:1–15.

Srikantan S, Gorospe M (2012) HuR function in disease. Frontiers in Bioscience 17:189–205.

Stöckel J, Safar J, Wallace AC, Cohen FE, Prusiner SB (1998) Prion protein selectively binds copper(II) ions. Biochemistry 37:7185–7193.

Stöhr J, Watts JC, Legname G, Oehler A, Lemus A, Nguyen HOB, Sussman J, Wille H, DeArmond SJ, Prusiner SB, Giles K (2011) Spontaneous generation of anchorless prions in transgenic mice. Proceedings of the National Academy of Sciences of the United States of America 108:21223–21228.

Taraboulos A, Scott M, Semenov A, Avraham D, Laszlo L, Prusiner SB (1995) Cholesterol depletion and modification of COOH-terminal targeting sequence of the prion protein inhibit formation of the scrapie isoform. Journal of Cell Biology 129:121–132.

Tattum MH, Jones S, Pal S, Khalili-Shirazi A, Collinge J, Jackson GS (2010) A highly sensitive immunoassay for the detection of prion-infected material in whole human blood without the use of proteinase K. Transfusion 50:2619–2627.

Telling GC, Parchi P, DeArmond SJ, Cortelli P, Montagna P, Gabizon R, Mastrianni J, Lugaresi E, Gambetti P, Prusiner SB (1996) Evidence for the conformation of the pathologic isoform of the prion protein enciphering and propagating prion diversity. Science 274:2079–2082.

Telling GC, Scott M, Hsiao KK, Foster D, Yang SL, Torchia M, Sidle KC, Collinge J, DeArmond SJ, Prusiner SB (1994) Transmission of Creutzfeldt-Jakob disease from humans to transgenic mice expressing chimeric human-mouse prion protein. Proceedings of the National Academy of Sciences of the United States of America 91(21):9936-9940.

Telling GC, Scott M, Mastrianni J, Gabizon R, Torchia M, Cohen FE, DeArmond SJ, Prusiner SB (1995) Prion propagation in mice expressing human and chimeric PrP transgenes implicates the interaction of cellular PrP with another protein. Cell.

Terry C, Wadsworth JDF (2019) Recent advances in understanding mammalian prion structure: A mini review. Frontiers in Molecular Neuroscience 12:169.

Tesar A, Matej R, Kukal J, Johanidesova S, Rektorova I, Vyhnalek M, Keller J, Eliasova I, Parobkova E, Smetakova M, Musova Z, Rusina R (2019) Clinical Variability in P102L Gerstmann–Sträussler–Scheinker Syndrome. Annals of Neurology 86:643–652.

Tobler I, Gaus SE, Deboer T, Achermann P, Fischer M, Rulicke T, Moser M, Oescht B, McBride PA, Manson JC (1996) Altered circadian activity rhythms and sleep in mice devoid of prion protein. Nature 380:639–642.

Tuzi NL, Cancellotti E, Baybutt H, Blackford L, Bradford B, Plinston C, Coghill A, Hart P, Piccardo P, Barron RM, Manson JC (2008) Host PrP glycosylation: A major factor determining the outcome of prion infection. PLoS Biology 6:872–882.

Vogel C, Marcotte EM (2012) Insights into the regulation of protein abundance from proteomic and transcriptomic analyses. Nature Reviews Genetics 13:227–232.

Wadsworth JDF, Asante EA, Collinge J (2010) Review: Contribution of transgenic models to understanding human prion disease. Neuropathology and Applied Neurobiology.

Wadsworth JDF, Collinge J (2011) Molecular pathology of human prion disease. Acta Neuropathologica 121:69–77.

Wadsworth JDF, Hill AF, Beck JA, Collinge J (2003) Molecular and clinical classification of human prion disease. British medical bulletin 66:241–254.

Wadsworth JDF, Hill AF, Joiner S, Jackson GS, Clarke AR, Collinge J (1999) Strain-specific prion-protein conformation determined by metal ions. Nature Cell Biology 1:55–59.

Wadsworth JDF, Joiner S, Linehan JM, Cooper S, Powell C, Mallinson G, Buckell J, Gowland I, Asante EA, Budka H, Brandner S, Collinge J (2006) Phenotypic heterogeneity in inherited prion disease (P102L) is associated with differential propagation of protease-resistant wild-type and mutant prion protein. Brain 129:1557–1569.

Wang H, Rhoads DD, Appleby BS (2019) Human prion diseases. Current Opinion in Infectious Diseases 32.

Wang S, Lai X, Deng Y, Song Y (2020) Correlation between mouse age and human age in anti-tumor research: Significance and method establishment. Life Sciences 242:117242.

Watts JC, Giles K, Serban A, Patel S, Oehler A, Bhardwaj S, Guan S, Greicius MD, Miller BL, DeArmond SJ, Geschwind MD, Prusiner SB (2015) Modulation of Creutzfeldt-Jakob disease prion propagation by the A224V mutation. Annals of Neurology 78:540–553.

Watts JC, Prusiner SB (2014) Mouse models for studying the formation and propagation of prions. Journal of Biological Chemistry.

Wells GA, Scott AC, Johnson CT, Gunning RF, Hancock RD, Jeffrey M, Dawson M, Bradley R (1987) A novel progressive spongiform encephalopathy in cattle. The Veterinary Record 121:419–420.

Westaway D, DeArmond SJ, Cayetano-Canlas J, Groth D, Foster D, Yang SL, Torchia M, Carlson GA, Prusiner SB (1994) Degeneration of skeletal muscle, peripheral nerves, and the central nervous system in transgenic mice overexpressing wild-type prion proteins. Cell 76:117–129.

White AR, Enever P, Tayebi M, Mushens R, Linehan J, Brandner S, Anstee D, Collinge J, Hawke S (2003) Monoclonal antibodies inhibit prion replication and delay the development of prion disease. Nature 422:80–83.

Will RG, Ironside JW, Zeidler M, Estibeiro K, Cousens SN, Smith PG, Alperovitch A, Poser S, Pocchiari M, Hofman A (1996) A new variant of Creutzfeldt-Jakob disease in the UK. The Lancet 347:921–925.

Williams ES, Young S (1980) Chronic wasting disease of captive mule deer: a spongiform encephalopathy. Journal of Wildlife Disease 16:89–98.

Windl O, Giese a, Schulz-Schaeffer W, Zerr I, Skworc K, Arendt S, Oberdieck C, Bodemer M, Poser S, Kretzschmar H a (1999) Molecular genetics of human prion diseases in Germany. Human genetics 105:244–252.

Wulf MA, Senatore A, Aguzzi A (2017) The biological function of the cellular prion protein: An update. BMC Biology 15:1–13.

Xiao X, Cali I, Dong Z, Puoti G, Yuan J, Qing L, Wang H, Kong Q, Gambetti P, Zou WQ (2013) Protease-sensitive prions with 144-bp insertion mutations. Aging 5:155–173.

Yam AY, Gao CM, Wang X, Wu P, Peretz D (2010) The octarepeat region of the prion protein is conformationally altered in PrPSc. PloS one 5:e9316.

Yang H, Wang H, Shivalila CS, Cheng AW, Shi L, Jaenisch R (2013) XOne-step generation of mice carrying reporter and conditional alleles by CRISPR/cas-mediated genome engineering. Cell 154:1370.

Yang S, Delgado R, King SR, Woffendin C, Barker CS, Yang ZY, Xu L, Nolan GP, Nabel GJ (1999) Generation of retroviral vector for clinical studies using transient transfection. Human Gene Therapy 10:123–132.

Yen ST, Zhang M, Deng JM, Usman SJ, Smith CN, Parker-Thornburg J, Swinton PG, Martin JF, Behringer RR (2014) Somatic mosaicism and allele complexity induced by CRISPR/Cas9 RNA injections in mouse zygotes. Developmental Biology 393:3–9.

Young K, Clark HB, Piccardo P, Dlouhy SR, Ghetti B (1997) Gerstmann-Straussler-Scheinker disease with the PRNP P102L mutation and valine at codon 129. Molecular Brain Research 44:147–150.

Zanusso G, Monaco S, Pocchiari M, Caughey B (2016) Advanced tests for early and accurate diagnosis of Creutzfeldt-Jakob disease. Nature Reviews Neurology 12:427.

Zanusso G, Petersen RB, Jin T, Jing Y, Kanoush R, Ferrari S, Gambetti P, Singh N (1999) Proteasomal degradation and N-terminal protease resistance of the codon 145 mutant prion protein. Journal of Biological Chemistry 274:23396–23404.

Zhang X, Li T, Ou J, Huang J, Liang P (2021) Homology-based repair induced by CRISPR-Cas nucleases in mammalian embryo genome editing. Protein and Cell 13(5): 316-335.

Zhang Y, Ge X, Yang F, Zhang L, Zheng J, Tan X, Jin Z-B, Qu J, Gu F (2014) Comparison of non-canonical PAMs for CRISPR/Cas9-mediated DNA cleavage in human cells. Scientific reports 4:1–5.